MODELLING AND ANALYSIS OF A CATERPILLAR SHAFT USING 2D AND 3D FEA

THESIS REPORT

by

PALASH MANISH KACHHY

to obtain the degree of

Master of Science in Civil Engineering

at Delft University of Technology

THESIS COMMITTEE

Chair and University Supervisor	: Dr. Ir. Wout Broere
Main Company Supervisor	: Ir. Thomas Aelen
Secondary University Examiner	: Dr. Ir. Kees Blom
Secondary Company Examiner	: Ir. Frank Kaalberg

ACKNOWLEDGEMENTS

In memory of my grandparents who died before they could see me graduate.

Lots of love and thanks to my parents, Col. Manish and Mrs. Manisha, my brother, Arnav, and my relatives for their unconditional and continuous support.

Thanks to my best friend (brother in fact) Saurabh, and his family, for their support and patience…and putting up with me for so long!

My sincere gratitude to the members of Witteveen+Bos for sharing their knowledge on the subject matter; especial thanks to Mr. Zhekang Huang for his guidance in modelling with DIANA FEA – a true wizard!

SUMMARY

An important part of a tunnel project is its access which is usually achieved through a shaft, either temporary or permanent. As bigger and deeper shafts are conceived, the conventional designs like rectangular or circular shafts do not fulfil project requirements well which is where caterpillar or peanut shaped shafts provide a solution. The caterpillar shape has been adopted recently in projects in Brazil, Hong Kong and the U.K. but not much information exists in the public domain about the caterpillar shafts' structural behaviour and design nuances; thus, this study explores these two aspects of the shaft. A 3-cell caterpillar shaft of 25m diameter, 52m d-wall depth, 40m excavation depth and d-wall cross-wall support was the main model analysed in this report using 2D and 3D FEM methods in DIANA FEA software (version 10.8 and 10.9).

The caterpillar shaft was reduced to a quarter size following the lines of symmetry for detailed analyses. The caterpillar shaft showed high rigidity with maximum cumulative deformation of 6.8mm in the middle cell d-wall panels and 6.9mm of deformation in the Y-panel when a portion of cross-wall was removed with no buttress support. This structural rigidity was because of the development of hoop forces in the d-wall panels and the presence of cross-walls. However, the high rigidity of the structure also meant that there was negligible movement in the soil which did not trigger any soil arching effect as the soil remained in the neutral state. 2D axisymmetric analysis, commonly used for the numerical analysis of a circular shaft, was compared to the circular section of the caterpillar shaft in the 3D model. Similarly, a 2D plane-strain analysis, which represents the

long side of a rectangular shaft, was compared to the junction of the adjacent cells at the Y-panel location of the caterpillar shaft in 3D to see if the results were comparable. The findings revealed that neither of the 2D models provided a reasonable estimation of forces when compared to the 3D model; this discrepancy was primarily due to the differences in the shaft designs and the distinct ways in which they deform – the caterpillar shaft deformed like an elliptical shaft with compression in the long end and elongation in the shorter end. The axisymmetric model underestimated the results of hoop forces in the circular 3D d-wall panels by about 15-20% only in the sections of wall above the depth of excavation but below excavation level the results deviated considerably. Likewise, the 2D plane-strain model could only be used to compare the Y-panel with multi-level struts support, and not the Y-panel with cross-wall support due to inherent geometric limitations, which overestimated the deformation by about 52% (±17%) and bending moment by 15-25%. The Y-panel in the 3D model was also tested with varying thicknesses of buttress which provided additional support to the Y-panel against bending moments. Adding just 1m thick buttress at the Y-panel reduced the bending moments in the Y-panel by up to 30% but increasing buttress thickness from 1m to 2m or 3m showed diminishing returns.

From this study, the structural response of the circular d-wall panels and the Y-panels was provided while also providing some 2D and 3D modelling insight. The caterpillar shaft provides great structural rigidity while experiencing forces which were within the design and feasibility limits. Such a structure can be employed in various cut-and-cover and excavation projects to reduce deformation and heavy strut support. The structure, however, requires 3D modelling for accurate assessment of shaft response. Further effort is required to adapt 2D analyses to the 3D using back-analysis and validate those with the results from field measurements.

TABLE OF CONTENTS

LIST OF TABLES

LIST OF FIGURES

1

INTRODUCTION

This chapter summarises the current excavation designs for rectangular, circular and caterpillar shafts. It highlights the research gaps and the motivation of this study. Lastly, it discusses the study's objectives, significance to community, scope and limitations.

Sub-chapters:

1. Research Context
2. Research Focus
3. Scope and Limitations

1.1. Research Context

Large underground infrastructure projects are on the rise due to rapid urbanisation and increasing experience in the field of tunnel engineering. An important component of such tunnel projects is the access to the tunnel alignment through shafts. Shafts are the main access points to the tunnels during, and sometimes after, the construction of tunnels. Depending upon the use-case, these can either be temporary or permanent structures; in the latter case, an open shaft is often repurposed for housing ventilation, emergency, or maintenance access points etc., or, in case of railways and metros, as a station.

In The Netherlands, and places with deltaic soil conditions, the construction of shafts is one of the most complex undertakings due to two main reasons: (i) the presence of (soft) soil strata; (ii) presence of groundwater table at or close to the surface. While the presence of the soil strata itself is not a problem, when paired with a high groundwater table, it adds significant lateral or inward force on the retaining structures. The presence of a high groundwater table also means that often wet excavation is adopted. The presence of water inside the shaft during the excavation makes it difficult to install bracings[1] to complement the retaining structure. These shafts are often constructed using sheet-piles and D-walls, but these become uneconomical as the shaft depth goes beyond 15-20m because to counteract the significant forces acting on the retaining walls, the solution is to install more struts/bracings at the cost of working space, install heavier walls or change the design of the shaft.

[1] also called props or struts

Shafts can be designed in different shapes depending on the pre-existing conditions. The three most common shapes are: rectangular, circular, and elliptical. Rectangular shafts are common when the length of the shaft is of significance like in the case of metro or railway stations. Most common advantages of having a rectangular shape are the ease of design and optimal space utilisation. Circular and elliptical shafts are commonly used for relatively smaller, but deeper, excavations such as to house ventilation equipment or pump stations, serve as access-points for the tunnels (during and post construction) or for building foundations. The inherent advantage of a circular and elliptical shape is that the curved shape distributes the lateral forces evenly in compression – called hoop forces – along its geometry. This reduces the shear forces and bending moments, and the need for internal bracing of the retaining structure, providing large, unobstructed working space.

The disadvantage of a rectangular shape becomes pronounced when dealing with deep excavations. The lateral forces and bending moments increase quickly as the depth increases, more so in presence of a high groundwater level when it cannot be lowered, which demands a heavy design for the retaining element complemented by a dense array of bracings/struts which significantly reduces the working area. Circular/elliptical shaped shafts do address this disadvantage of rectangular shape, however, these become suboptimal in terms of space utilisation when there is also a need for additional space lengthwise.

Figure 1-1: A typical cut-and-cover excavation of a rectangular shaft. Notice the web of struts required to keep the shaft in place. Photo: oasys-software.com

1.1.1. Intro to Caterpillar Shaft

To address the respective disadvantages of rectangular and circular/elliptical shapes, a hybrid is considered which is the **peanut** or **caterpillar shape**[2] for the shafts. Caterpillar shafts utilise the circular shape for an even compressive force distribution to concentrate all the forces at the junction of adjoining circular shafts which adds length to the shaft as shown in Figure 1-2.

[2] 'Peanut shaft' if it has 2 cells, and 'caterpillar shaft' for 3 or more cells. In this study, the term 'caterpillar shaft' is used as a blanket term for all sizes.

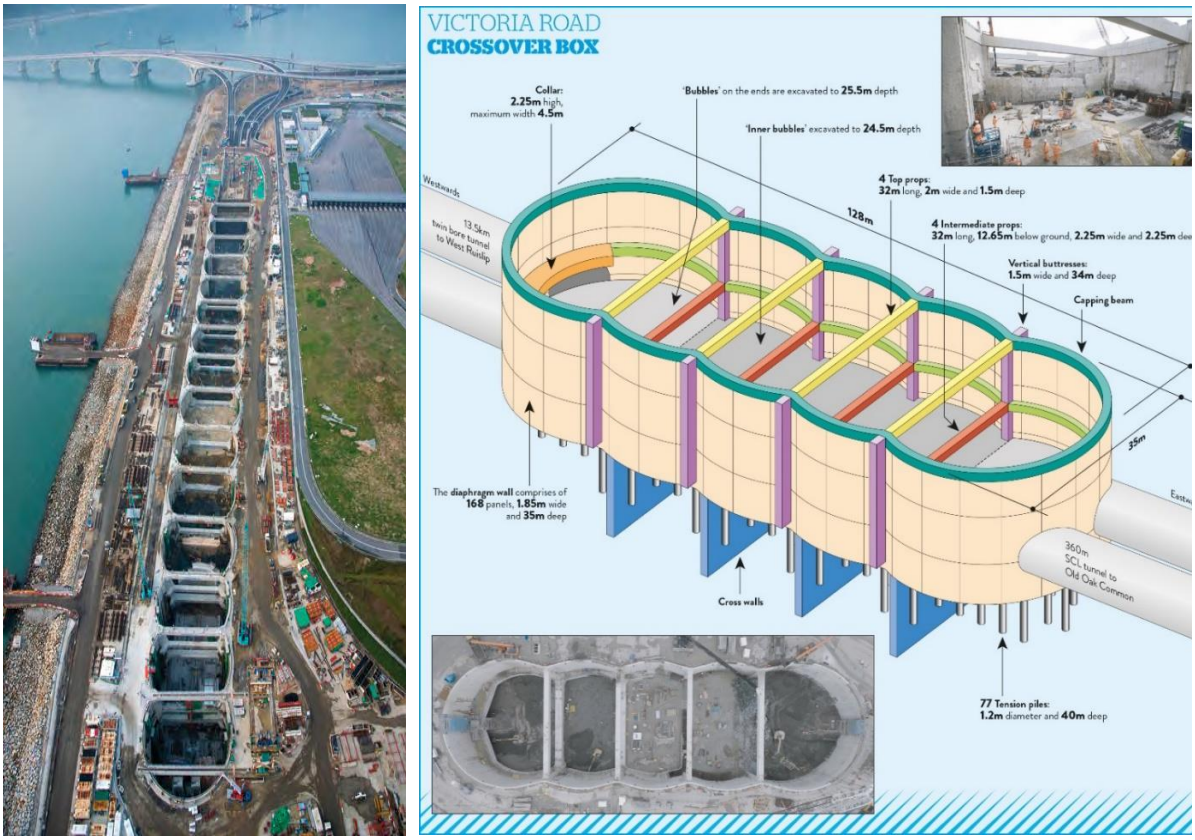

Figure 1-2: A 15-cell caterpillar shaft executed in Tuen Mun – Chek Lap Kok Link in Hong Kong (left). Photo: issuu.com; Schematic diagram of Victoria Road Crossover Box from the U.K. (right)

The caterpillar or peanut shaped shaft comes as a good hybrid of rectangular and circular shapes while addressing the disadvantages of the two. It is expected that the circular section of the shaft would generate compressive hoop forces in the circular panels and concentrate them at the junction of the adjoining shafts which can then be supported by heavy struts. This would leave the mouth of the shafts unrestricted during construction. Thus, a caterpillar shaft proves especially beneficial when:

(i) Dealing with large lateral forces (depth greater than 25m),

(ii) There is a need for unrestricted opening of shaft mouth

(iii) There is also a need for space lengthwise.

1.1.2. Background for Research Project

The thesis project stems from a project based in Eemshaven. Eemshaven is a seaport in the province of Groningen in the north of the Netherlands. It is also regarded as the 'energy port' as a third of all energy is supplied to the Netherlands from here.

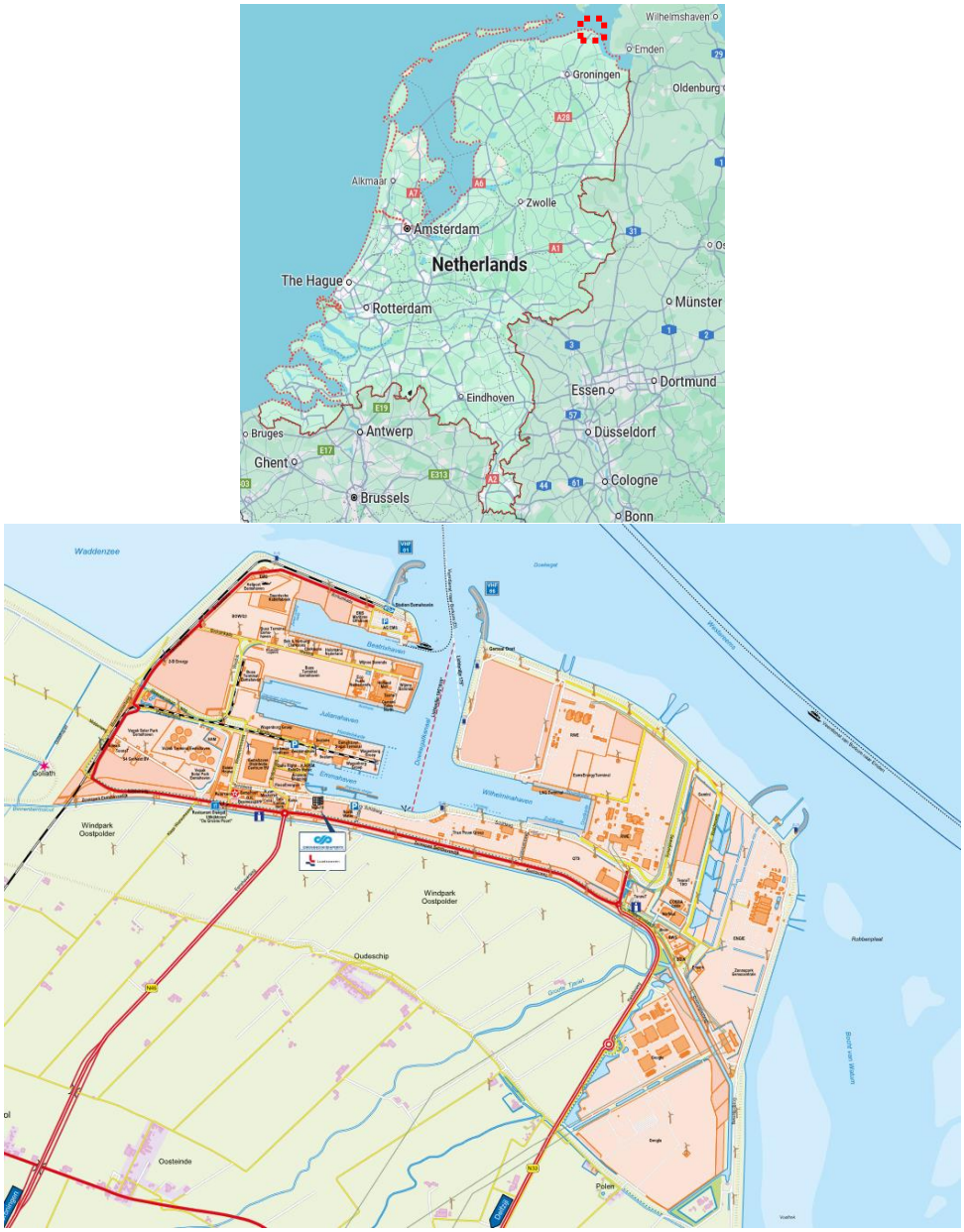

Figure 1-3: Map of Eemshaven

The project requires a tunnel construction with approx. 10m internal diameter TBM or a combination of two smaller TBMs. Given the difficult geological conditions and project requirements, the tunnel

alignment is placed 40m below the surface level. Access to the tunnel alignment depth requires the construction of a shaft which will not only serve as the launching shaft for the TBM during construction but also as a permanent structure to house ventilation, firefighting, emergency back-up systems, access for powerlines and act as an access point to the tunnels.

In The Netherlands, the presence of high groundwater table present across the country, eliminates the possibility to have a rectangular shaft for this project due to practical and economic constraints; additionally, the project requirements demand a long and wide, unrestricted working space which also eliminates the circular shape. Hence, a proposal for a two- or three- cell caterpillar shaft of 25m diameter each with a depth of 40m to the base was made by Witteveen+Bos. The idea for this shape stemmed from the other projects [19][20][21] which have been or being executed elsewhere. However, a shaft of this magnitude or this shape, has not been executed before in Dutch conditions.

Another motivation for this study is that limited knowledge on such structures is currently available in public databases. Although, caterpillar shafts have been executed successfully in some cases, the design challenges and the structural response of the shaft, especially at the Y-panel, largely remain undisclosed; hence, the analysis of caterpillar shaft was proposed as a thesis topic to fill-in these gaps.

1.2. Research Focus

As previously mentioned, a project of this shape and magnitude has not been executed in The Netherlands before and limited knowledge is available in the public domain. From the literature that is available on caterpillar shafts (discussed in Chapter 2), it is seen

that the soil-structure interaction of the shafts was carried out in a combination of 2D and 3D analyses. 2D axi-symmetric analysis was employed to derive the forces experienced by the d-wall in the circular section of the shaft which were then used to create the 3D model. However, not much information is available about the design/modelling considerations, comparison of 2D and 3D results with field measurements, and structural response of the shaft under various soil and structural conditions.

Thus, this thesis aims to close this knowledge gap and provide a base for further design development of caterpillar shafts. This research aims to answer the question: "What is the structural response of a caterpillar shaft and how does it vary under various soil and structural conditions". This will give an insight on the benefits of using such a structure and what a preliminary design analysis of such a structure entails. In doing so

(i) forces developed in the perimeter D-wall panels and the Y-panel will be studied.

(ii) modelling considerations for the construction and excavation of the shaft will be discussed. A caterpillar shaft based on the project requirements will be modelled to study the forces associated with this non-circular shape.

(iii) equivalent 2D realisations of rectangular and circular shapes will be modelled using finite element analysis and results like deformations and structural forces will be compared to the results from the 3D caterpillar model.

1.3. Scope and Limitations

This research aims to serve as an exploratory work. As such

(i) The model presented here does not represent the detailed design of the final structure.

(ii) Many assumptions are made to simplify the model, such as simplified stratigraphy and connections between structural members due to lack of experimental and field data.

(iii) External factors such as presence of utilities, existing super-structures are not considered.

(iv) Launching of TBM is not considered in the model.

2

LITERATURE REVIEW

This chapter discusses some of the literature relevant to rectangular shafts, circular shafts, elliptical shafts and caterpillar shafts

Sub Chapters:

1. Rectangular, Circular and Elliptical Shafts
2. Caterpillar Shafts

2.1. Rectangular, Circular and Elliptical Shafts

Deep excavations are a common practice in civil engineering and in mining engineering. ITA classifies excavations from 70-90m as shallow shafts whereas ‘medium depth’ shafts in mining range from 90-300m [1]. In context of urban civil projects, shafts beyond 20-30m depth can be classified as deep shafts.

The biggest factor affecting the stability of a shafts, besides good execution, is the shape of the shaft. As already mentioned, rectangular shaped shafts exhibit large bending moments and shear forces in the retaining structure that require internal strutting/bracing which reduces the open area from the shaft mouth and are difficult to place in case of a wet excavation. The circular or elliptical shape is often adopted as the circular shape relies on compressive forces to carry the lateral loads and requires less internal bracing; besides, given that concrete exhibits greater strength in compression, such a circular design reduces the need for excessive steel reinforcement [2]. These compression forces generated due to the circularity of the structure are called ‘hoop forces’ which act around the entire wall. The consequence of hoop forces is that the shaft deforms uniformly.

The deformation characteristics of the retaining walls from site monitoring data have been studied by various researchers to draw empirical relationships depending on the soil type. The earliest study, and most notable one, has been by R.B. Peck [2]. This study presents general deformation behaviour of vertical structure with cross supports and settlement of soil beside it which is reproduced in Figure 2-1.

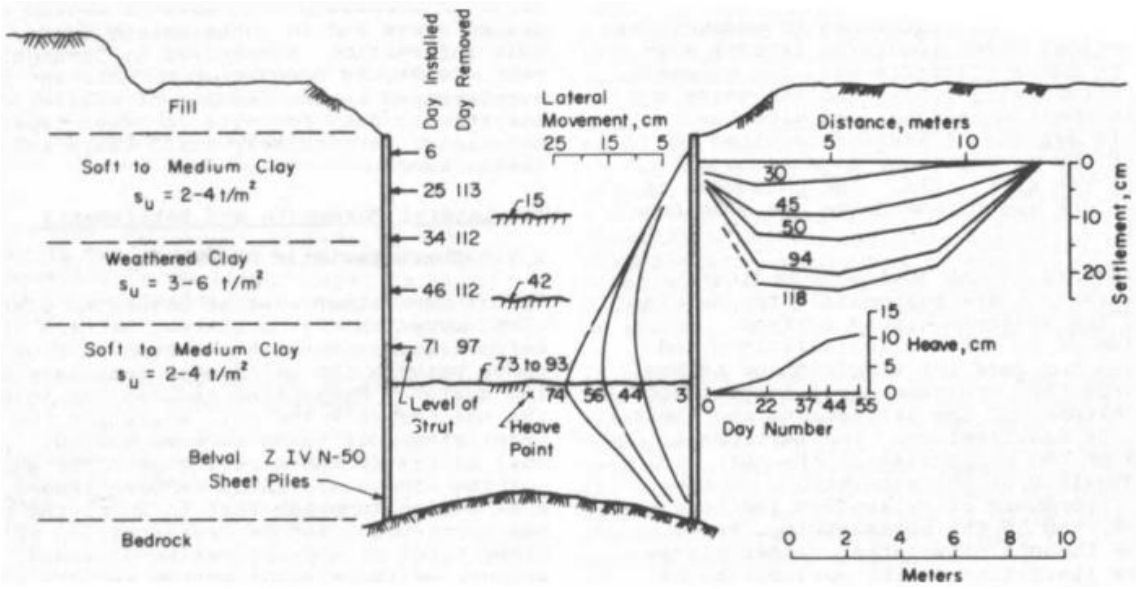

Figure 2-1: Relation of lateral movement of retaining structure and adjacent soil as proposed by R. B. Peck.

More recently, a database of excavation cases, first by M. Long [3] and then by C. Moormann [4], mostly of rectangular excavations, has provided insight in the behaviour of shaft in various soil conditions and type of retaining structures employed. Some select findings from the study [4] are summarised below:

(i) For majority of the excavation in soft soil (cu < 75 kN/m2) the wall displacement to the max. depth of excavation ratio was noticed between 0.5%-1%; the same for non-cohesive soils was 0.27% on average.

(ii) For deep excavations in soft and stiff cohesive soils, the maximum horizontal wall displacement uh_{max} is usually observed at the final depth of excavation or, as in 67% of the case histories, at a depth ratio of 0.5-1.0 of the max. depth of excavation below ground surface.

(iii) For 70% of all case histories the maximum soil settlement (behind retaining wall) is measured at a horizontal distance from the retaining wall that is smaller than half the excavation depth; in

soft clays the distance can also increase up to 2x the excavation depth.

(iv) The wall displacements seem to be independent of the magnitude of the embedded length of the wall (although a minimum embedded length cannot be zero).

(v) There is no direct or at least no linear correlation between the system stiffness[3] and the movements; an increase in the system stiffness does not result in a corresponding decrease in the displacements.

A circular shaft utilises the arching effect which reduces the shear and bending moments in the retaining structure by developing hoop forces throughout the structure. In an ideal case where the shape of the shaft is perfectly circular and the panels are perfectly aligned, the shaft would experience only hoop forces and no radial forces which act towards the centre of the circle (see Figure 2-2 [16]). The forces experienced by a cylinder can be formulated as follow:

$$\sigma_a = 0$$

Eq: 1

$$\sigma_{hoop} = \frac{-P \times r_o^2 \times (r_i^2 + x^2)}{x^2 \times (r_o^2 - r_i^2)}$$

Eq: 2

$$\sigma_r = \frac{-P \times r_o^2 \times (x^2 - r_i^2)}{x^2 \times (r_o^2 - r_i^2)}$$

Eq: 3

[3] Retaining wall and support (struts/bracings)

Where:

P = external pressure [kPa]

r_o = outer radius [m]

r_i = inner radius [m]

x = radial position in cross-section [m]

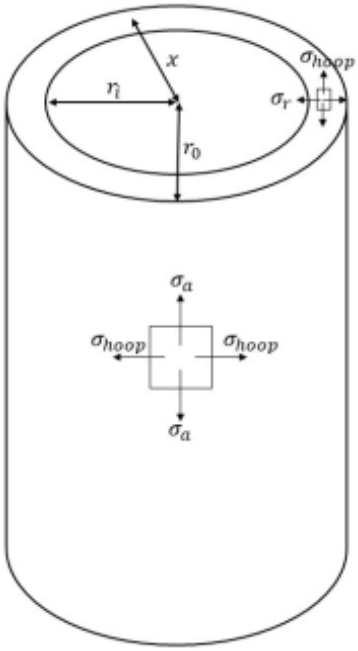

Figure 2-2: Stresses developed in a cylinder

In case of an excavation shaft, the external pressure would primarily be the horizontal soil pressure calculated using Eq: 4.

$$\sigma_H(z) = K \times \sigma'_V(z) + u_W(z)$$

Eq: 4

Where:

K = lateral earth pressure coefficient [-]

σ'_V = effective vertical earth pressure [kPa]

u_W = pore water pressure [kPa]

The lateral earth pressure coefficient depends on movement of the retaining structure in relation to the position of the soil which has three states – active (K_a), neutral (K_0) and passive (K_p). Active and passive lateral earth pressure coefficients are analytically derived from two main methods – Coulomb and Rankine. For simplicity, only Rankine's method for calculating K_a and K_p are discussed here.

$$K_0 = (1 - sin\phi') \times \sqrt{OCR}$$

Eq: 5

$$\mathrm{K_a} = \tan^2(45° - \frac{\phi'}{2})$$

Eq: 6

$$K_p = \tan^2(45° + \frac{\phi'}{2})$$

Eq: 7

Unlike for rectangular shafts, an extensive database does not yet exist for circular/cylindrical shafts. Two databases of circular shafts [5][6] have provided some insight on circular shafts; although, both databases are exclusively based in the U.K. One such database, by N.E. Faustin [6], has site data from 27 constructions undertaken in the U.K. The study categorised the shaft construction in two: support before excavation (SBE) and excavation before support (EBS). It reported the maximum soil settlement of 0.02-0.04% of the maximum excavation depth and negligible settlement at a distance 1-1.5 of maximum excavation depth for SBE. This study did not comment on the horizontal movement experienced by the shaft due to limited data; however, if Peck's [2] postulate of constant volume displacement (vertical:horizontal) is to be applied here, then a similar displacement for the wall movement could be expected which would result in considerably lower values when compared to rectangular shafts (although this was disproved in later studies [4]). In another

study which looked at the site monitoring data of a large and deep circular excavation pit (30m dia. x 56m deep) [7], it was observed that the circular shaft deformed in two stages as seen in Figure 2-3: in the first stage, the circumferential compression deformation was caused by the joints between the diaphragm walls. Once the joints were compressed and the external loading was greater, vertical bending dominated the deformation mode. The maximum deformation observed for this structure was about 7mm at final excavation stage.

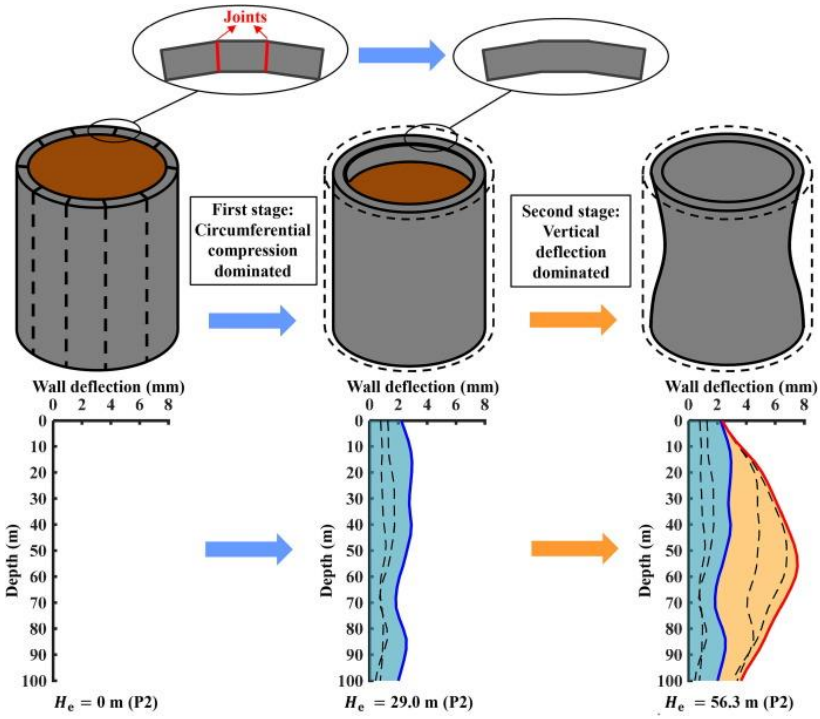

Figure 2-3: Two-stage wall deflection observed for a large and deep excavation [7]

The absence of high-quality monitoring data from circular excavation has been a drawback when trying to document the behaviour of circular shafts. Consequently, empirical methods are not common or reliable when describing the behaviour of circular shafts; those that exist are often based on a specific project. For example, one such empirical method available was derived from the monitoring data of only one shaft constructed using caisson sinking method in the U.K. [8] which is not relevant for this study.

Despite limited data, it is evident that the circular (or cylindrical) shafts exhibit a much lower deformation in the structure and the soil around it as compared to rectangular (or cuboidal) shafts. A consensus can be made that the circular shafts show an approx. deformation between 0.01-0.02%. These low deformations in circular shafts are attributed to the soil arching effect, in which lateral earth pressure will experience compression and extension in tangential and radial directions, respectively. The soil arching effect is famously described by K. Terzaghi [8] using a trapdoor model who provided the analytical solution which was then refined by Feng et al [9]. Later these analytical solutions for arching effect were extended by applying the slip-line method in the axisymmetric model [10][11]. These models were used to describe the said effect in tunnel construction, from where the idea for the application in vertical shafts could be established.

For an analytical analysis, a centrifuge test was conducted using kaolin clay with varying degrees of undrained shear strength to develop an empirical solution to predict subsurface soil displacements induced by circular shafts [13] and compared the lab results to the monitoring data from other projects. The study provided equations to evaluate vertical soil settlements and horizontal wall movements as shown in Figure 2-4. The study also concluded that maximum surface vertical displacement is significantly larger than the maximum horizontal displacement. Although this study showed good agreement of empirical equation and field data, this study is verified on very limited case studies.

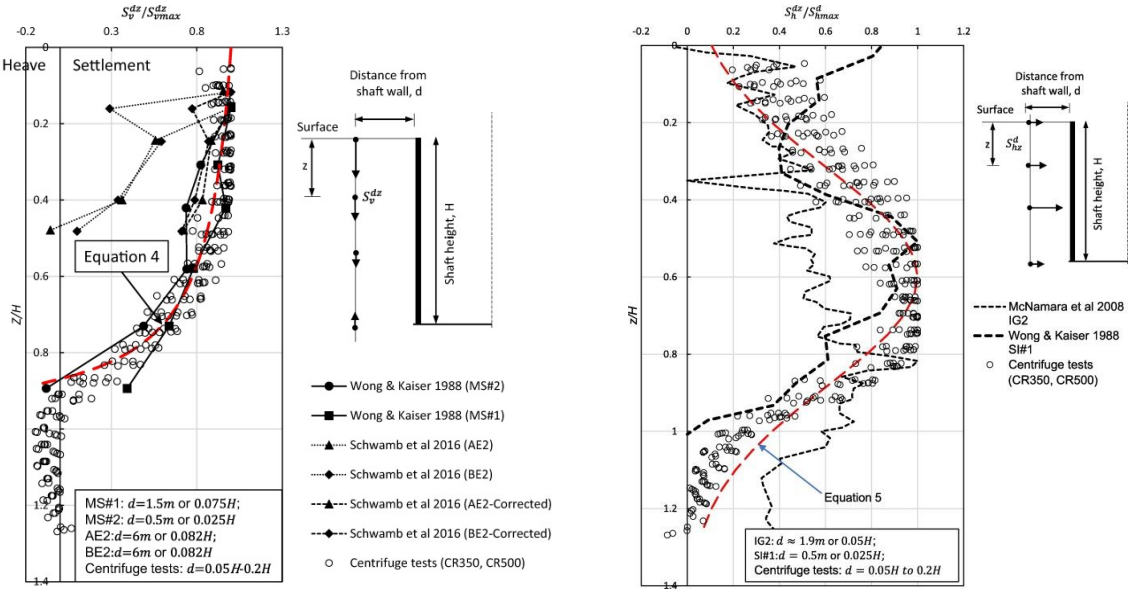

Figure 2-4: Subsurface vertical and horizontal movements [13]

For numerical evaluation of circular shafts, there have been multiple case studies available. One such study considered 20m diameter and 120m deep cylindrical model. The study provided normalized lateral earth pressure theory for excavated shafts by considering the 3D arching effect obtained from parametric studies using various levels of shaft stiffness [14]. It was found that the previous analytical models [8][11] underestimated the earth pressure acting on the cylindrical shaft because they did not consider the accurate arching effect. This study showed that the tangential stress increased while the radial stress decreased as the excavation progressed (Figure 2-5); additionally, this pattern was less obvious as the shaft stiffness was increased.

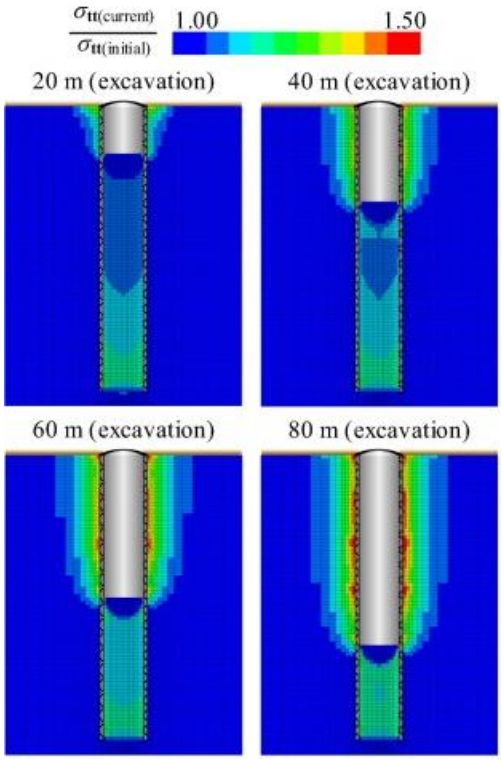

Figure 2-5: Tangential stress ratio contour at various excavation stages [14]

From these studies on circular shaft, it is evident that the circular shape offers to be a rigid structure, even at great depths. Naturally, any deviation from an ideal circular shape would not result in such an efficient design. In an elliptical shaft, for example, the deformation of the shaft walls does not show a uniform convergence as seen in Figure 2-3. Instead, the shaft converges at the long end and elongates in the short end as shown in Figure 2-6 [15]. Consequently, bending moment experienced by the shaft walls in the short end was greater than that experienced by the walls in long end. The ratio of 0.45 between the short and long diameters of an ellipse was found to be optimal [16].

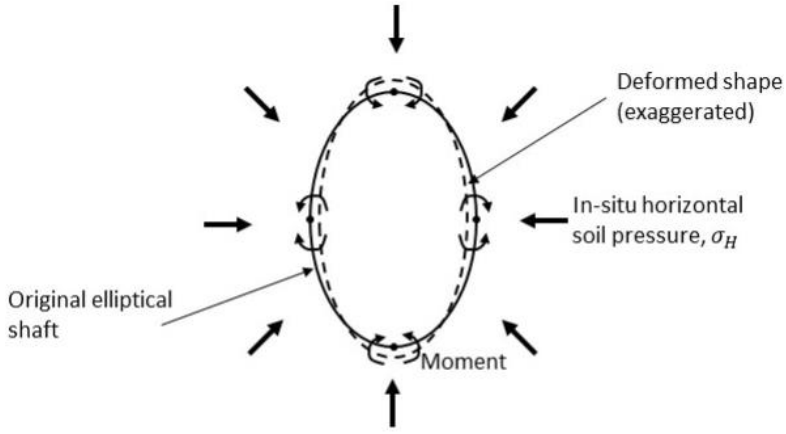

Figure 2-6: Stresses in elliptical shaft lining [15]

A case study on the underground parking garage in Garenmarkt, Leiden, The Netherlands, provides a good comparison of field and numerical results [17]. The parking garage was shaped like an elliptical shaft – hippodrome shape – which was analysed with 2D axisymmetric, 2D plane-strain and 3D analyses.

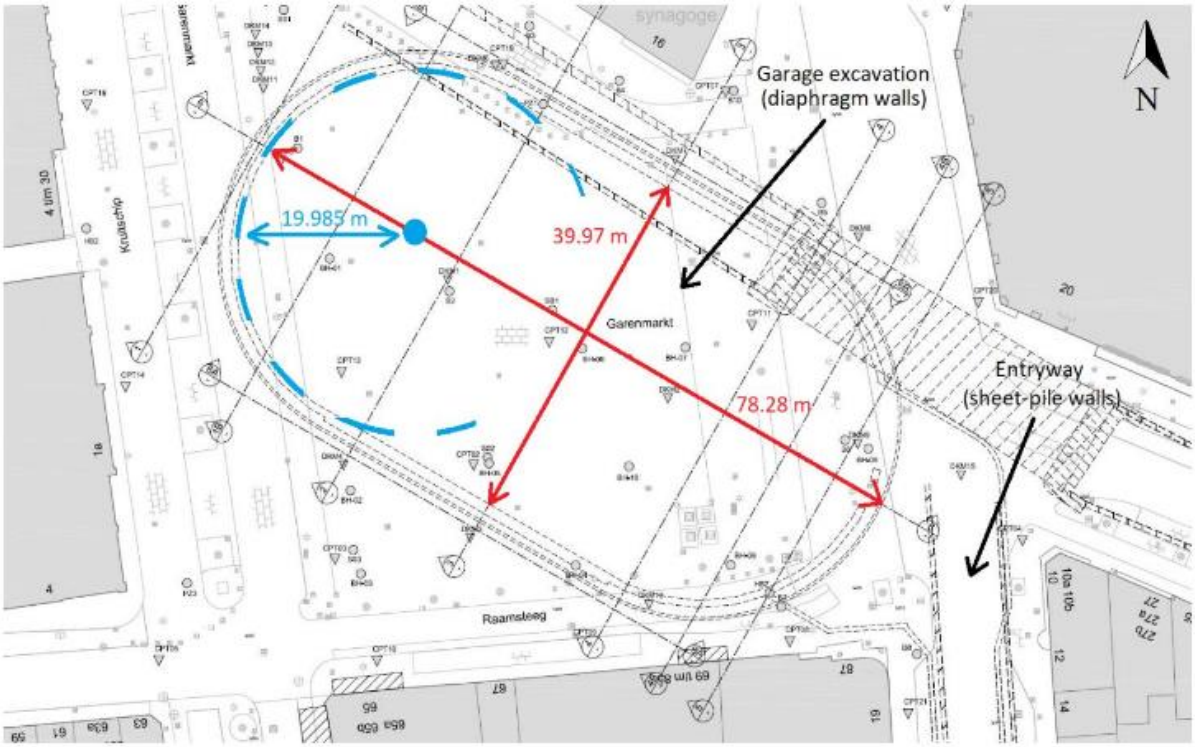

Figure 2-7: Excavation dimensions of the Garenmarkt parking garage in Leiden, The Netherlands [17]

The wall deformation results showed that the all the wall panels moved into the soil before moving towards the excavation side; measurement error was ruled out and no clear explanation was defined for such a behaviour. Overall, it was seen that none of the initial analyses, 3D or 2D, accurately predicted this deformation behaviour and all the analyses overestimated the max. deformation in the d-wall panels (see Figure 2-8); except in the case of transition zone, where the curved wall meets the straight wall, which reported 1-2mm difference (see Figure 2-9). The field measurements for the curved walls were deemed faulty so a comparison could not be made.

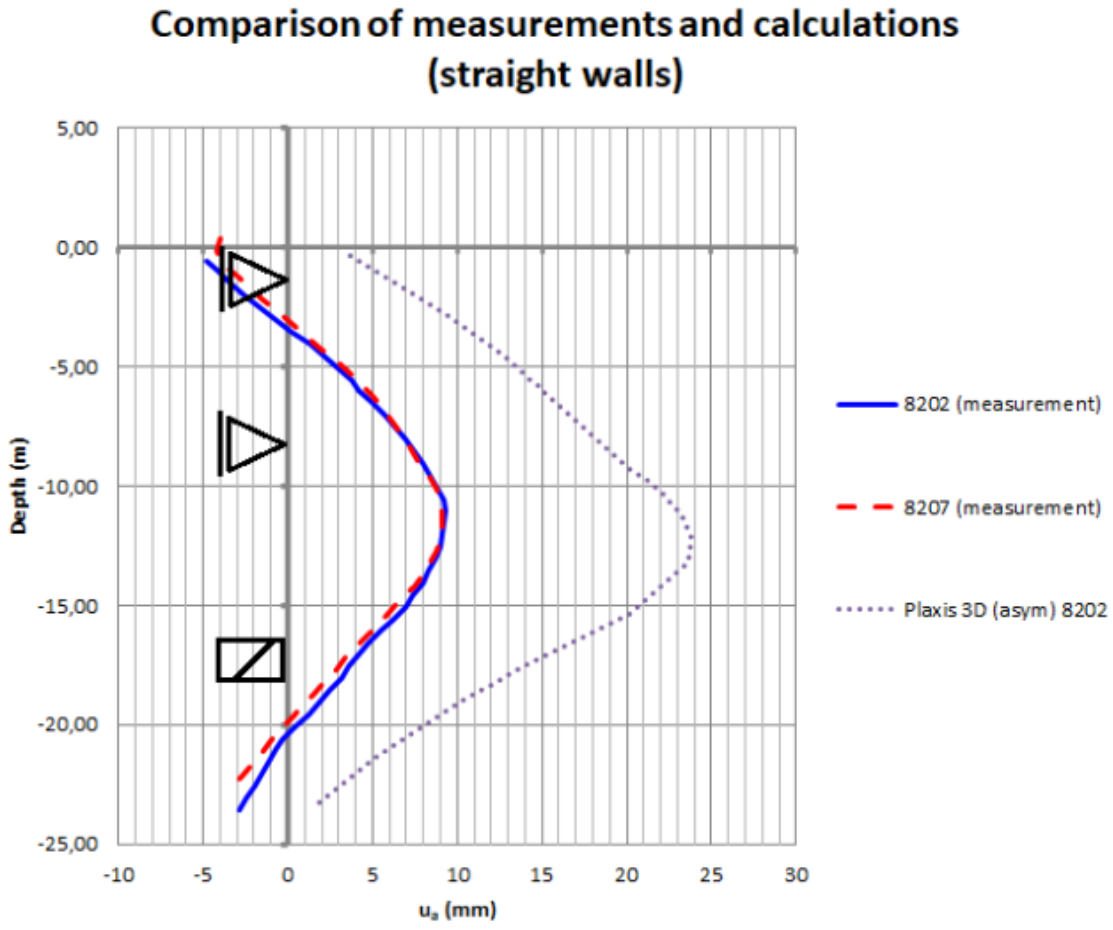

Figure 2-8: Comparison of the measured and calculated (best prediction only) displacements near the centre of the straight walls

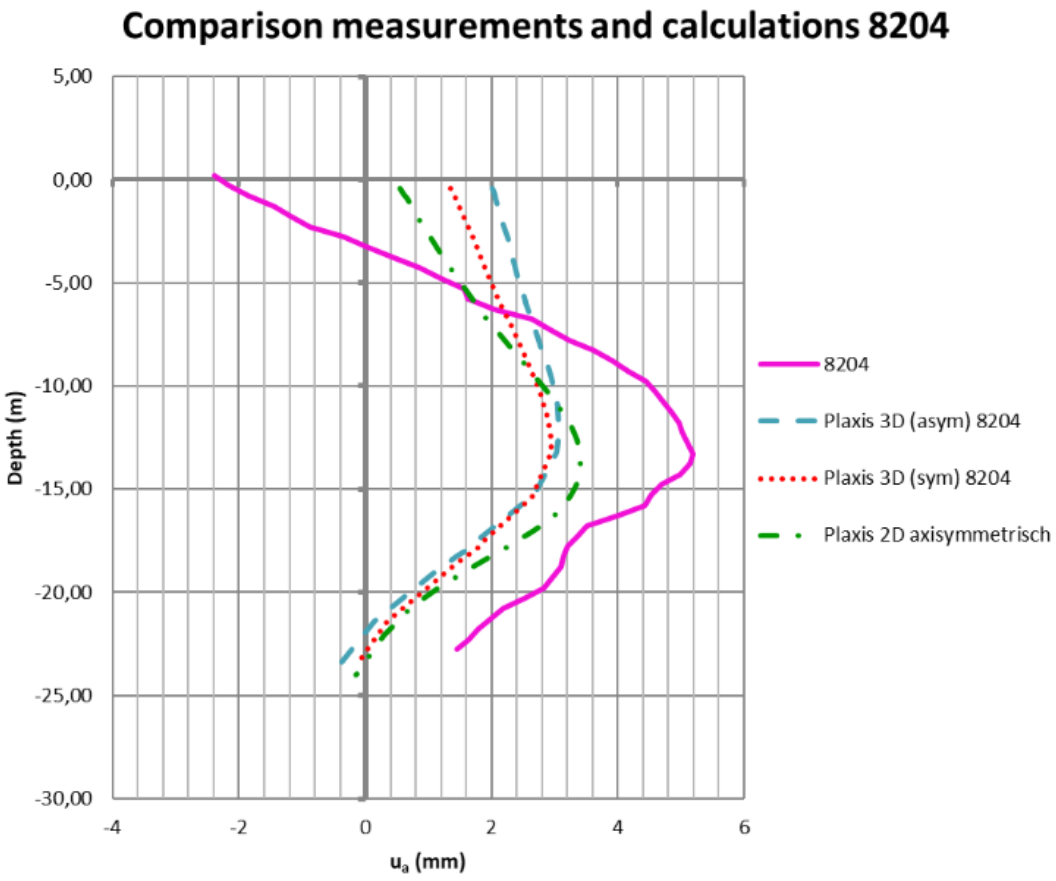

Figure 2-9: Comparison of the measured and calculated displacement in the transition zone

2.2. Caterpillar Shafts

Moving to caterpillar shafts, there have been no technical papers that detail analytical, empirical or numerical analyses for such a design. Although there have been many instances of caterpillar shaft construction in recent years, documentations of these structures are limited; what exists are articles reported by third parties which do not delve into the design, construction techniques and soil-structure interaction. It could be that due to the novel nature of these projects, either the information is deliberately not shared, or not enough research has been done to warrant publication of a peer-reviewed paper on the subject. Following subchapters summarise some of the literature that has been gathered on caterpillar shaft.

2.2.1. Design Of Sheet Pile Cellular Structures Cofferdams & Retaining Structures

The earliest mention of caterpillar shaft-like structure can be found in the manual by U.S. Army Corps of Engineers published in 1990 [17]. It details the construction of cofferdams using 'cellular structures' as they "are economical for this type of construction since stability is achieved relatively inexpensively". The manual proposes three types of cellular structures: circular cells, diaphragm cells and cloverleaf cells as shown in Figure 2-10. It is recommended that the diaphragm cells be constructed such that the arcs are connected by 120° intersection pieces or cross-walls (diaphragms), and the radius of the arc matches the cord-length of the arc to have equal tension in the arc and the diaphragm. Additionally, diaphragm cells are not independently stable and failure of one cell could lead to failure of the entire cofferdam.

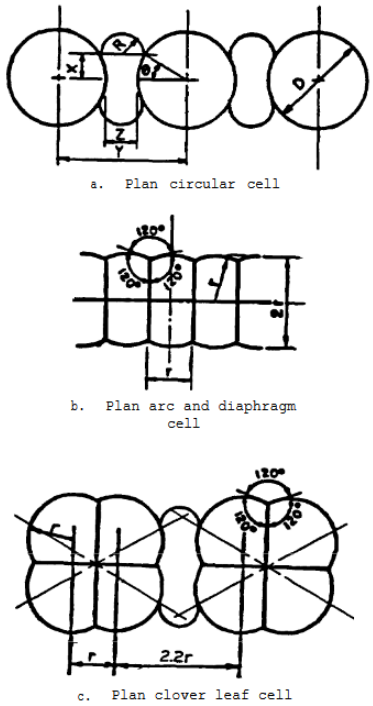

Figure 2-10: Typical arrangement of circular, diaphragm and cloverleaf cells

2.2.2. Brooklin Station of the Sao Paulo Metro, Brazil

Brooklin Station of Sao Paulo, Brazil, was constructed in October 2013 concluding a 13-month construction period [19]. It consisted of a 5-cell caterpillar shaft, each 36m in diameter and 27m in depth. Geology of the site consisted of sandy and clayey layers, multilevel aquifers and a high groundwater table at 1m below surface level.

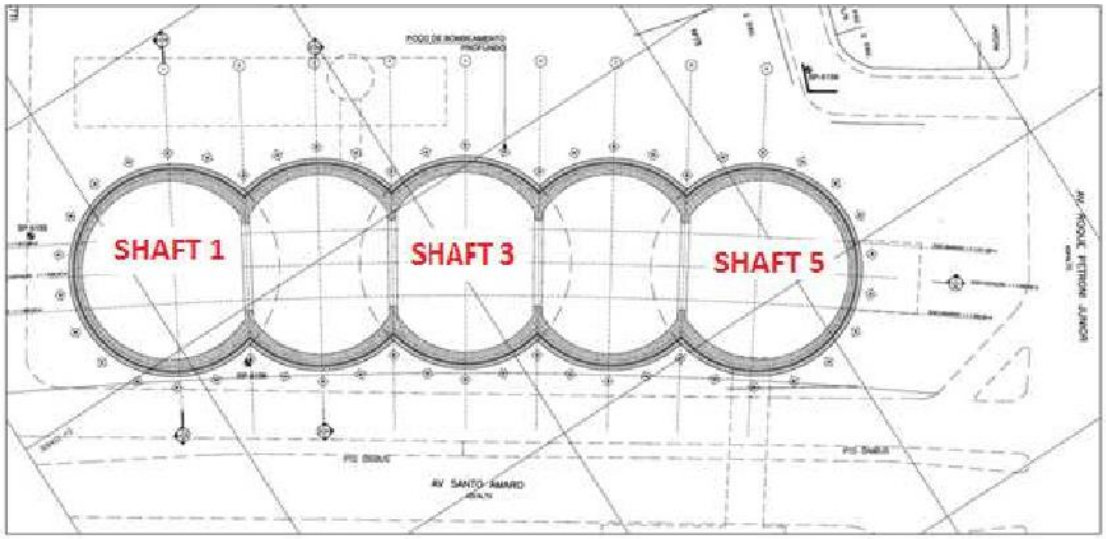

Figure 2-11: Plan view of Brooklin Station

The shaft was analysed using a combination of 2D axi-symmetric model, to verify shaft stability during excavation, and 3D analysis for overall impact of station excavation on the surroundings using finite difference method (FDM). The result of FDM analyses were verified by site monitoring data and both results showed similar results. The site monitoring data recorded a max. surface settlement of 15mm at 20m distance (0.56 times shaft diameter) and the inclinometers embedded within the d-walls showed a cumulative horizontal displacement of 20-35mm, with max. displacements located in cells 2, 3 and 4.

2.2.3. Tuen Mun - Chek Lap Kok Link in Hong Kong

This 15-cell caterpillar shaft was constructed to accommodate a 630m long dual two-lane sub-sea cut-and-cover tunnels which was 33m wide and 43m deep [20]. The site geology consisted mainly of reclamation fill followed by marine clay and alluvial clay with seams of alluvial sand. The coffer dam was constructed using D-wall panels and utilising slurry-trench technique for its construction. The lateral forces from the circumferential D-wall panels were borne by Y-shaped panel installed at the interface which directed the force to the struts installed inside the shaft. The article claims that compared to the traditional design (the specifics unmentioned) this caterpillar shape was more efficient in load distribution and significantly reduced the number of struts required to stabilise the structure.

The geotechnical analysis was done using both 2D and 3D FEM software and the structural analysis was done using 3D FEM analysis. Seepage analyses and staged excavation were considered in the PLAXIS axisymmetric analyses to calculate the lateral earth pressures and pore water distribution inside and outside the excavation, resulting from pumped dewatering below the excavation. Three-dimensional structural analyses of the caterpillar cofferdam were then performed using the computer programme SAP 2000. The perimeter arc D-wall, cross walls, struts and Y-panels were represented by a series of thin-shell elements and the ground medium surrounding the perimeter D-wall was represented by a series of area springs perpendicular to the shells. In case of tension, the ground springs were ignored, and no reaction was given to the D-wall. PLAXIS 3D analysis, which accounted for the soil-structure interaction, was used to study the overall behaviour of the shaft, in terms of movement and induced forces, and compared with SAP2000 models.

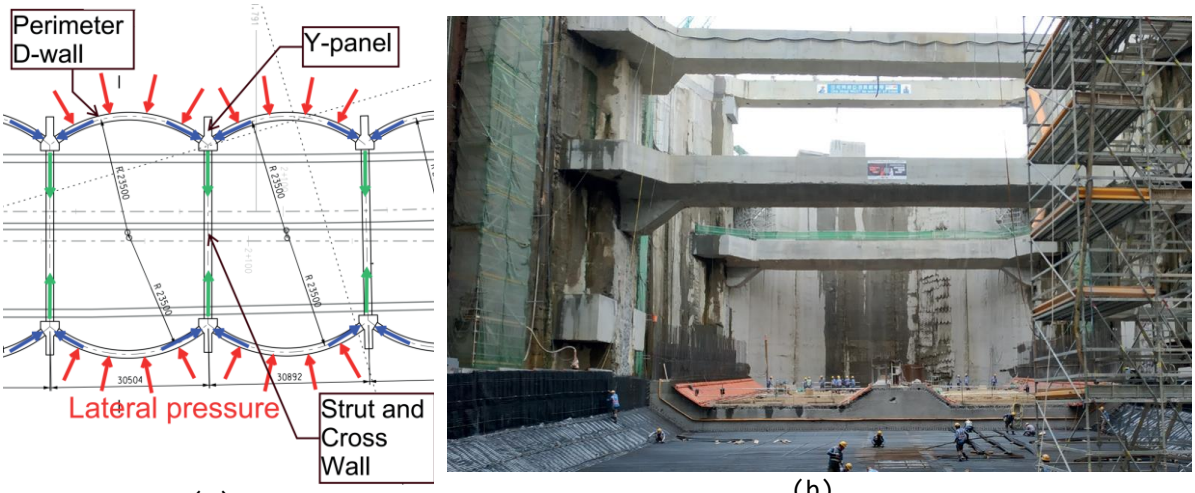

Figure 2-12: (a) Typical arrangement of Caterpillar cells and load transfer; (b) Cross section showing lateral support

The shear stress of around 73,000 kN and bending moments of about 310,000 kN-m were reported, and a heavy rebar cage (maximum 135 t) was employed for the Y-panel to support the reported forces; however, no further explanation or context is provided for the reported values.

2.2.4. Victoria Road Crossover Box

This was the first caterpillar shaft being excavated in the United Kingdom (UK) [21]. This 5-cell permanent structure was designed to be used as a station with 6 tracks while also serving as launching-shaft for one of the two tunnel boring machines (TBMs). The shaft is 128m long, 35m wide, 25.5m deep. The diaphragm wall around the perimeter comprised of 168, 1.85m wide and 35m deep panels. The hoop forces are transferred to the buttress elements (Y-panel) where each cell connects with its neighbouring cell. The buttresses ran vertically and were supported by top and intermediate props (or struts) as well as cross walls under the base slab. The vertical buttresses were 1.5m wide and reached a depth of around 34m; with two wing reinforcement cages on the sides and a main buttress reinforcement cage in the middle. The top struts were 2m wide by 1.5m deep, while the four intermediate props – 12.65m below ground – were 2.25m wide by 2.25m deep. All props were approximately 32m long.

Figure 2-13: Victoria Road Crossover Box (U.K.) overview

Initially, a rectangular shaft was proposed but was discarded in favour of this caterpillar shaft as it proved to be more economical and eco-friendlier in comparison. The designers claimed that this caterpillar design "enabled a 49% reduction in VRCB's length compared to the original design. The number of tension piles was reduced by 69% to 77%", resulting in a reduction in the volume of concrete needed from 100,000m^3 to 57,000m^3. Consequently, "the carbon footprint of this part of the project was lowered with a 42% reduction in embodied carbon to 40,490t CO_2e." The methodology for this comparison, however, was not accompanied with the article. There were also no details regarding the design and modelling process, or about the structural response of the shaft observed during the analyses phase and construction phase.

3

OBJECTIVES AND METHODOLOGY

3.1. Objectives

From the literature review it was seen that much of the case studies available in the public domain are limited to the traditional vertical retaining walls, rectangular in shape. When focusing on the circular shafts, the available data is considerably less, and limited work has been done to summarise and normalise the shaft behaviour in various conditions. For example, it was seen that Long [3] and Moormann [4] has summarised the shaft behaviour from over 530 case studies and has provided extensive comparative analyses in their paper. Faustin et al [15] have attempted to provide a similar study for circular shafts but all the 27 case studies presented in their report are limited to United Kingdom which greatly limits its applicability.

For the peanut or caterpillar shaft, case studies that address the overall structural behaviour of the shaft and design considerations do not yet exist in the public domain. While there are a few examples from projects executed in Brazil, Hong Kong and the U.K., they do not provide extensive monitoring data, or the design considerations made, especially for the Y-panel. The availability of such data in the public domain may prove beneficial for the engineering community to adopt such a complex and novel design at large, given the claims of significant economic and environmental benefits of this design over the traditional ones by the respective projects in Hong Kong and the U.K.

The lack of deeper understanding of the structural behaviour of caterpillar shaft is the very essence of this current report; consequently, the objective of this report is to address the gaps that currently exist in understanding of these structures and provide FEM considerations for the designers.

3.1.1. Objective-1: Sensitivity Analysis

Sensitivity analysis aids in assessing the influence of various input parameters on model. There are multiple ways to execute a sensitivity analysis depending on the desired outcome of the study. In this project, the key objective is to understand the structural behaviour of the Y-panel in the caterpillar shaft and overall structural response of the structure.

To achieve this, a global sensitivity analysis will be executed on a base model – the control – by introducing the following variations:

(i) Changing soil stratum: the stratum will be varied globally from cohesion to cohesionless soil. Since there is only one field test (CPT) conducted at the site location, there is not enough information to reliably derive the mean soil properties. Hence, representative soil properties of sand, silt and clay will be derived using Dutch National Annex of the Eurocodes (NEN-EN 1997-1+C1+A1:2016/NB:2019) which will be used in the analyses.

(ii) Effect of the buttress: in other caterpillar projects executed it is seen that the Y-panels are accompanied with a buttress support on the outer-side of the shaft possibly to reduce the bending moments in the Y-panel. However, it is not mentioned how the thickness of the buttress was chosen and what benefits were realised due to its addition in the design. Thus, iterations with varying buttress thicknesses will be made to understand that.

3.1.2. Objective-2: Comparison of 2D and 3D Analyses

During the inception phase of any project, the first step is to assess various design solution quickly to check the feasibility of the solution. In other time sensitive cases it is not always possible to prepare a 3D model from ground up or make quick changes in an existing model. Thus, in practice, rectangular shafts are generally analysed using 2D plane-strain models whereas the circular shafts are analysed using 2D axi-symmetric models.

In this study, the perimeter d-wall panels will be idealised as a 2D axi-symmetric model, and the Y-panel junction will be idealised as a plane-strain model and results from each case will be compared with the equivalent 3D model. If the results of 2D models do not match with those of 3D model, then it would be interesting to know how different the results are, to what extent and why; else, it would provide a confirmation to conduct 2D analyses during the feasibility-check phase.

3.1.3. Additional Checks

The following additional checks or analyses were undertaken but are not discussed here as it would extend the intended scope of this report:

(i) 3D full-scale model was compared with a quarter model of the same type to check if the scaled-down version gave similar results.

(ii) A 3D model with reduced dimensions (cell diameter 20m and cells' centre-to-centre distance of 14m) is created to validate the base/control model; essentially, it is created to see if the sensitivity carried out on the base model showed similar observations in a separate model of different

dimensions. This is not presented in the report but was performed as a check.

⚠ **Note:**

A quarter model of a 3-cell shaft of 25m diameter, 17.5m c/c cell distance, no buttress support on the Y-panel, with cross-wall support, up to the shaft depth, across the Y-panels and in uniform sand stratum was chosen as the control for this study

3.2. Summary

All the objectives and the methodology adopted discussed thus far are summarised in Table 3-1.

Table 3-1: Summary of key objectives for this study

Sr. No.	Test / Comparison	Objective / Aim	Method / Action
01a.	Shaft in different soil conditions	Observe the changing structural response of the shaft with changing soil strata	Prepare models with sand, silt and clay stratum and compare the results.
01b.	Y-Panel without Buttress vs With Buttresses	See what the impact is of adding a buttress to the Y-Panel.	Prepare and compare different thicknesses of buttress for the 25m diameter 3D model: - 0m (without buttress) - 1m thickness - 2m thickness - 3m thickness

Sr. No.	Test / Comparison	Objective / Aim	Method / Action
02a.	3D vs. 2D Axisymmetric	See if it is possible to compare the hoop forces derived from 2D model to those derived from the 3D model	- Prepare a 25m diameter 3D caterpillar shaft model, with no buttress support, and an equivalent 2D axisymmetric model to compare hoop forces in the circular wall panels of the caterpillar shaft. - Prepare also a caterpillar shaft with 20m diameter to confirm if the observed response in 25m diameter model is replicable
02b.	3D vs. 2D Plane-Strain	See if it is possible to compare the Plane-strain model with the 3D model (2D Plane-Strain model represents a rectangular shaft which should exhibit maximum bending moments on the shaft walls)	- Prepare a 25m diameter 3D model and an equivalent 2D plane-strain model to compare bending moments and deformations in the Y-panel - Prepare also a shaft with 20m diameter to confirm if the observed response in 25m diameter model is replicable
03.	3D Full Scale vs 3D Quarter Model	Confirm/observe the line of symmetry to reduce computation time for various analyses Highlight important observations on the behaviour of the shaft	- Prepare a full-scale 3D model and an equivalent quarter model. - Compare various parameters at various construction stages.

4

MODELLING OF THE SHAFT

This chapter describes the considerations made for the FEM model of the caterpillar shaft with respect to the site conditions, geometry, meshing, material properties and excavation sequences. A 25m diameter, 3-cell caterpillar shaft is considered as the standard for all design decisions.

Sub chapters:

1. Project Requirements and Site Conditions
2. Material Properties
3. 3D Geometry of the Shaft Model
4. 2D Geometry
5. Excavation Sequence

4.1. Project Requirements and Site Conditions

A brief introduction is already provided in Chapter 1.1 which forms the basis for this study. The design was already proposed before the start of this study; hence, the focus is not made on optimising or redefining the project parameters, but on evaluating the caterpillar shaft which was proposed as one of the solutions for the project.

The project is in Eemshaven which is a seaport located in north of The Netherlands. The subsurface data of Eemshaven area extracted from the available public records DINOloket[4] is shown in Figure 4-1. The area comprises of clean sand with seams of clay in the first 20m and a band of silt between 20-30m depth. The water level was observed to be fluctuating between 4-5m below surface level. At the time of writing this report, the exact location for the shaft is undetermined, hence, further information regarding existing structures and utilities, historic data and other relevant information cannot be determined and, consequently, will not be included in the model.

[4] dinoloket.nl

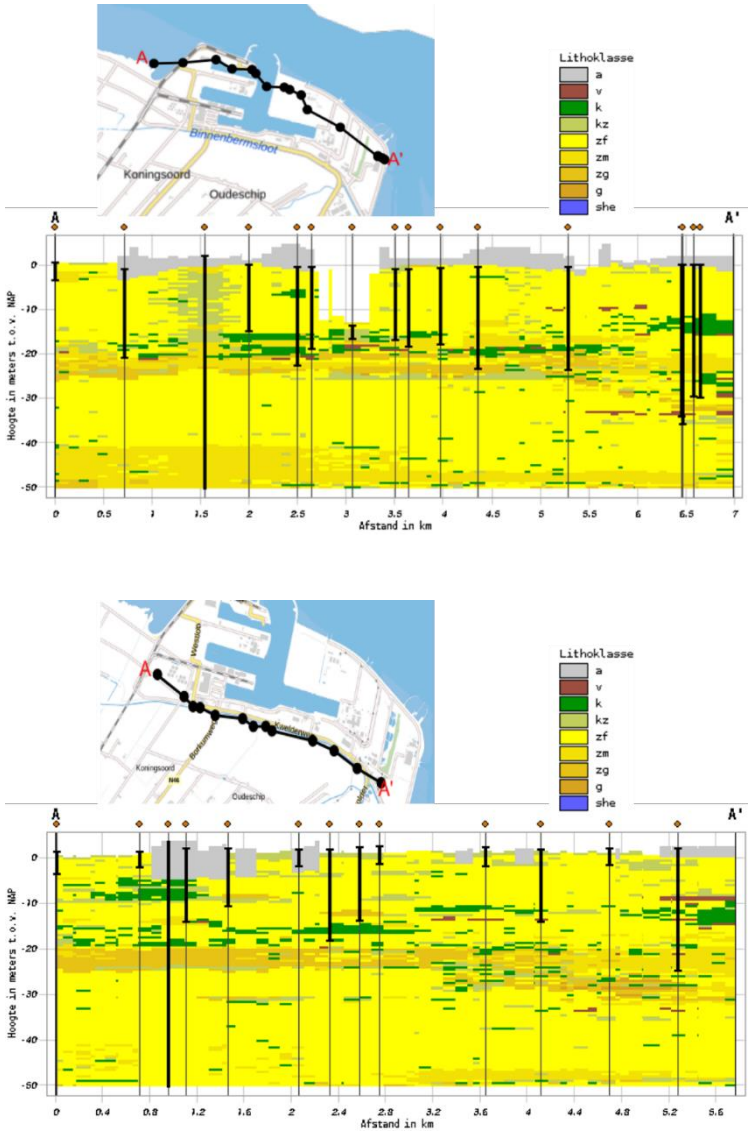

Figure 4-1: Subsurface soil data of Eemshaven extracted from DINOloket

One CPT analysis was done in the vicinity which was used to form the stratigraphy of the area and derive soil parameters. The complete stratigraphy derived from the CPT is presented in Table 4-1 and the soil parameters used for the analysis are discussed in the following chapters.

Table 4-1: Soil interpretation from the lone CPT investigation done at site

Formation	Depositional Environment	Lithology (per Table 2b*)	qc [MPa]	Elev. Start [mNAP]	Elev. End [mNAP]	Thickness [m]
Naaldwijk	Tidal Deposits	Weakly Sandy Clay; Loosely Packed	0.5-5.0	surface	0.0	2.0
Naaldwijk	Tidal Deposits	Strongly Clayey Sand; Loosely Packed (semi-undrained)	0.5-5.0	0.0	-11.0	11
Naaldwijk	Tidal Deposits	Silty Sand; Loosely to Moderately Packed	5.0-15.0	-11.0	-15.0	4
Naaldwijk	Tidal Deposits	Weakly Sandy Clay; Moderately Packed	1.0-2.0	-15.0	-20.0	5
Boxtel	Periglacial Deposits	Clean Fine Sand; Loosely to Moderately Packed	10.0-20.0	-20.0	-25.0	5
Eem	Marine Deposits	Clean Medium Coarse Sand; Moderately Packed	10.0-20.0	-25.0	-30.0	5
Dirente	Fluvio-glacial Deposits	Clean Coarse Sand (possible boulders)	10.0-30.0	-	-	-
Peelo	Fluvio-glacial Deposits	Clean Medium Coarse Sand; Tightly Packed	10.0-30.0	-30.0	-55.0	25
Appelscha	Fluvio-glacial Deposits	Clean Coarse Sand; Tightly Packed	10.0-30.0	-55.0	-60.0	5
Peize / Waalre	Fluvio-glacial Deposits	Clean Medium Coarse Sand; Moderately Packed	10.0-30.0	-60.0	-130.0	70

As can be seen from the CPT interpretation, strata are mostly composed of sand with mix of clay and sometimes silt. In the upper layer, strong presence of clay mixed with sand is seen with cone resistance (q_c) varying greatly. Patches of silty-sand and sandy-clay can be observed from -11 to -20 mNAP. These results from the CPT somewhat follow the observations from the soil profile extracted from DINOloket. However, these results cannot be considered conclusive as the data is extracted only from one CPT, and the location of this CPT with respect to the shaft is known; in all likeliness, given the large

horizontal variability observed in Figure 4-1, the clay and silt layers may not extend beyond a few meters horizontally.

Project requirements detailed by the client demand that the shaft must provide sufficient space for the installation and assembly of the TBM, assuming a single tunnel tube with an internal diameter of 10m; consequently, the minimum internal width is kept at 17m, length at 60m and clear space from the base of the shaft at 12m. The base of the shaft is at 40m below surface level. Consequently, the shaft walls extend beyond the excavations depth (44m) to a depth of 52m below surface, with 4m additional excavation reserved for underwater concrete floor (UWC/UCF) and working platform.

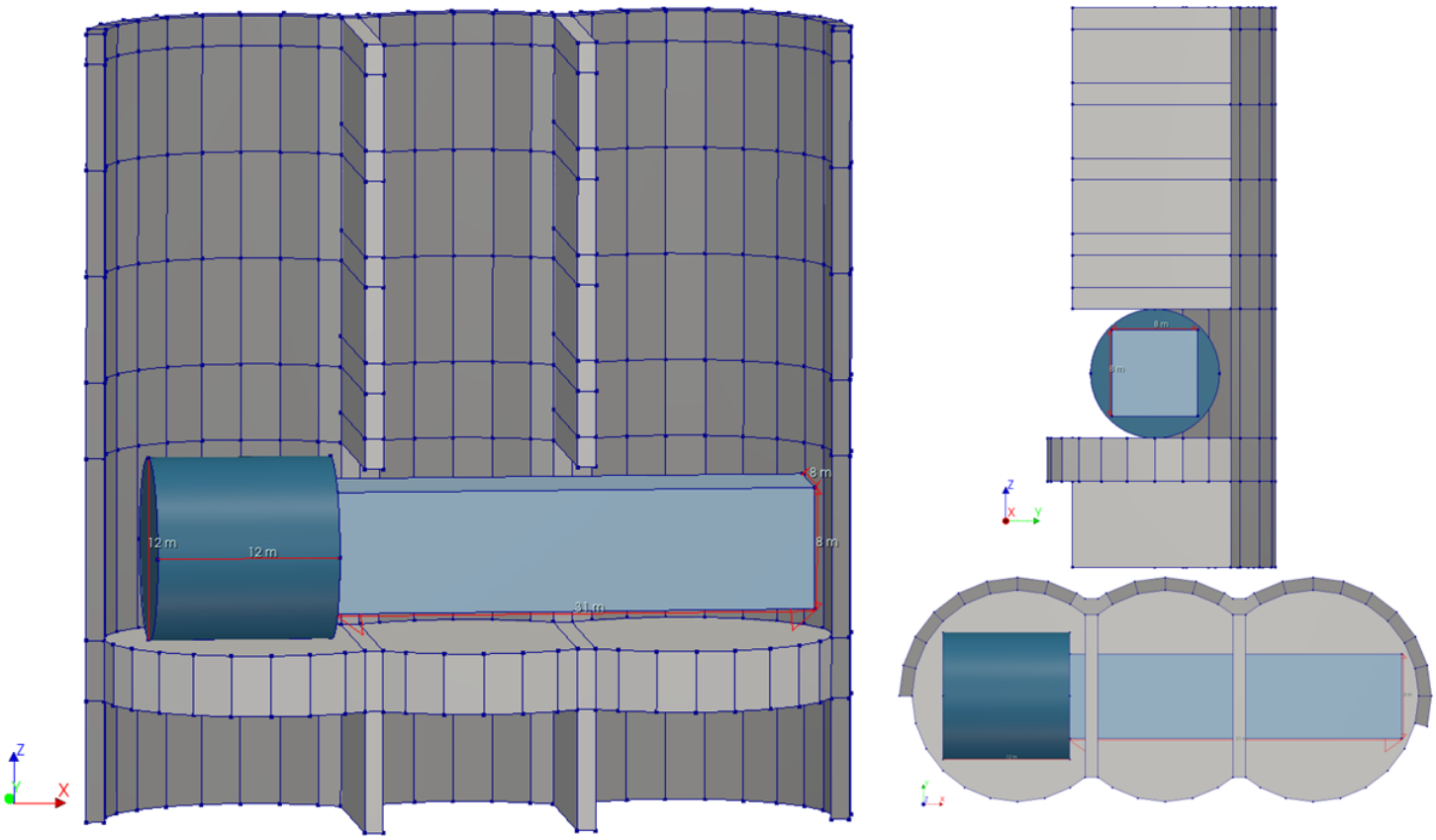

Figure 4-2: Placement of TBM within the shaft

4.2. Material Properties

4.2.1. Soil

The stratigraphy of the project location was simplified into three major categories: Clean Sand, Sandy Silt and Weakly-Sandy Clay. These three characterisations ensured that the shaft behaviour could be observed moving from cohesionless to cohesive soils. Since the objective of the study is to understand how this peculiarly shaped shaft behaves, it was decided to analyse the shaft with uniform soil stratum and compare the variation in progression. Had only the actual site stratigraphy been used for the analyses it would have made it difficult to ascertain the factors that were most influencing the behaviour of the shaft.

The lack of soil investigation and testing also makes it difficult to choose an appropriate material model for soil as the soil behaviour is unknown. A simple linear-elastic perfectly plastic model with Mohr-Coulomb (MC) failure criterion could be good for a first order approach but fails to account for stress-dependent stiffness which may prove to be overly conservative; Hardening Soil (HS) model, on the other hand, captures non-linear behaviour reasonably well for soils and is better alternative than MC model for modelling excavations [23]. Thus, a Hardening Soil model is used and Table 4-2 summarises the material model input used in the study. The properties are arranged as per the user-interface input of DIANA FEA.

Table 4-2: Soil properties used in this study

Parameters	Clean Sand	Sandy Silt	Weakly-Sandy Clay
Type	Medium dense	Medium dense	Medium dense
Initial stress	✓	✓	✓
Groundwater flow	✓	✓	✓
Yield function type	Mohr-Coulomb	Mohr-Coulomb	Mohr-Coulomb
Flow rule type	HS Standard	HS Standard	HS Standard

Parameters	Clean Sand	Sandy Silt	Weakly-Sandy Clay
Ref. triaxial secant stiffness [kN/m²]	30,000	20,000	3,000
Unloading-reloading stiffness [kN/m²]	120,000	80,000	15,000
Ref. oedometer tangent stiffness [kN/m²]	30,000	20,000	3,000
Poisson’s ratio	0.2	0.2	0.2
Cohesion [kN/m²]	1*	5	10
Friction angle at shear failure [°]	32.5	30	22.5
Dilatancy angle at shear failure [°]	2.5	0	0
Failure ratio qf/qa	0.9	0.9	0.9
Stress-dependency exponent	0.5	0.5	0.8
Reference pressure [kN/m²]	100	100	100
Pre-overburden pressure [kN/m²]	50	20	20
Tension cut-off value [kN/m²]	0	0	0
(Dry) Density [T/m³]	1.733	1.733	1.631
Porosity	0.3	0.2	0.01
K_0	0.5	0.5	0.7
Directional dependency (groundwater flow)	Isotropic	Isotropic	Isotropic
Hydraulic conductivity [m/s]	1e-04	1e-05	1e-10

Parameters	Clean Sand	Sandy Silt	Weakly-Sandy Clay
Elastic storativity [/m]	0.26**	0.15**	0.05**

⚠ **Note:**

All input values are representative due to lack of reliable soil investigation and testing.

* For Clean Sand, cohesion was taken as unity to avoid numerical imbalances. It is a general practice to not take cohesion as zero (0) as it might lead to numerical issues, although there has been no conclusive evidence of it. One way to gauge if low values of cohesion may cause numerical imbalances is to conduct sensitivity analysis. In this study, such a procedure was not conducted.

** The correct implementation of 'elastic storativity' in DIANA FEA, although documented[5], is somewhat obscure when compared to other literature [26][27]. Elastic storativity or coefficient of storage or yield coefficient as unitless quantities but in DIANA input is in 'per meter' unit; the known values for yield coefficient were used [27] assuming an unconfined aquifer condition. It is understood that this parameter only affects transient waterflow analysis and not steady-state analysis, which is implemented in this study, so the effect on the result is negligible. Readers are advised further reading into this matter.

4.2.2. Concrete

For the structural elements, the concrete properties chosen were kept uniform across all structure components. Additionally, a relatively higher concrete class was chosen to eliminate convergence errors arising due to the failure of concrete per se. Table 4-3 summarises the concrete properties used for this study.

[5] DIANA Users' Manual / Theory Manual / Materials / Groundwater Flow

Table 4-3: Concrete material properties

Parameters	Concrete C30/37
Class	Concrete design codes
Material Model	Eurocode 2 EN 1992-1-1
Concrete type	Normal weight
Concrete class	C30/37
Aggregate type	Quartzite
Cement type	Class N
Young's modulus, Ecm [kN/m^2]	3.28366e+07^
Poisson's ratio	0.2^
Thermal expansion coeff.	1e-05^
Density [T/m^3]	2.4^
Mean uniaxial tensile strength, Fctm [kN/m^2]	2896.47^
Mean compressive strength, Fcm [kN/m^2]	38000^
Compression curve	Eurocode 2 EN 1992-1-1^

^ default concrete properties as per Eurocodes

4.2.3. Interface

In DIANA FEA, the need for defining an interface arises due to the implementation of 'connections[6]' between shapes: "The concept is that when no connection is defined explicitly, all coincident topology is automatically connected. When a connection is defined explicitly between shapes, or between a shape and its surroundings, all coincident topology that is neither part of the source or the target, will be disconnected, and the selected connection type is created between the source and the target. Therefore, it may be necessary to reunite coincident topology that is either part of the source, or the target of the connection, but are not part of the connection itself." The above implementation implies a necessity to explicitly define a connection between different components in the model to ensure that

[6] DIANA User's Manuals / Theory Manual / Modelling / Geometry / Connections

there are no unintended open connections between nodes of adjacent shapes. The software offers the following options for connections:

Interface	Absorbing boundary
Unite	Rigid
Boundary interface	Distributed
Spring	Hinge
Boundary spring	Slide
Free-field	Disconnect

Table 4-4 lists the connections defined in the model.

Table 4-4: List of connections defined in the model

Connection between components	Material type	Connection type
Adjacent d-wall panels (incl. Y-panels)	Concrete-concrete	Interface
Struts/cross-wall and Y-panels	Concrete-concrete	Rigid
UCF and d-wall	Concrete-concrete	Interface
Shaft and inner/outer soils	Concrete-soil	Interface
Soil layers with same property	-	Unite

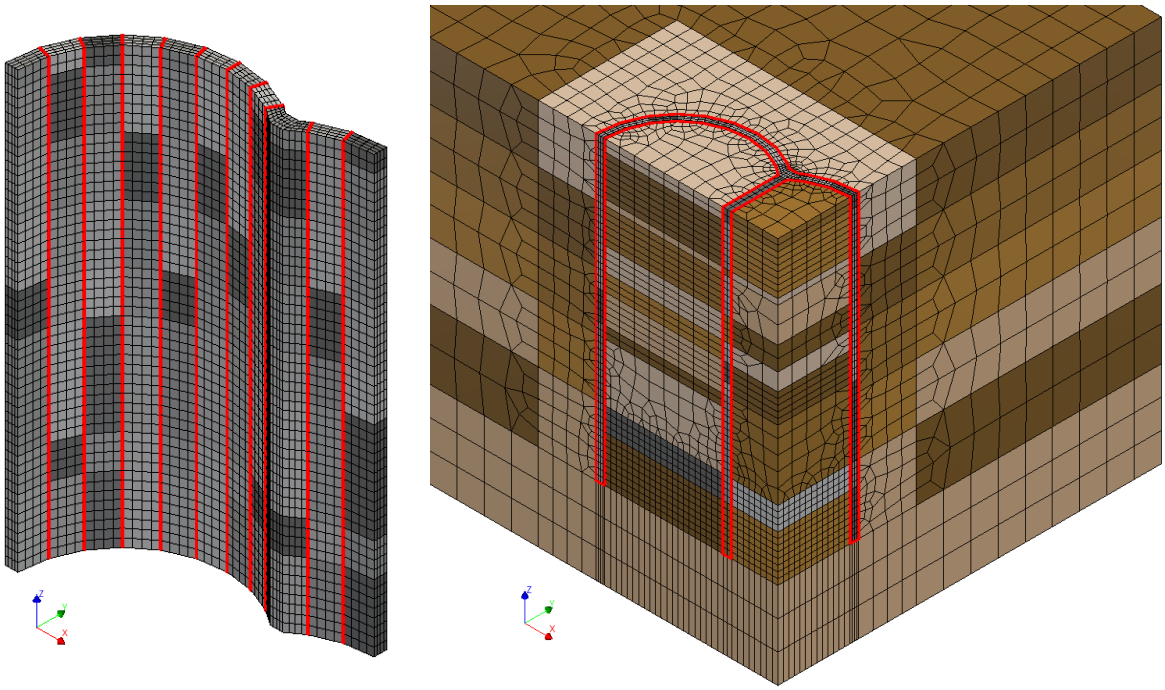

Figure 4-3: Concrete-concrete interface (in red) for adjacent d-wall panels (left); concrete-soil interface (in red) between shaft walls and soil (right)

For structure-soil connection, it is difficult to determine the properties for the interface that exists between them. In this D-wall construction, for example, bentonite slurry is used to keep the guide walls in place, which is replaced by concrete when it is poured in bottom-up process; in such an approach, concrete never fully replaces bentonite slurry, and the slurry may or may not have an influence on the interface. Since the objective of this study is not to analyse the interface behaviour, a simple Coulomb Friction model was adopted and was applied across all structure-soil interfaces. Cohesion was taken as unity to avoid numerical imbalances.

The structure-structure interface is highly dependent on the construction technique, material used and the skill of the contractor during construction. Again, as in the case of structure-soil interaction, it is difficult to confidently assign interface properties during the initial design stage. Some reference values could be extracted from the studies conducted by Mohamad et al [23] and Justyna Botor [25] which examined the concrete-concrete interface

behaviour using empirical and numerical methods; although, the conditions do not strictly apply to this case, the estimated values for Coulomb Friction (CF) model were derived from their respective studies which are good for the initial analysis of this nature.

Table 4-5: Interface material properties

Parameters	Interface: Concrete-Concrete	Interface: Concrete-Soil
Class	Interface elements	Interface elements
Material model	Coulomb friction	Coulomb friction
Type	3D surface interface	3D surface interface
Normal stiffness modulus-z [kN/m³]	1e+09	1e+08
Shear stiffness modulus-x [kN/m³]	1e+07^	1e+06^
Shear stiffness modulus-y [kN/m³]	1e+07^	1e+06^
Cohesion [kN/m²]	3620	1
Friction angle [°]	63.66	26
Dilatancy angle [°]	0	0
Interface opening model	No opening	No opening

^ shear stiffness is generally taken as 1/2 of normal stiffness to avoid numerical errors; here, it was assumed to be 1/100.

4.3. 3D Geometry of the Shaft Model

This chapter explains the decisions and process of defining the final geometry used for this thesis study. Images of the final geometry are presented here, with dimensions and detailed explanations regarding the chosen dimensions presented in the following sub-chapters.

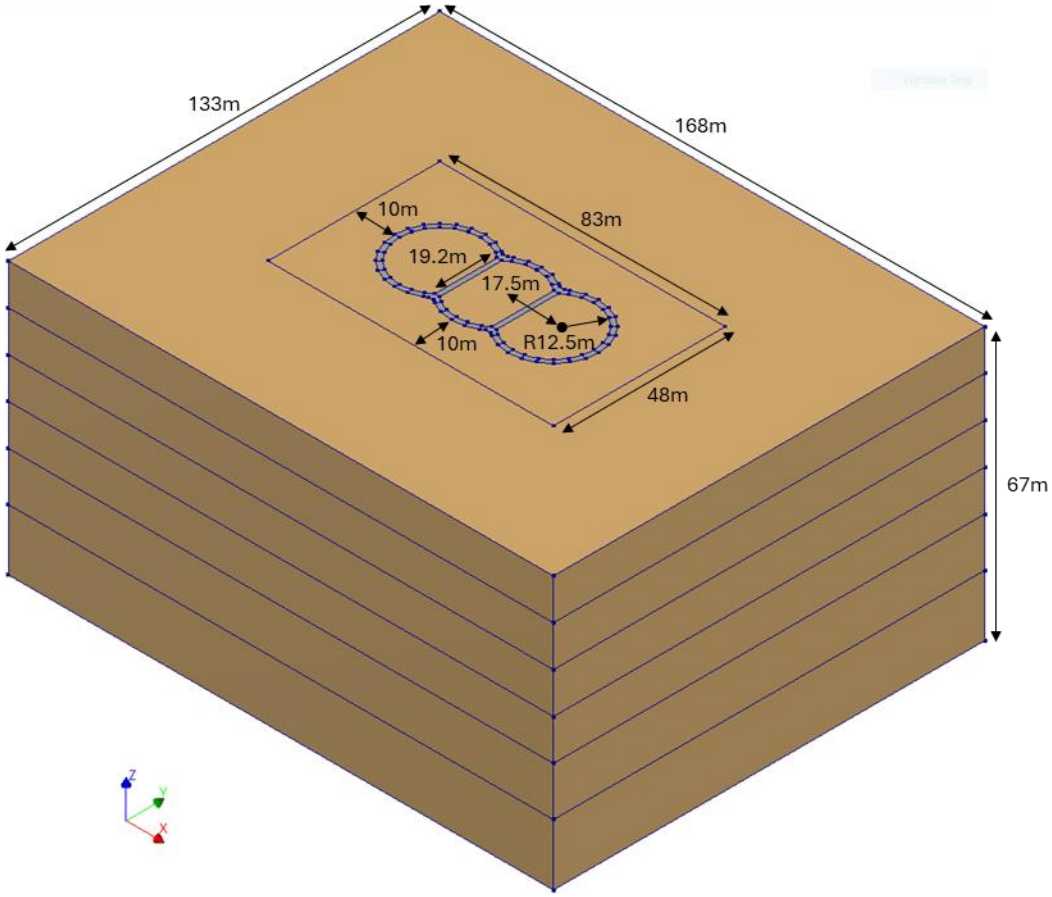

Figure 4-4: Full-scale 3D model of caterpillar shaft

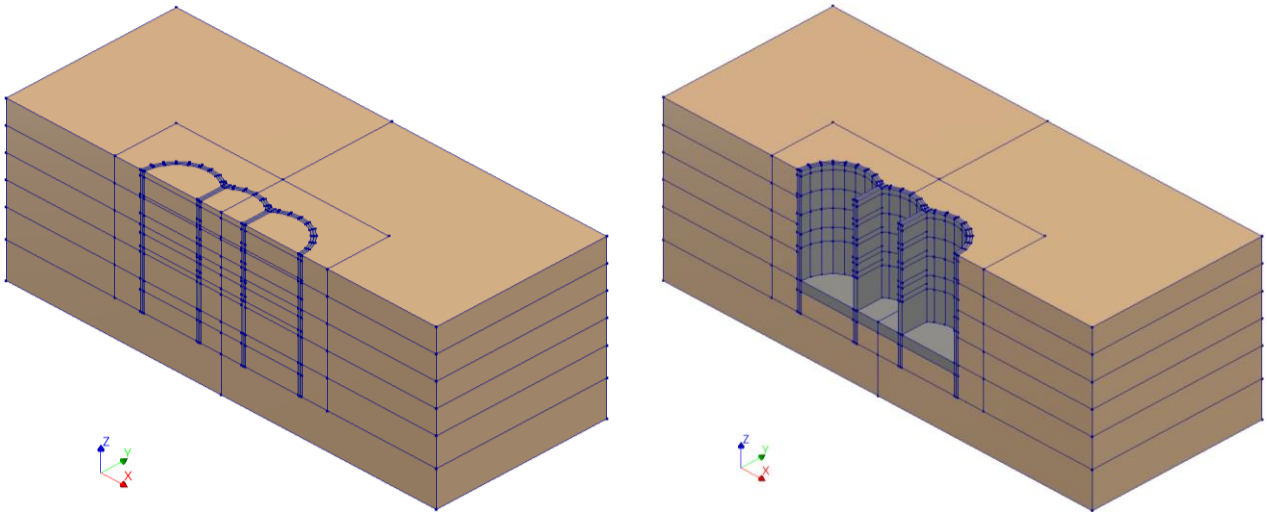

Figure 4-5: Half-scale model of 3D caterpillar shaft

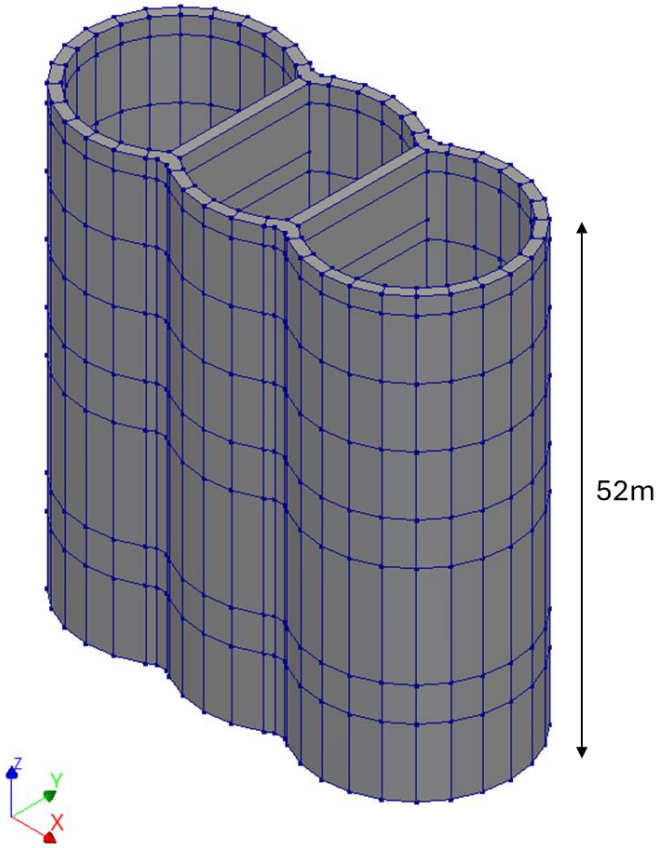

Figure 4-6: Full-scale 3D model of structural elements of caterpillar shaft

4.3.1. The Panels

Reinforced concrete D-walls are chosen for shaft construction. D-wall is constructed in-situ from the surface by use of hydraulic grabs. D-walls are made panel-by-panel where each panel is reinforced by steel cages.

shows the top view of the ideal orientation of these panels.

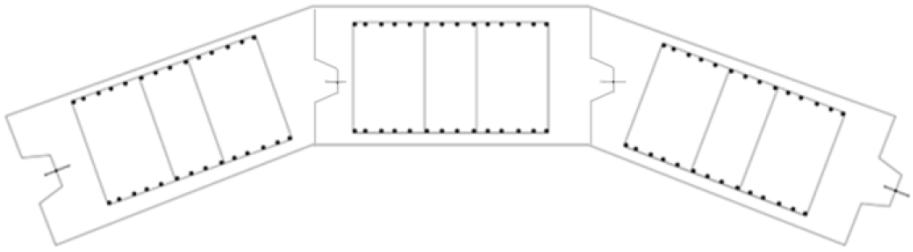

Figure 4-7: Representative top-view orientation of D-wall panels. Image: Witteveen+Bos

In the model, the circular shaft walls were considered as regular polygons instead of being considered a perfectly circular ring. Regular polygons (or ‘N-gons’) are polygons with ‘n’ sides and ‘n+1’ vertices where all sides and internal angles are equal. Figure 4-8 defines the key parameters of a polygon.

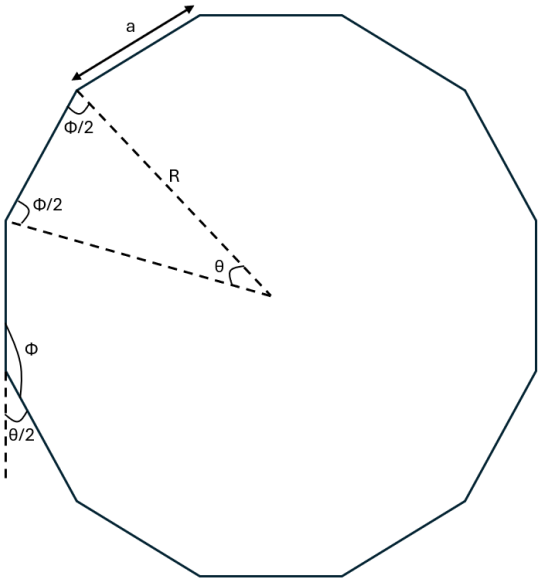

Figure 4-8: Geometric elements of a regular polygon (see Table 4-6 for details)

To form this regular polygon, the key input parameters are the number of sides (*N*) and the radius of the polygon (*R*). The radius is dictated by the project requirements, while the number of sides of the polygon are the decision of the designer. The greater the number of sides, the more circularity will be offered by the polygon. Maintaining the circularity of the shaft structure is essential in ensuring that the arching effect is utilised fully; effective stress transfer in adjacent panels is achieved when the line of thrust is in the middle of the wall thickness as seen in Figure 4-9.

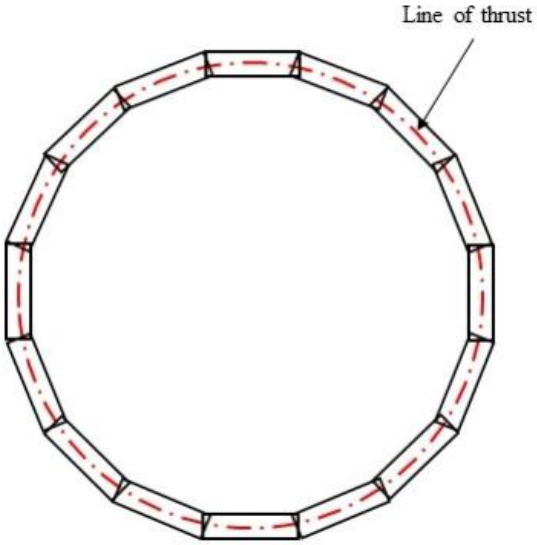

Figure 4-9:Line of thrust in a circular diaphragm wall structure

By increasing the number of sides, the panel length (a) reduces, and the line of thrust is better embedded within the wall thickness (t). Reducing the panel length too much would make the construction impractical as sufficient space will not be left for tremie pipes; reduced panel length would also lead to less area being occupied by reinforcement (cage) and more by unreinforced concrete which could lead to development of more cracks at the joints. Other factors that influence the number of sides chosen could also depend on the size of the equipment used for the construction, the size of the structure, construction method, etc. For this study, 24 number of sides were chosen, while the excavation radius of 12.5m was dictated by the project requirements. All structural components of the shaft were designed as volume elements.

The thickness of the panels was chosen as 1.5m which gave the outer radius of 14m. The thickness of 1.5m was found out to be over-designed for this purpose (see APPENDIX-2: PANEL THICKNESS VERIFICATION) and a thinner element could be used for the purpose. Since this could only be verified after the analysis, the focus of this study is not on optimisation or reinforcement design, and to

avoid convergence errors due to thinner elements, the thickness was chosen as 1.5m as a preliminary design.

The key parameters of the polygon for this study are summarised in Table 4-6.

Table 4-6: Dimensions of D-wall panels used in this study

Number of sides, *N* [-]	: 24
Inner radius, *Ri* [m]	: 12.5
Thickness, *t* [m]	: 1.5
Outer radius, *Ro* [m]	: 14
Interior angle, Φ [°]	: 165
Central angle, θ [°]	: 15
Length of inner side, *ai* [m]	: 3.272 (approx.)
Length of outer side, *ao* [m]	: 3.586 (approx.)

D-wall panels created in the 3D modeller are shown in Figure 4-10.

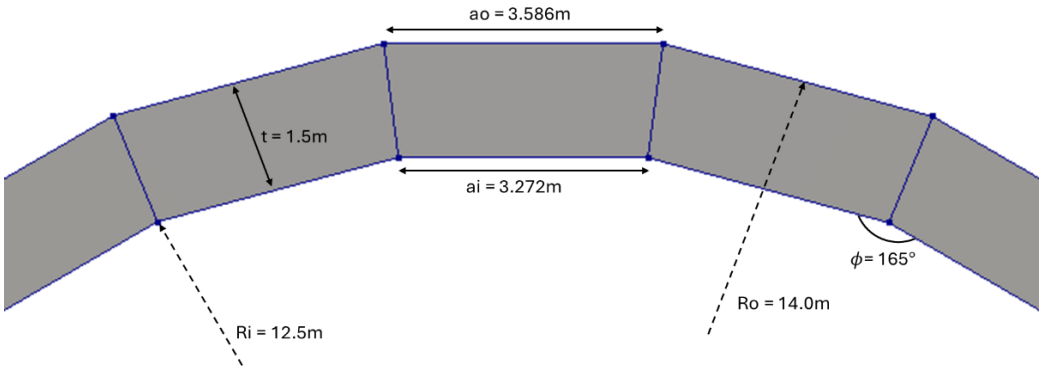

Figure 4-10: Top-view model of D-wall panels used in this study

Remark:

(i) While the length of panel – 'ai' or 'ao' – is governed by the size of the grab, which is usually available in max. size of 2.8m, it is still possible to use multi-phase excavation to achieve the desired lengths which are greater than the available size of the grab. For example, the Y-panel (discussed in Chapter 4.3.4) can be excavated in multiple phases by the grab to achieve the desired shape [19].

(ii) If N is an even number, half of the axes pass through diagonally opposite vertices and the remaining ones, pass through the midpoints of opposite edges. On the other hand, if N is odd, all the axes of symmetry, pass through a vertex and the midpoint of its opposite edge. It was found easier to work with even number of sides.

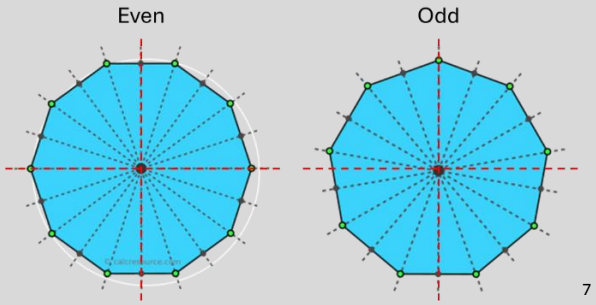

[7]

[7] calcresource.com

(ii) if the number of panels, N, is a multiple of 6 then the interior angle, Φ, and central angle, θ, will be whole numbers which make the geometry easier to work with

4.3.2. Dummy/Composed Elements

The main objective of dummy elements is in the post processing of analyses results which help in capturing the forces and bending moments that the volume elements experiences. In DIANA FEA, the concept of dummy elements is implemented by 'Composed Elements'[8]. These composed elements do not have any mechanical properties of their own, such as stiffness and mass, and hence do not influence the behaviour of the finite element model. DIANA FEA offers two variants of composed elements – Composed Lines and Composed Surfaces. In models created for this study, 'compose surface elements' have been utilised which are placed in the middle of the volume elements. In composed surface elements the distributed local forces and bending moments along a line normal to a reference surface is calculated from the primary Cauchy stresses in solid elements; thus, the output for forces is given in units of Kilo Newtons per Meter [kN/m] and for bending moment it is given in Kilo Newtons [kN] or [kN-m/m].

Composed elements could be made using the same concept of polygons as done for the shaft walls. The length of the composed elements, however, was kept more than the length of side ('a') obtained from averaging the inner and outer radii. This was done to capture the nodal data of the outer radius which would not align with the nodes of composed surface as shown in Figure 4-11.

[8] DIANA User's Manuals / Theory Manual / Elements / Composed Elements

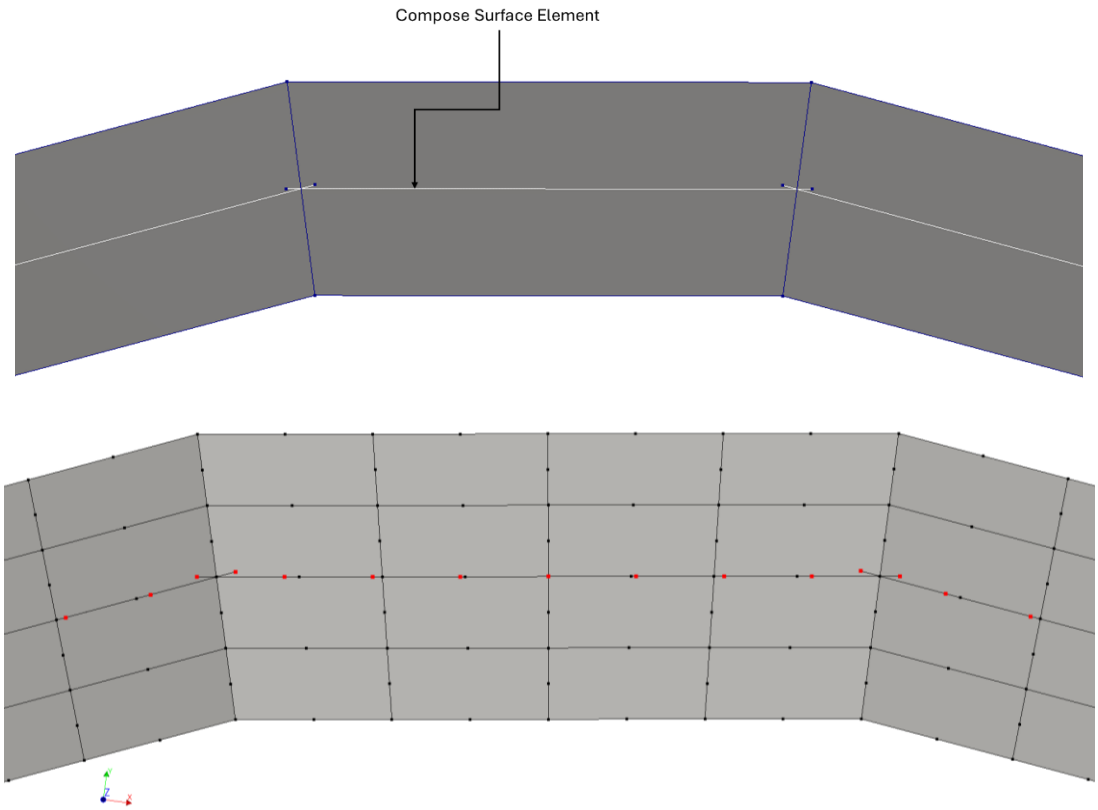

Figure 4-11: Top-view of D-wall panels with composed surface elements and their nodes (in red)

4.3.3. Total Length of Shaft and Cell Distance

A caterpillar shaft is a combination of at least two overlapping circular shafts, each called a 'cell'. One can even think of these structures as enlarged versions of secant piles. The number of cells is governed by how much length is required for the project. For example, in London project [21], 4 cells were executed to house the station whereas in case of Hong Kong project [19] 15 cells were executed for the cut-and-cover section. For this study, a 3-cell shaft was considered as the standard which was governed by the project requirements as detailed in Chapter 4.1.

The distance between the centre of adjacent cells depends on the angle at which the cells converge, which in turn will determine how much clear working area will be available. Setting a higher ratio of cell distance to shaft radius will result in longer shaft but will

reduce the width of the opening, while setting a lower ratio with increase the width but reduce the length of the shaft, as demonstrated in Figure 4-12. Ratio of 1.4 for cell distance to cell radius was optimum for this study given the space requirements mentioned in Chapter 4.1 and following the 120° arc as suggested in Figure 2-10.

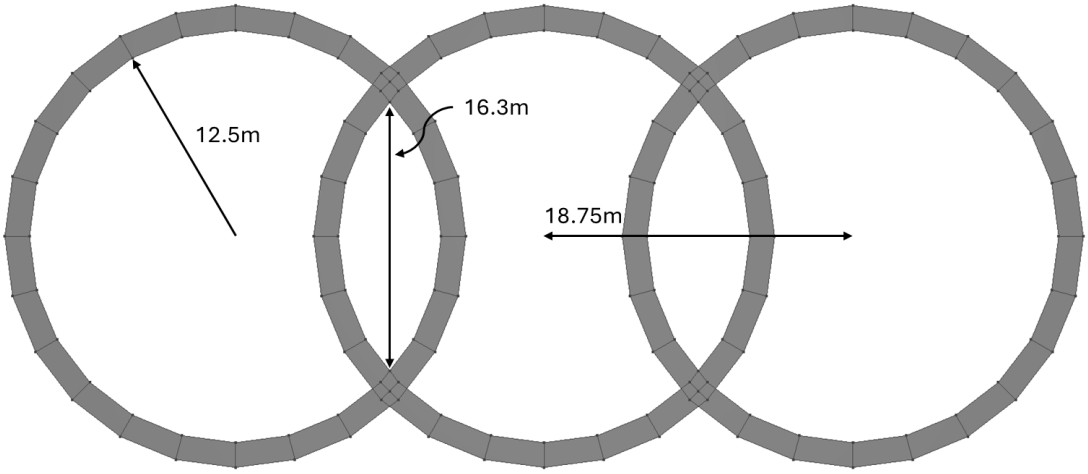

(a)

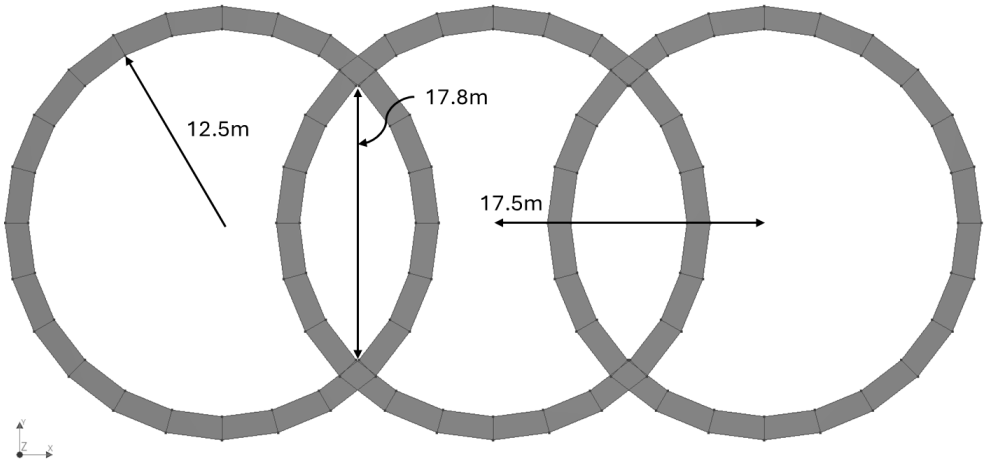

(b)

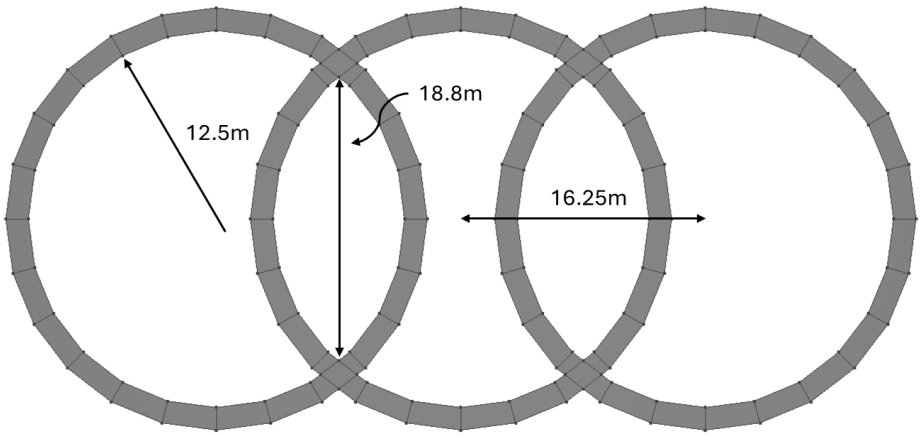

(c)

Figure 4-12: With radius of the shaft fixed: (a) Caterpillar rings with shaft-cell distance to radius ratio of 1.4; (b) Caterpillar rings with shaft-cell distance to radius ratio of 1.5; (c) Caterpillar rings with shaft-cell distance to radius ratio of 1.3

Thus, the caterpillar shaft for this study constitutes of 3 cells, each separated by 17.5m from centre-to-centre, making the ratio of cell distance to cell radius to 1.4. The effect of changing ratio could be a topic for study in future.

4.3.4. The Y-Panel

The Y-Panel is used to connect the two adjacent shaft cells and to concentrate these loads to the struts. The upper part of the 'Y' shape, referred to as the wings/flanges, continue from the circular shaft walls and to the lower part of the 'Y' shape, the stem/web, and to the struts. The flanges follow the 1.5m thickness of the permitter d-wall panel to avoid the effect of eccentricity due to changing thickness. The web of the Y-panel is given a rectangular shape with width as 1.5m and height as approx. 1.9m. The width of the web is kept to match the width of the struts and to accommodate buttress (discussed in the following chapters). Figure 4-13 shows the dimensions of the Y-panel. As mentioned earlier, such a shape can be achieved by excavating in different phases using the grab.

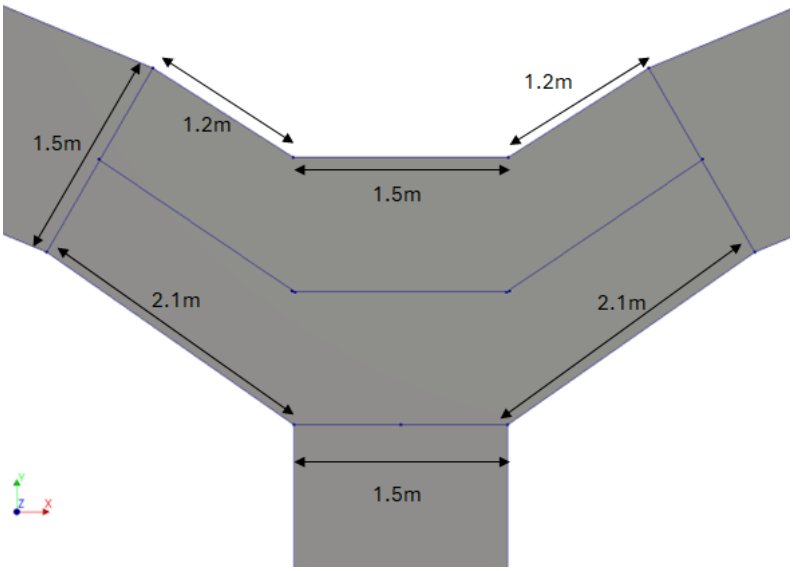

Figure 4-13: Top-view of Y-panel with dimensions

The compose surfaces for the Y-Panel were chosen at three locations – at the two wings and at the centre as shown in Figure 4-14. Like the composed surfaces of D-wall panels, the compose surfaces of Y-panels also extend slightly to capture all nodal information normal to their axes.

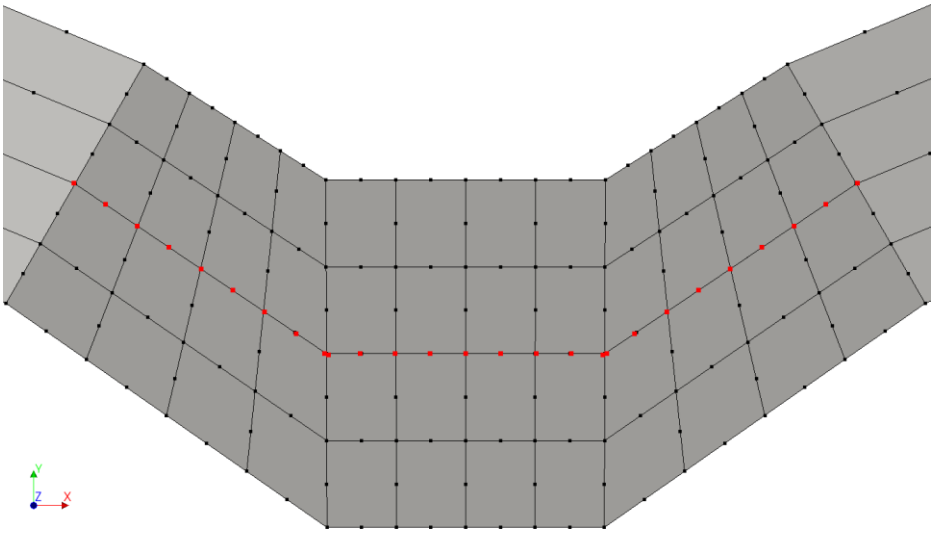

Figure 4-14: Nodes and mesh elements of the Y-panel and its composed surface in red (top-view)

4.3.5. The Struts

The project site has a high groundwater table, very close to the surface level. Such a situation warrants a wet excavation especially when water drawdown is not an option. To provide support to the excavated shaft, two design approaches could be adopted - placement of temporary struts underwater during excavation followed by in-situ construction of permanent struts after dewatering of the shaft, and placement of D-walls across opposite Y-panels from the surface before excavation.

The former approach, during wet excavation, is usually executed by placing high load capacity steel hydraulic struts which can be lowered in place during excavation process. After the completion of excavation, under-water concrete floor (UWC or UCF) is placed, and the shaft is dewatered; if required by the project, permanent struts are installed in place of hydraulic struts after dewatering. This approach, although feasible, involves high risk, results in high concentrated forces at the strut locations and higher deformation in the structure since there is always some downtime between the excavation being completed and the struts being installed. Analysing such an approach using 3D FEM adds high computational time given the increased number of steps involved, in adding temporary struts during excavation and then replacing those with permanent struts The number of steps could be reduced by installing permanent struts in place of temporary struts in the numerical analysis, but it may not produces accurate results.

The latter approach, which involves constructing a D-wall cross-walls was considered for this study as it is simpler of the two approaches to execute. The idea is to construct the cross-walls alongside the shaft walls and Y-panel. This wall would extend till -52.0m (shaft wall depth) and would connect the two opposite Y-panels

as shown in Figure 4-15. The thickness was maintained at 1.5m to match the Y-panel width. Since a continuous support is already present before the excavation is executed, the deformations and bending moments experienced by the structure would reduce significantly and would avoid concentration of loads at strut locations. Such a design also ensures a better connection between the Y-panel and the cross-walls (almost a rigid connection if executed properly) when compared to strut installed afterwards. This approach was finalised for the detailed study of the shaft.

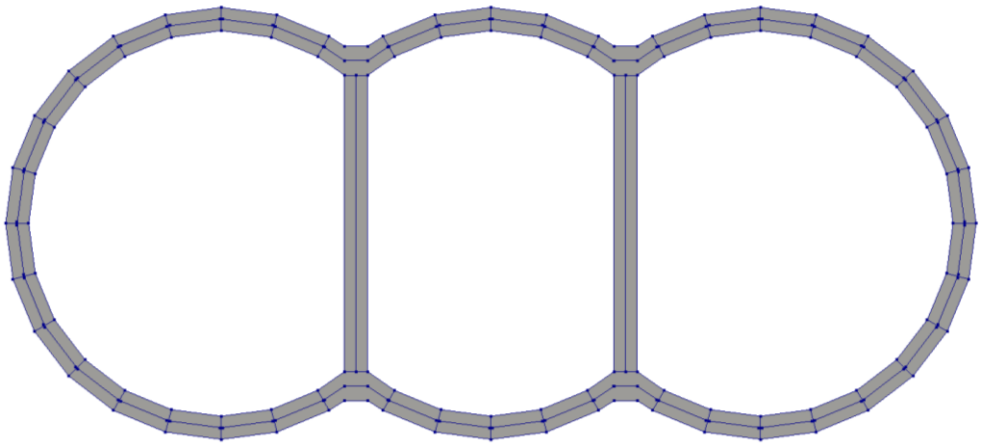

Figure 4-15: Top-view of D-wall panels, Y-panel and struts with composed elements as modelled in DIANA FEA

4.3.6. The Buttress

In the London and Hong Kong projects, it was observed that a buttress was added to the Y-panel on the exterior side. In both cases, the application of buttress was not explained. It is presumed, reading the literature, that the buttresses provided additional structural support by reducing the bending moments in the Y-panel. To fully understand the effect, buttresses, as shown in Figure 4-16, were introduced in the model. The buttress is modelled as a volume element of concrete connected rigidly to the Y-panel. In this study, four cases are considered: no buttress, 1m, 2m and 3m buttress.

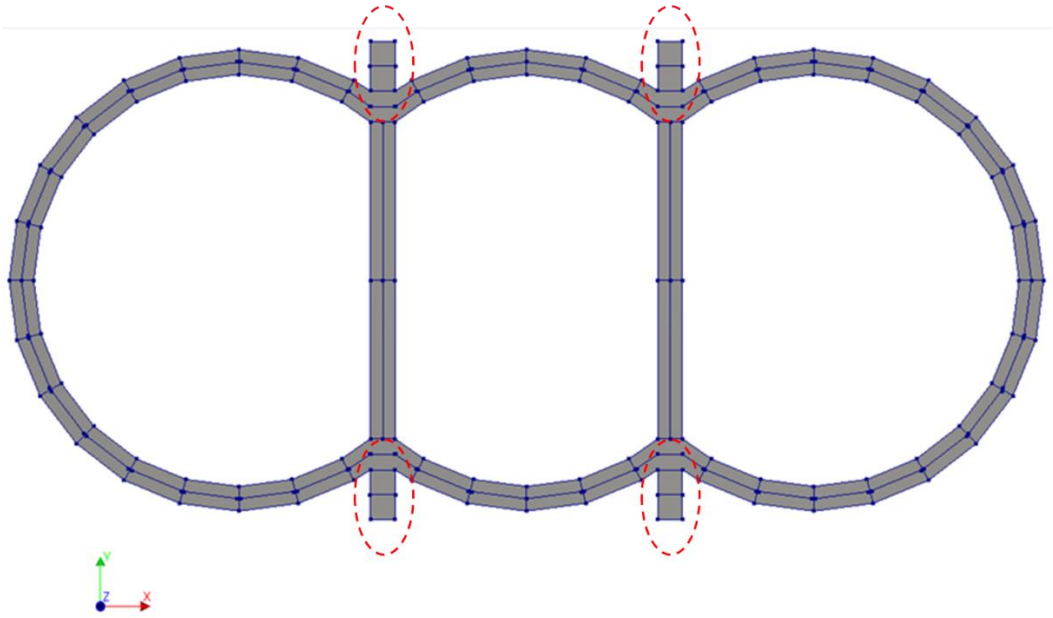

Figure 4-16: Top view of structural elements of caterpillar shaft with (3m) buttress

4.3.7. The Boundary Limits

For most tunnelling and excavation projects, the zone of influence usually does not extend beyond 2-2.5 times the excavated diameter in horizontal direction, albeit this is dependent on various factors. The field results of the project in Sao Paulo [19] suggested a max. observed settlement of about 15mm at a distance of 20m, which is about 0.56 times the shaft diameter; using this knowledge and trend seen in other circular shaft constructions, it was decided to start the analysis with a boundary of about 2*diameter.

After an initial FEM analysis, this presumption was confirmed when the highest observed cumulative subsidence was <1mm at a distance of 2*diameter from the wall extrados as seen in Figure 4-17. Thus, 2.1*diameter of excavation (or 52m of soil from the wall extrados) was finalised as the limits for the analyses as 1-2mm subsidence can be considered negligible for all practical purposes.

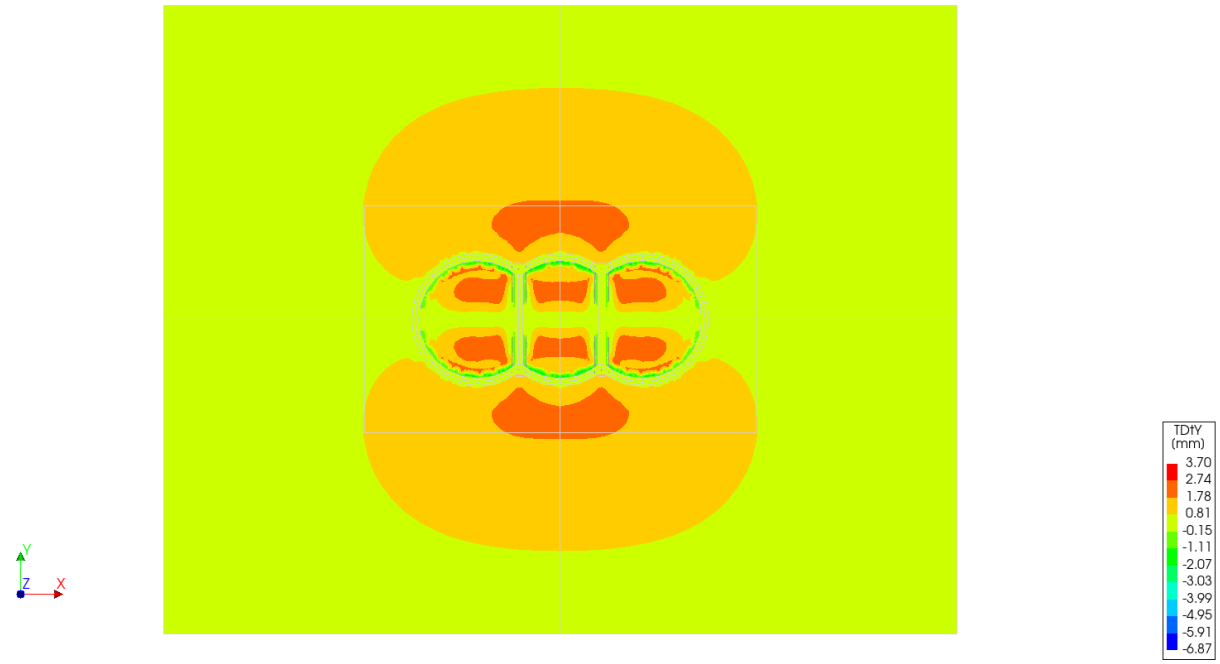

(a)

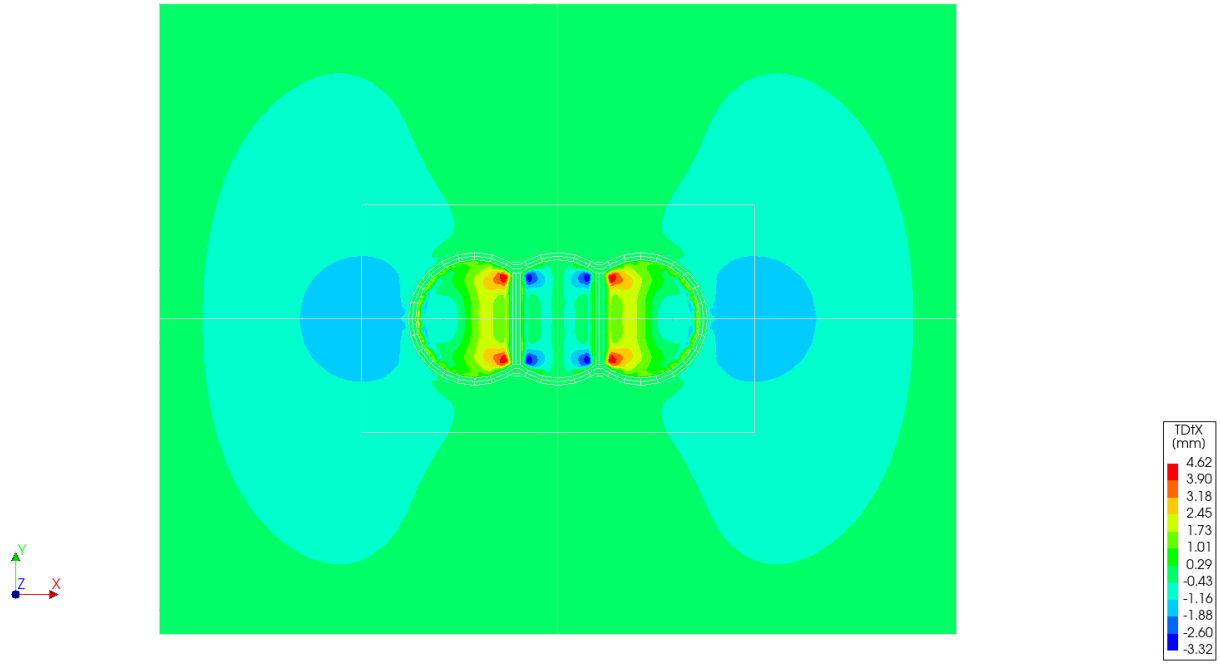

(b)

Figure 4-17: (a) Top view of deformation in global y-direction; (b) Top view of deformation in global x-direction

For mesh-refinement purposes, a block of soil was created which extended 10m from wall extrados in either direction. This is shown in Figure 4-18. For the boundary limits in vertical direction, a distance of 15m from the end of shaft walls was taken as the limits as the

initial analysis showed negligible effect at that depth; thus, the total height of the model was fixed at 67m.

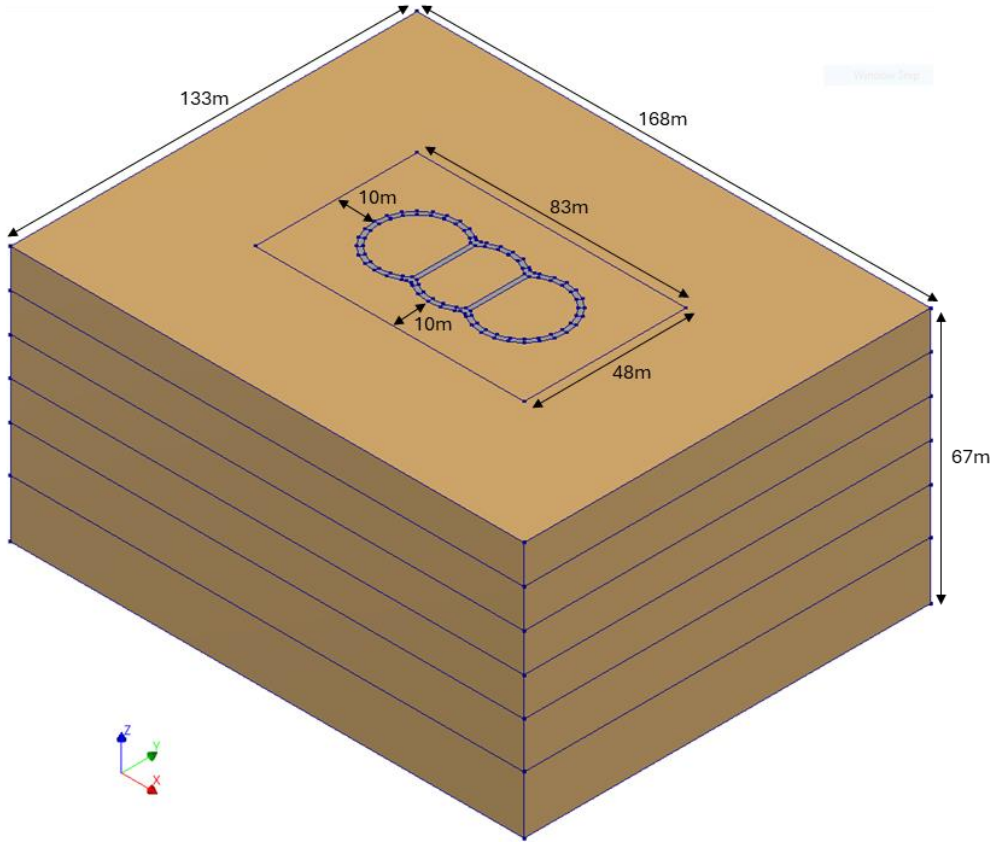

Figure 4-18: Isometric view of the full-scale model with dimensions of the boundary limits

Thus, a model of 168m x 133m x 67m was created as the boundary limit while a soil block of 83 x 48m was created 10m from the wall exterior for mesh refinement purposes (see Chapter 0).

4.3.8. Boundary Conditions

Supports were added to the faces of the geometry with fixed translations in the direction they were facing, i.e., roller supports).

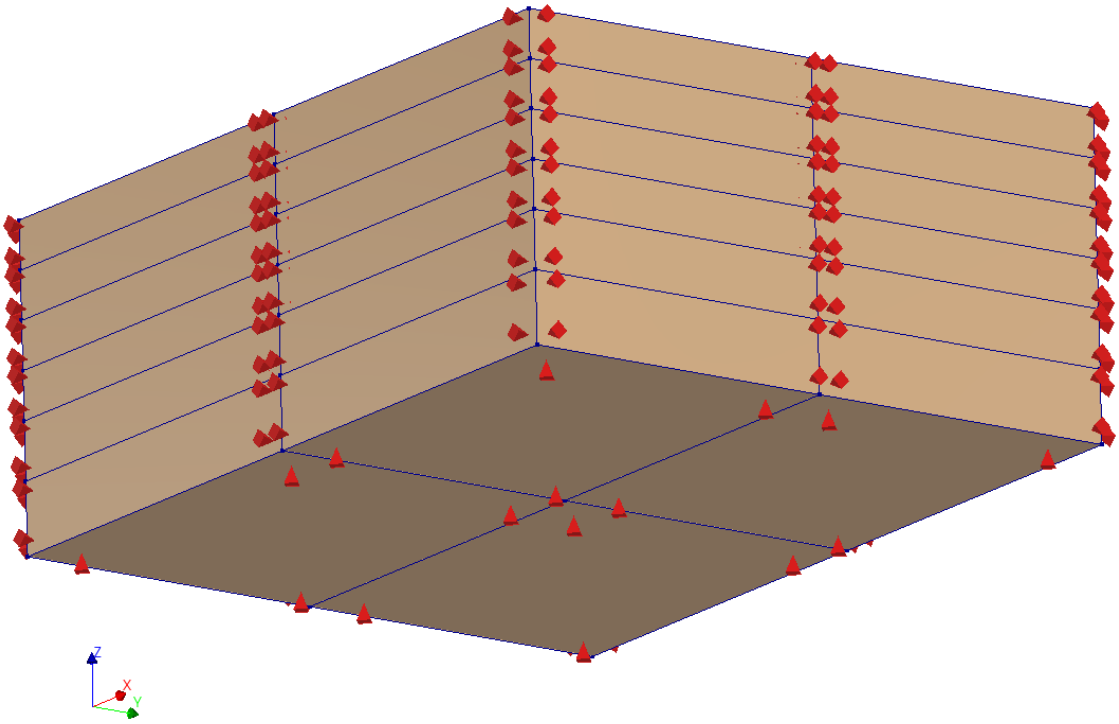

Figure 4-19: Isometric view of the full-scale model showing the boundary supports

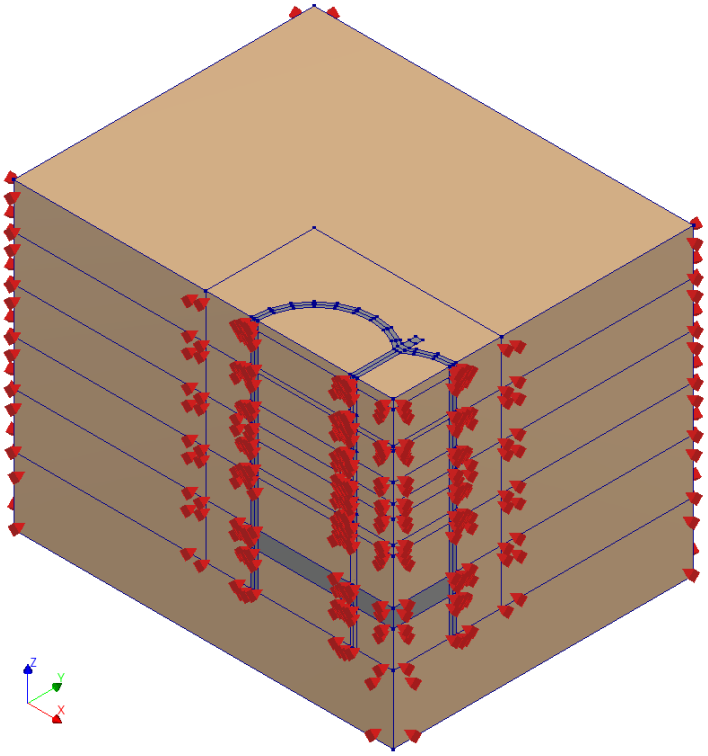

Figure 4-20: Isometric view of quarter-scale model showing the boundary supports

4.3.8.1. Water Boundary condition

In DIANA FEA there are at least two ways to add the water level. One is to define the water level using 3D coordinates and the other is to add a ‘fixed potential’ with a ‘prescribed [water] head’; the latter was chosen to properly simulate pore pressure in the soil body. Using this method also simulated uplift pressure experienced in the shaft after adding the UWC layer. The topmost faces of the outer soil were chosen as the boundaries to add the fixed water head of 0m; that is, the water level was set at the surface level.

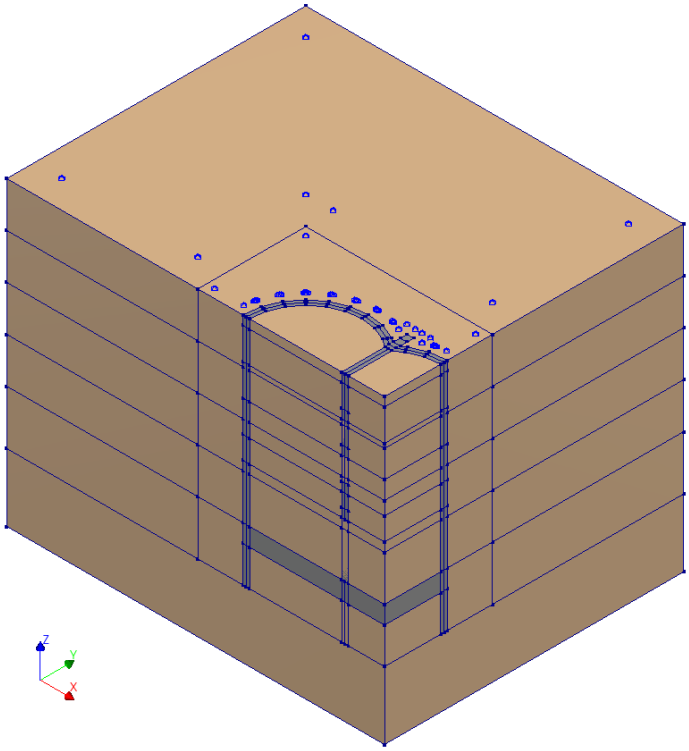

Figure 4-21: Isometric view of the quarter model showing water boundary condition

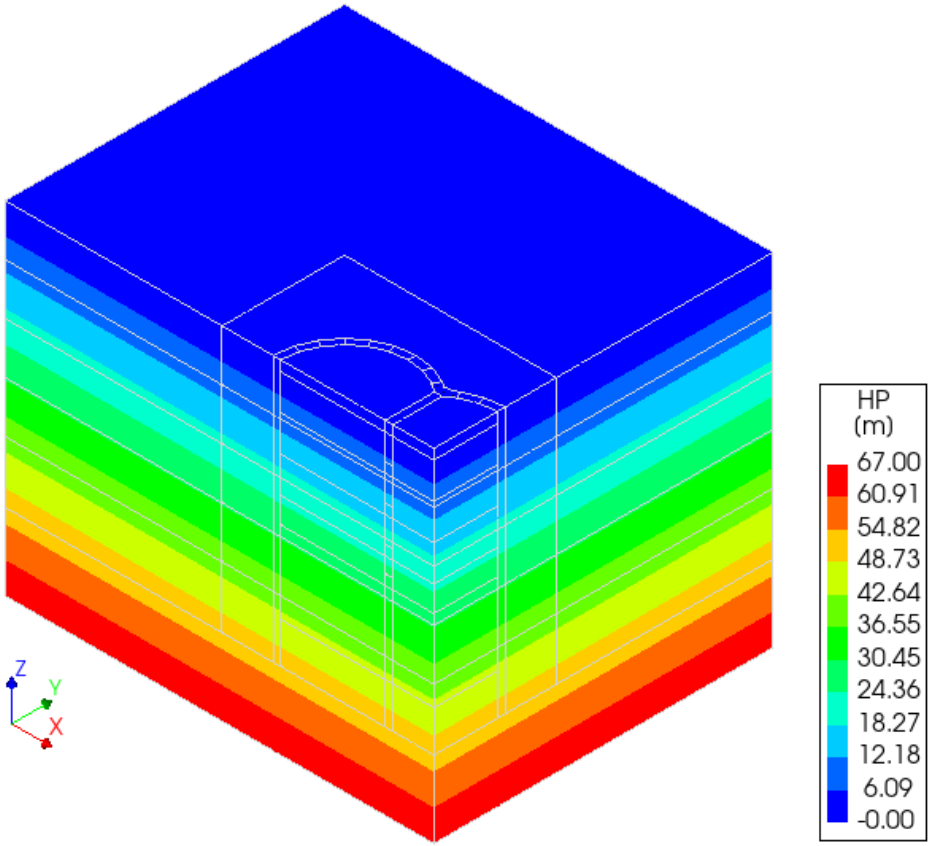

Figure 4-22: Isometric view of the quarter model showing pressure head

4.3.9. Meshing of the Model

The mesh for this model was defined manually instead of relying on the auto-mesh feature of the software as the auto-mesh feature proved to be unreliable around curved edges. The default mesher-type was set to 'quadrangle/hexahedron' using 'quadratic mesh order' with 'linear interpolation'. Some key rules[9] to consider while meshing were:

(i) In DIANA FEA, the mesh seed are looked up in a hierarchical manner with highest preference given to edge seeds, then face and lastly to shape seeds.

[9] DIANA User's Manuals / Theory Manual / Modeling / Mesh / General Properties

(ii) When conflicting target element sizes are found for a set, the smallest target element size is deemed optimal

'Extrusion Mesher' and 'Adaptive element size' features of the software were enabled while generating the mesh. With Extrusion mesher enabled, it is sufficient to assign a mesh seed to just one edge that extends in the extrusion direction; mesh seeds propagate along chains of extruded shapes. This feature is very useful in obtaining uniform meshes. By enabling adaptive element size, the software automatically refines the mesh in in curved parts of the model.

The total number of elements for a full-scale model averaged around 370,000.

> 💡 **Remark:**
>
> a model with about 150,000 elements required about 60 GB of RAM in this setup.

4.3.9.1. D-wall Panels and Y-Panels

Wall panels are the focus of the study. Multiple iterations were done to refine the mesh to make it efficient. Given the panel length and thickness, an edge division of 4 was considered optimum for the top and bottom faces to allow the composed elements to capture the data from volume elements properly. Thus, each panel had a grid of 4x4 elements (16 elements) on the top and bottom faces as shown in Figure 4-23.

Defining shape element size would dictate the number of elements in depth. For example, if the element size is chosen to be 0.5m, the data could be extracted at every 0.5m of the panel length over the 52m panel length; however, given that the smallest element size also governs the element size of the adjoining geometric elements as

discussed earlier, it would mean that the soil blocks would also have element size of 0.5m resulting in a fine mesh even for the soil elements which are farther away. While a finer mesh may lead to more accurate results, it would greatly reduce the efficiency of the model.

Having 2m element size for the panels would give results at every 2m elevation which would lead to loss of data between elements. Thus, 1m was considered optimal mesh size, striking a balance between data accuracy and computational optimisation.

D-wall panels and Y-panels were assigned the following properties:

- Edge division of 4 on top and bottom edges
- Element size of 1m for the entire shape

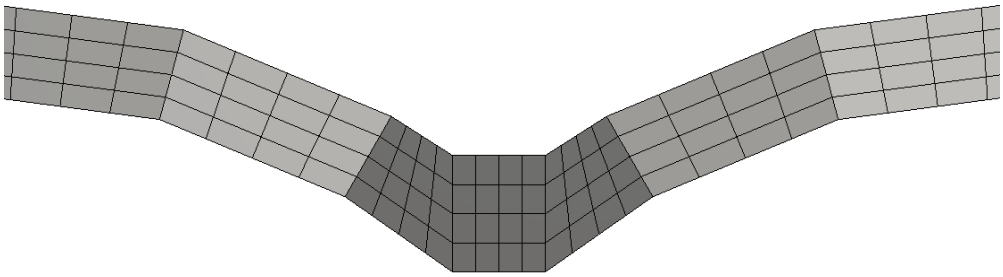

Figure 4-23: Top view of D-wall panels and Y-panels showing mesh with edge division of 4

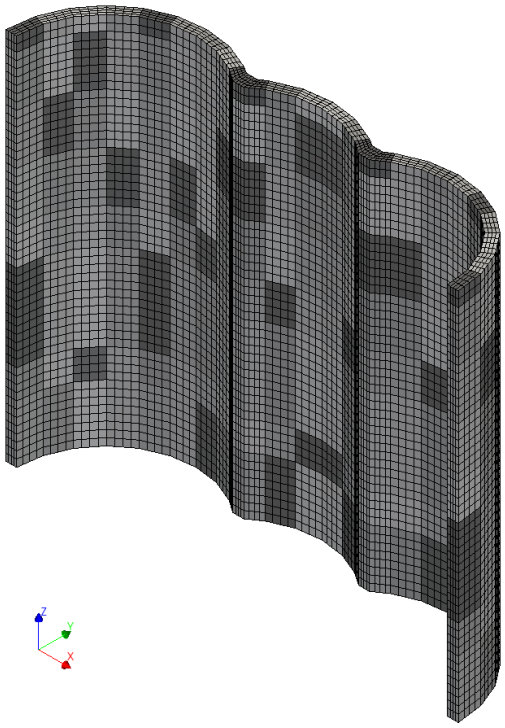

Figure 4-24: Isometric view of half-model showing mesh for D-wall and Y-panels with 1m element size

4.3.9.2. Inner and Outer Soils

It was imperative to keep the mesh of the soil next to the shaft walls fine to ensure a good soil-structure interaction. The inner and outer (10m from the shaft) soil shapes were thus assigned the edge division of 2.5m for top and bottom faces given the diameter of inner soil at 25m and soil-block of 10x10m surrounding the shaft walls; in z-direction, the element size followed the specifications of the panels (1m size) given the meshing rules of DIANA as explained earlier. Increasing the fineness of mesh for soil even slightly lead to a significant increase in the number of elements given the large size of soil body; even with mesh size of 1.5m to 2m, the total number of elements reached close to half-a-million. Thus, 2.5m was observed to be quite reasonable refinement with 'adaptive element size' option checked.

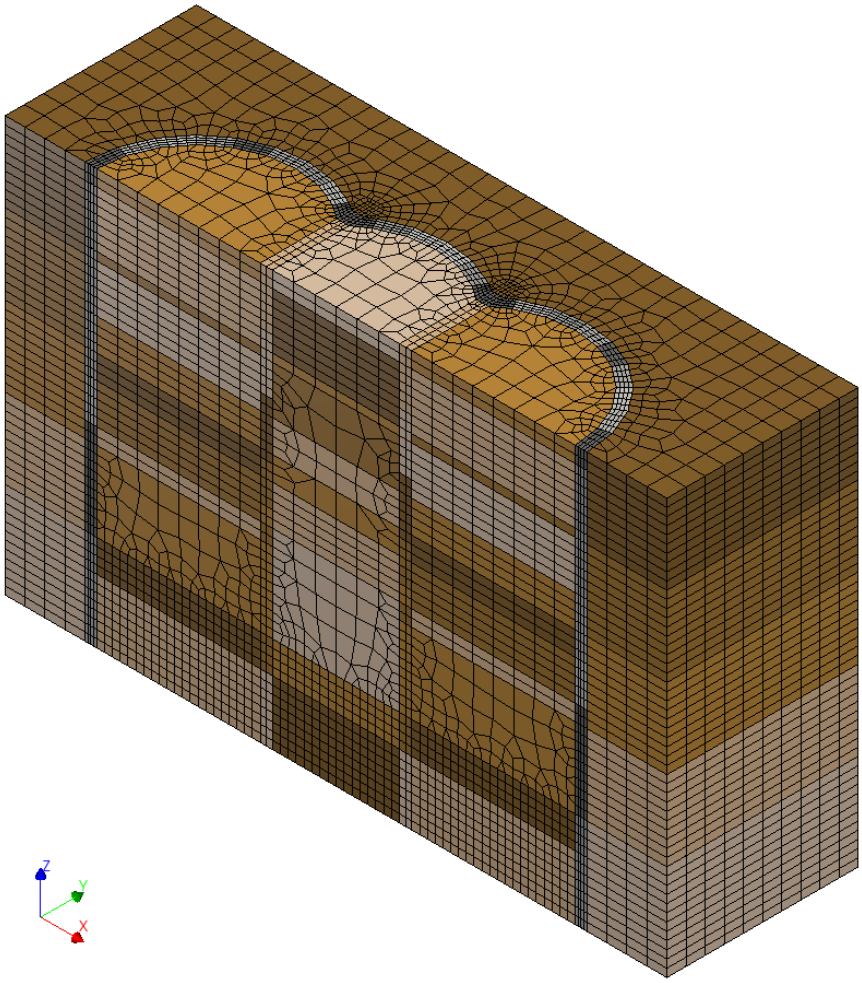

Figure 4-25: Isometric view of inner and outer soil (up to 10m from shaft walls) with mesh size of 2.5m

Soil beyond 10m were assigned the element size of 5m, with 'adaptive element size' checked, which seemed reasonable given that the influence of the shaft diminished significantly around 1*diameter distance.

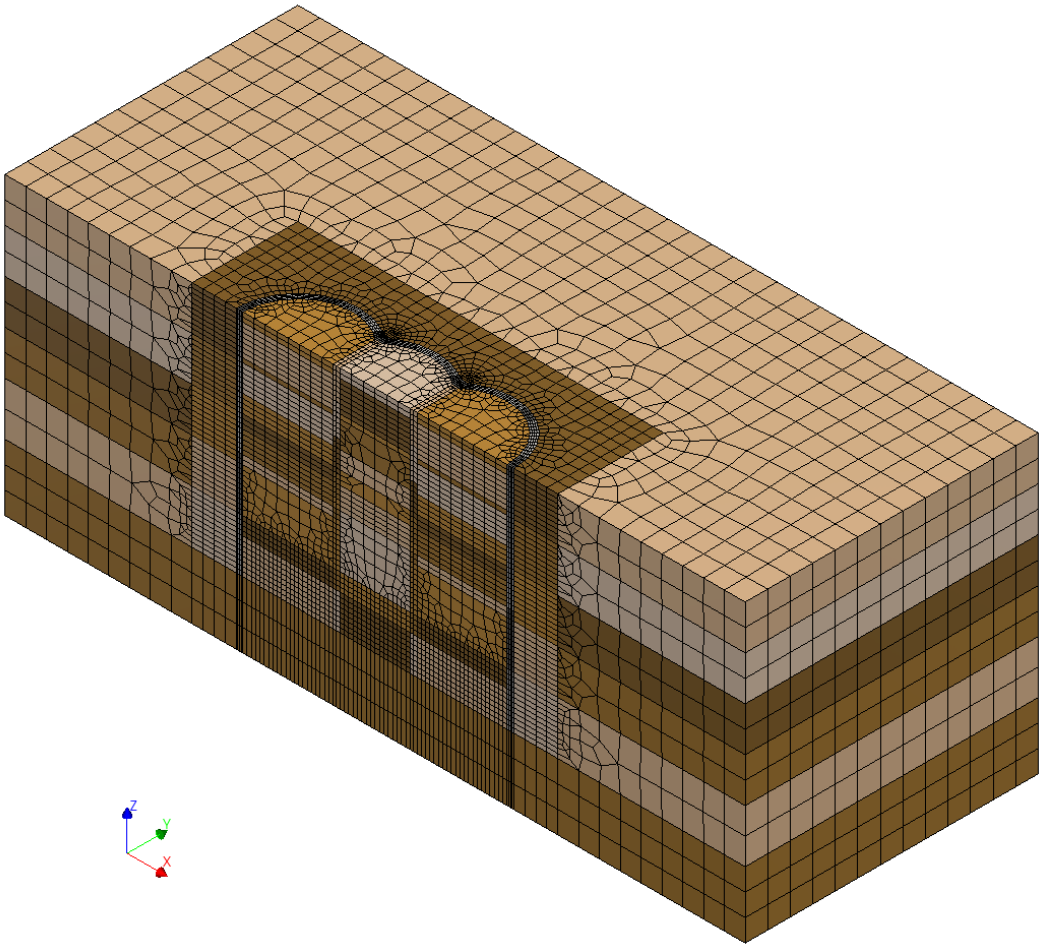

Figure 4-26: Isometric view of outer soil (beyond 10m from shaft walls) assigned the mesh size of 5m

4.3.9.3. Interface and Composed Surface Meshing, and Local Element Axes

The interfaces automatically adopt the mesh of the parent elements so there is no need to explicitly assign it a mesh size. For example, the composed surface of D-wall panel had 4 divisions on top and bottom edges and 1m element size in z-direction.

At this stage, one must also ensure that the local axes for the elements are all aligned uniformly to guarantee accurate results. Designers are encouraged to manually define the local axes for interface for greater control over the output. In these models, the

vertical interfaces and vertical composed elements have their local x-axis in global z-direction, and horizontal interfaces and horizontal composed elements have their local x-axis in global x-direction. An example of a uniform interface mesh is shown in Figure 4-27. Note that the local axes are different from the global axes which is intentional.

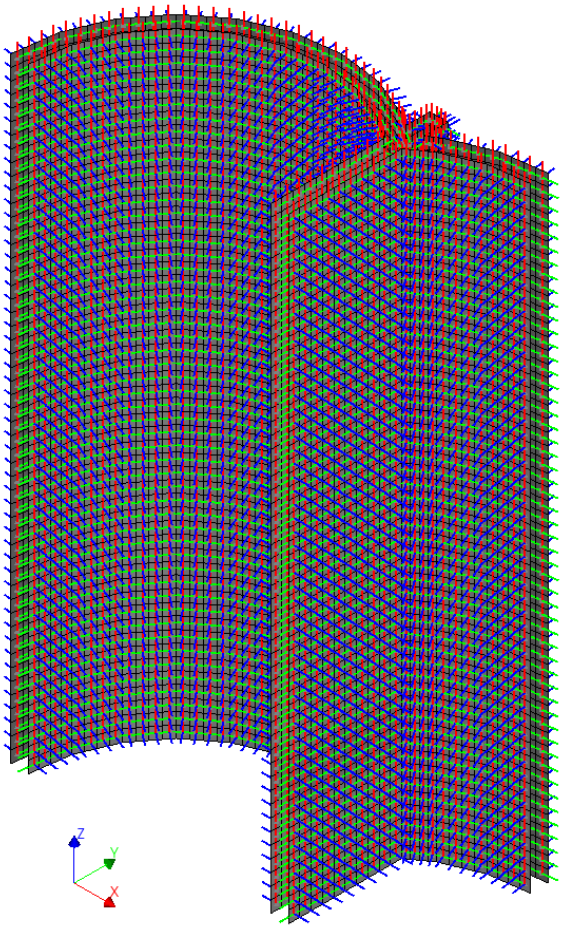

Figure 4-27: Isometric view of interface between inner soil and shaft walls with local element axes shown

This implies the following for the vertical interfaces and composed elements:

- Nxx: represents the normal force in the element
- Nyy: represents the hoop/tangential forces in the element

- Mxx: represents vertical bending moment in the element
- Myy: represents tangential bending moment in the element

4.4. 2D Geometry of the Shaft Model

The 2D geometries for the axisymmetric and plane-stain models follow the same design principles as the 3D model but differ in aspects that are inherent to these respective analyses.

4.4.1. Axisymmetric Model

The axisymmetric model was made to compare it with the circular geometry of the 3D shaft. The aim is to see whether the 2D model can reproduce the forces and deformation patterns derived from the much larger and numerically intense 3D model. In DIANA FEA, the axisymmetric model is setup as shown in Figure 4-28 and the final setup of the model is shown in Figure 4-30.

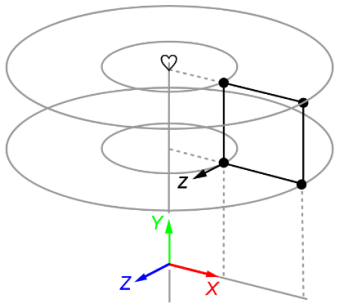

Figure 4-28: Axisymmetric implementation in DIANA FEA

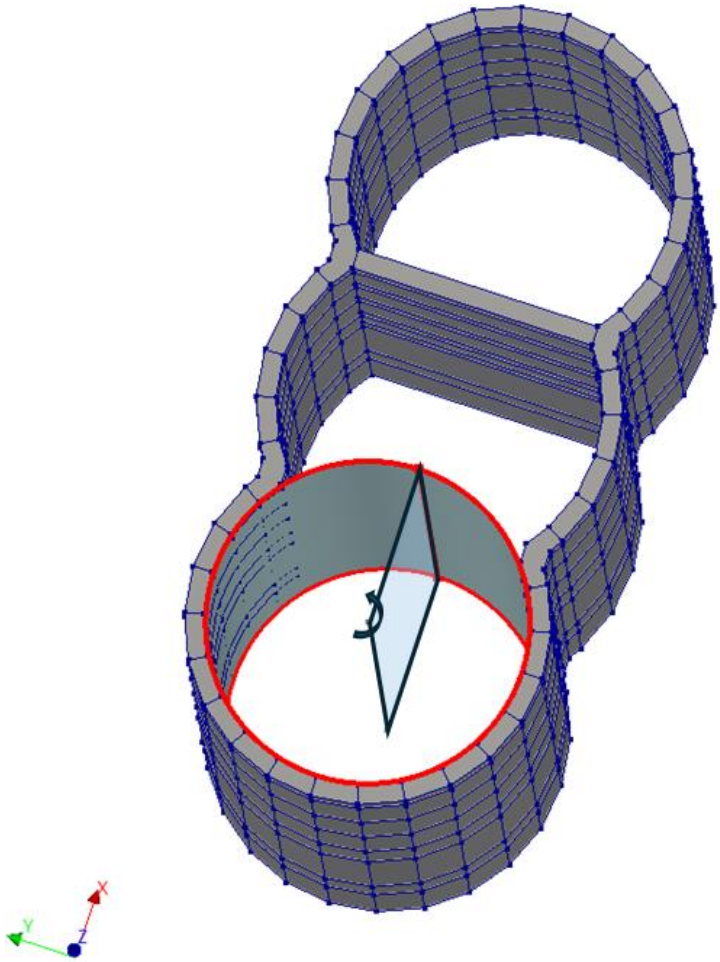

Figure 4-29: Theoretical implementation of axisymmetric analysis in the 3D model

- The D-wall was made using ‘flat shells of revolution’ of 1.5m thickness.
- For the mesh, the entire model was assigned a shape element size of 1m giving a total number of 4,700 elements (approx.).
- Struts were not modelled in this axisymmetric analysis.

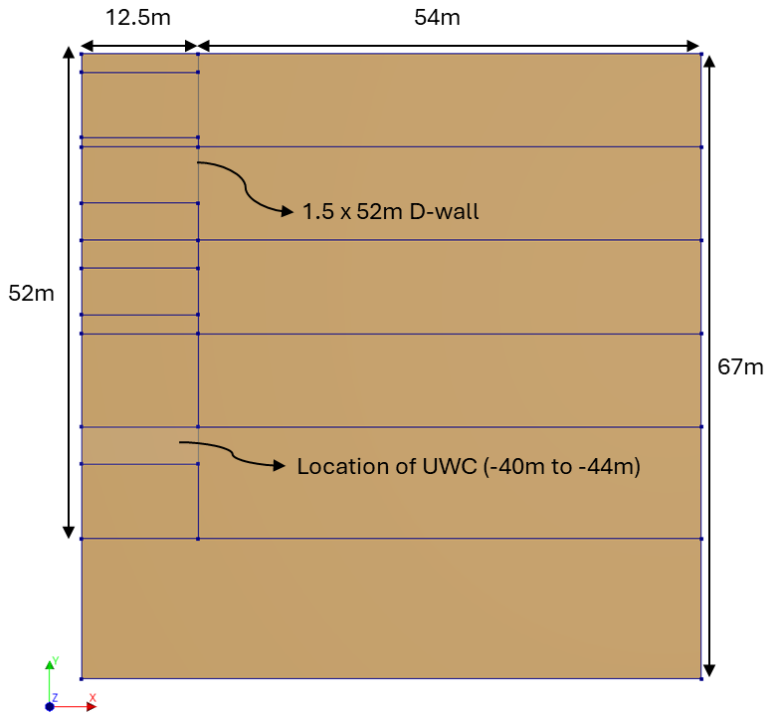

Figure 4-30: Axisymmetric model created in DIANA FEA for this study

Remark:

(i) when defining the interface between the D-wall and soil, in this case, two interfaces must be assigned – one between D-wall and inner soil and the other between D-wall and outer soil while ensuring that the local element axes of both interfaces are pointing in opposite direction as shown:

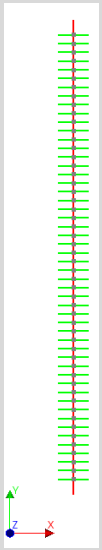

(ii) a ‘rigid’ connection could be defined between inner and outer soils instead of ‘unite’ connection for the ‘initialisation stage’ which should be disabled during ‘installation stage’ to avoid numerical issues arising due to installation of D-wall.

4.4.2. Plane-Strain

In practice, a 2D plane-strain model is used to mimic the behaviour of a 3D rectangular shaft in 2D for both sides of the shaft (minus the corners); the idea is to assume an infinitely long side out-of-plane and analyse the cross-section with the worse conditions. A similar 2D approach could be adopted for the caterpillar shaft at the Y-panel to compare it against the 3D model to see if there is any resemblance in the behaviour and the magnitude of forces. Since the circularity of the shaft breaks at the Y-panel, it is presumed that a plane-strain model could replicate the response of the Y-panel; although, it could not be an exact replication given the loads experienced by the Y-panel are expected to be the contribution of the hoop forces from the circular section of the shaft and the laterally inward forces from the soil.

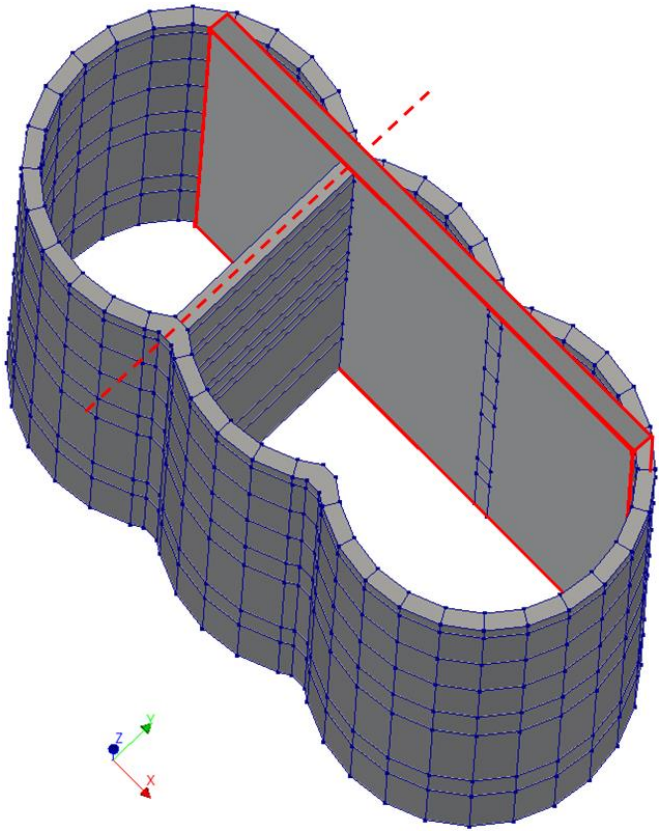

Figure 4-31: Theoretical implementation of plane-strain analysis in the 3D model

In plane-strain, however, it was not possible to model the cross-wall of the shaft along with stage-wise excavation of inner soil. This is because in the 3D equivalent cross-section, the soil portion is replaced by cross-wall at Stage-B (installation of the structure) as shown in Figure 4-31; hence, in a 2D model, it is not possible to have the strut wall in place while also performing stage-wise excavation of the shaft.

4.5. Excavation Sequence

Table 4-7 shows the excavation sequence adopted for this study.

Table 4-7: Excavation sequence adopted for this study

Stage	Description	Remarks
A	Initialisation of stresses in soil elements	Surface is considered at 0.0m elevation.
B	Installation of shaft walls, Y-panels and Cross-walls	D-wall panels, Y-panels and cross-walls are installed till the depth of -52.0m. Composed elements, and structure-structure and structure-soil interfaces are also activated.
1	Excavation of inner soil till -2.0m	Hydrostatic loads are activated on the inner shaft walls till -2.0m and on the top face of unexcavated inner soil with the hydraulic head set at 0.0m to simulate wet condition for excavation
2	Excavation of inner soil till -9.0m	Hydrostatic loads are activated on the inner shaft walls till –9.0m and on the top face of unexcavated inner soil with the hydraulic head set at 0.0m
3	Excavation of inner soil till -16.0m	Hydrostatic loads are activated on the inner shaft walls till –16.0m and on the top face of unexcavated inner soil with the hydraulic head set at 0.0m
4	Excavation of inner soil till -23.0m	Hydrostatic loads are activated on the inner shaft walls till –23.0m and on the top face of unexcavated inner soil with the hydraulic head set at 0.0m
5	Excavation of inner soil till -28.0m	Hydrostatic loads are activated on the inner shaft walls till –28.0m and on the top face of unexcavated inner soil with the hydraulic head set at 0.0m
6	Excavation of inner soil till -40.0m	Hydrostatic loads are activated on the inner shaft walls till –40.0m and on the top face of unexcavated inner soil with the hydraulic head set at 0.0m.
7	Excavation of inner soil till -44.0m	Hydrostatic loads are activated on the inner shaft walls till –44.0m and on the top face of unexcavated inner soil with the hydraulic head set at 0.0m.
8	Installation of UWC between -40.0m to -44.0m	Hydrostatic loads are activated on the inner shaft walls till –40.0m and on the top face of UWC with the hydraulic head set at 0.0m. Interfaces connected to UWC are also activated now.
9	De-watering of shaft	Hydrostatic loads are removed from inner faces of the shaft walls. Vertical hydrostatic pressure is maintained on top

Stage	Description	Remarks
		face of UWC to simulate presence of tension piles.
10	Cross-wall is excavated/removed between -28.0m and -40.0m	This 12m of wall is removed to make space for TBM and placement of ancillary equipment inside the shaft. An alternate analysis is also conducted where this wall is not entirely removed, and some portion is left to act as a buttress for the Y-panel on the inner-side (see Chapter 5.6 for details)

⚠ **Note:**

No barettes or tension piles were modelled in this study. Instead, hydrostatic pressure was applied to counteract uplift pressure experienced after installation of UWC and de-watering of shaft. Barettes or tensions piles also help to counteract the basal heave effect, but no measure was taken to counteract basal heave in this study. Ideally, barettes would be installed concurrently during the installation of D-walls for the shaft structure from the surface itself before the start of excavation.

💡 **Remark:**

All interfaces can be activated at Stage-1 and DIANA FEA will automatically determine which interfaces are to be activated based on the current stage of the analysis. However, users are advised to activate only stage-specific interfaces (and composed elements) manually instead of relying on the software to gain more control over the stability of the analysis. For example, a structure-structure interface that exists between D-walls and UWC is not activated until Stage-10, when the UWC is activated, although this interface could be activated at Stage-1 as well to allow the software to automatically disable it until Stage-10.

5

RESULTS

Sub chapters:

1. General Observations
2. Changing Soil Strata
3. 3D vs. 2D Axi-symmetric Model
4. Arching Effect in Soil
5. Comparing Buttresses
6. Stage-10: Wall Removal

5.1. General Observations

A full-scale model was developed of the 3-cell shaft which was then reduced to a quarter size based on the line of symmetry identified from the initial analysis as seen in Figure 5-1. The results of the quarter model were compared with the results of the full-scale model which revealed a deviation of about 1% which was found acceptable; hence, the quarter model was used for all further analyses.

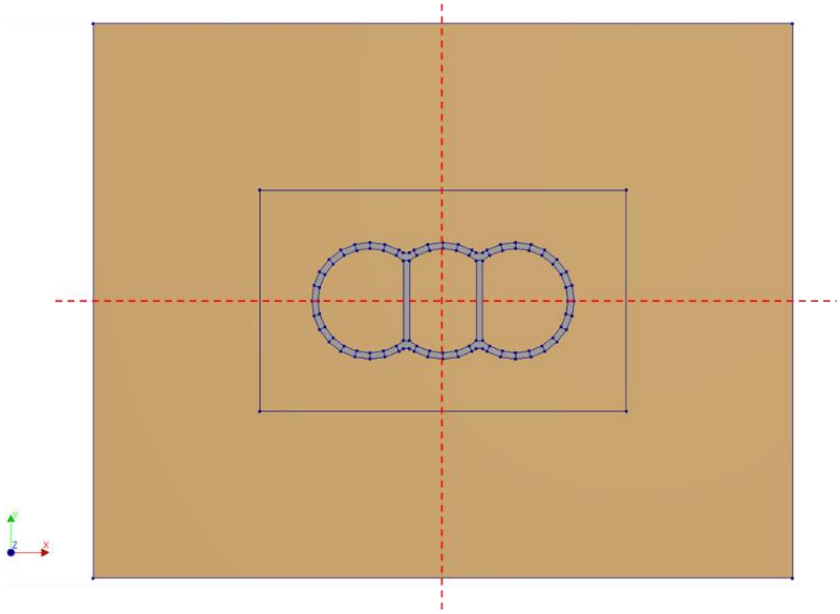

(a)

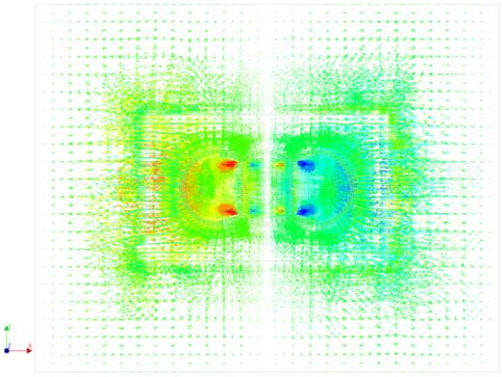

(b)

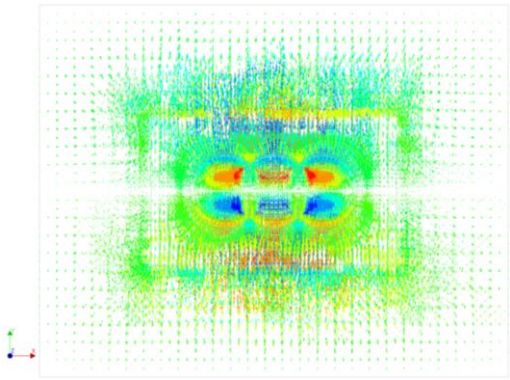

(c)

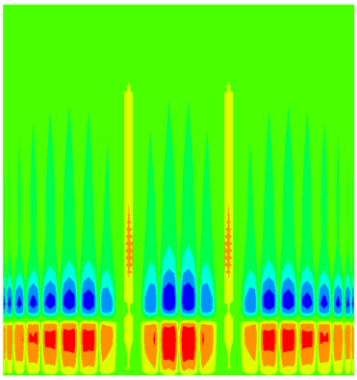

(d)

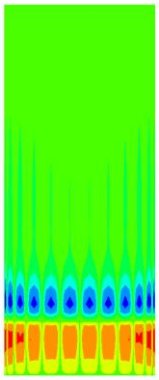

(e)

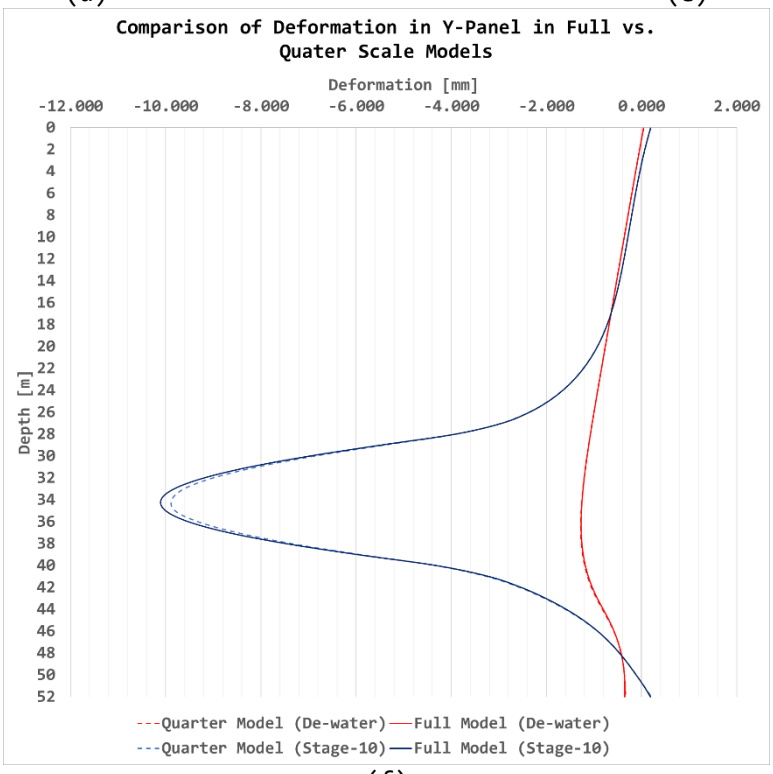

(f)

Figure 5-1: (a) line of symmetry defined on the full-scale model; (b) top view of displacement vectors in global x-axis; (c) top view of displacement vectors in global y-axis; (d) side view of Mxx on shaft walls; (e) front view of Mxx on shaft walls; comparison of deformation in the Y-panel of full and quarter models (20m diameter model in sand)

Some general observations that were made on the shaft behaviour:

- The shaft deforms laterally inwards at the Y-panels and elongates outwards at either end to form a shape like a hyperboloid. The maximum cumulative deformation is around 4-5mm in Stage-10 (wall removal) for the d-walls panels at the ends.

- There is also an upward movement of the shaft, as the excavation proceeds, in the range of 2-3mm (magnitude would vary with changing stratigraphy and wall-length). This is an expected heave effect from the stress release of the soil.

- The shaft deforms only 2-3mm (cumulative) laterally inwards after Stage-9 (de-watering) and large development of hoop forces (Nyy) is observed in the d-wall panels. These deformation values are about 1/10th of those observed in other projects (see Chapter 2) deformation which could be attributed to the cross-walls installed before the excavation which make the shaft very rigid.

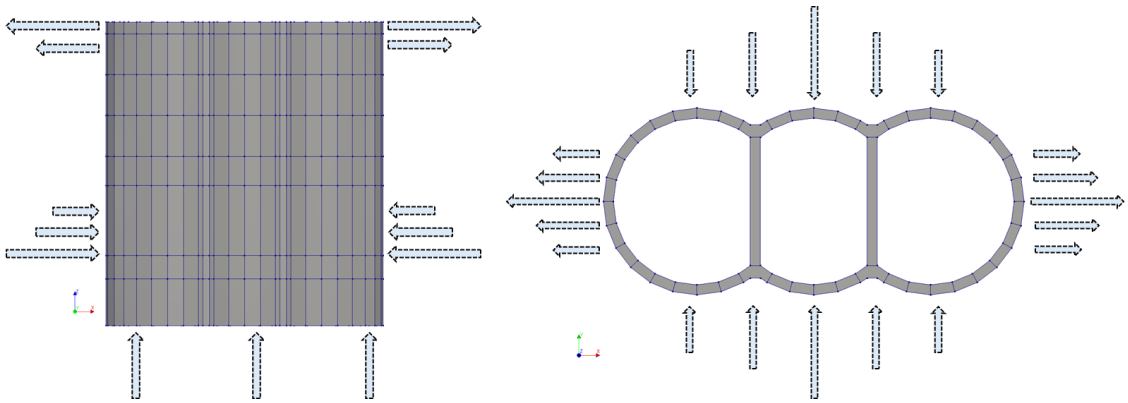

Figure 5-2: Side view (left) and top view (right) of deformation behaviour of the caterpillar shaft. Note: arrows are representative only and are not to scale.

- The Cauchy total forces principal components, [10] as seen in Figure 5-3, shows the stress distribution in the shaft; it is seen that the stress is transferred from the circular/perimeter d-wall panels to the struts, via Y-panels, as expected from this design.

[10] DIANA User's Manuals / Theory Manual / Results / Stresses / Cauchy Stresses

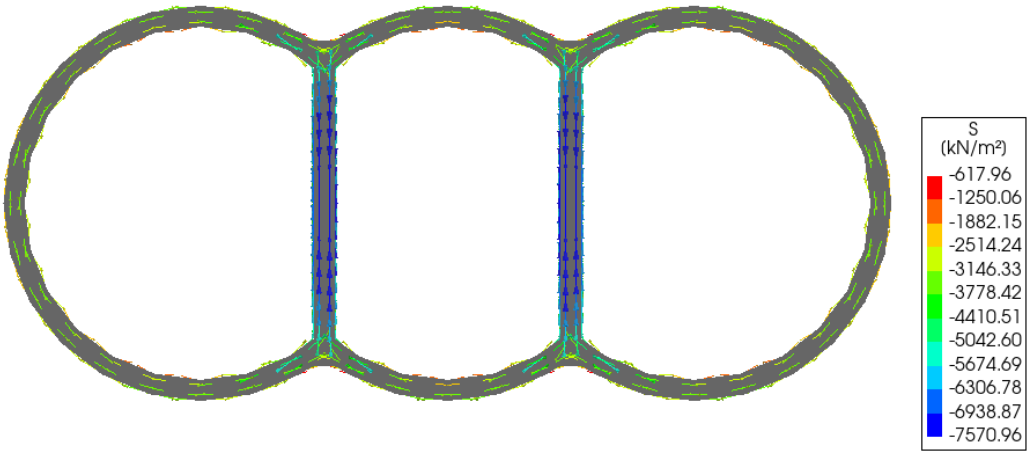

Figure 5-3: Cauchy total forces principal components in the shaft structure as seen at Stage-5

Figure 5-4 shows the panel numbering for the data presented in the charts that follow.

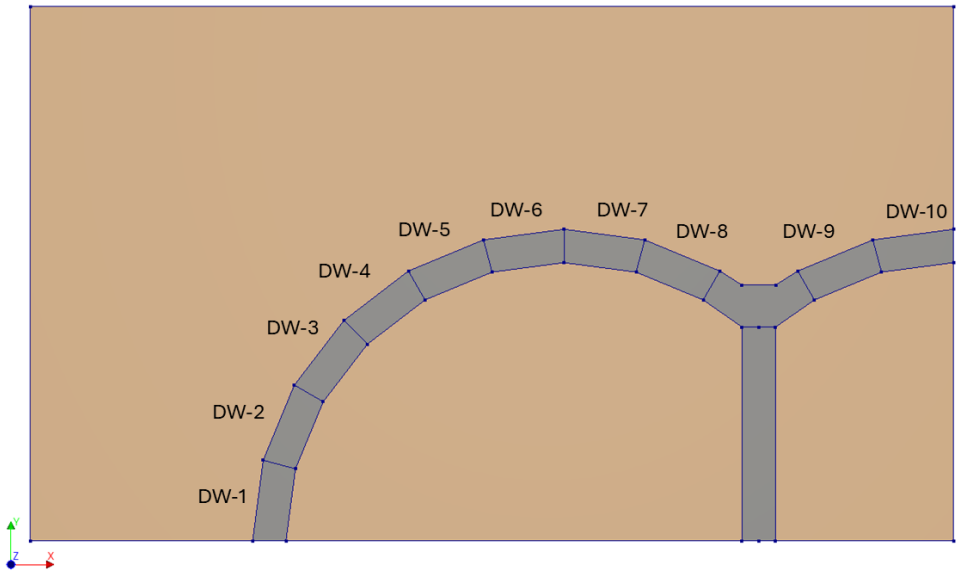

Figure 5-4: Panel identification numbers

5.1.1. The Circular/Perimeter D-wall Panels

- The maximum bending moments and deformations in the permitter d-wall were observed in the panels of middle cell (DW-10 and DW-9) as was also the case in the Sao Paulo project [19]

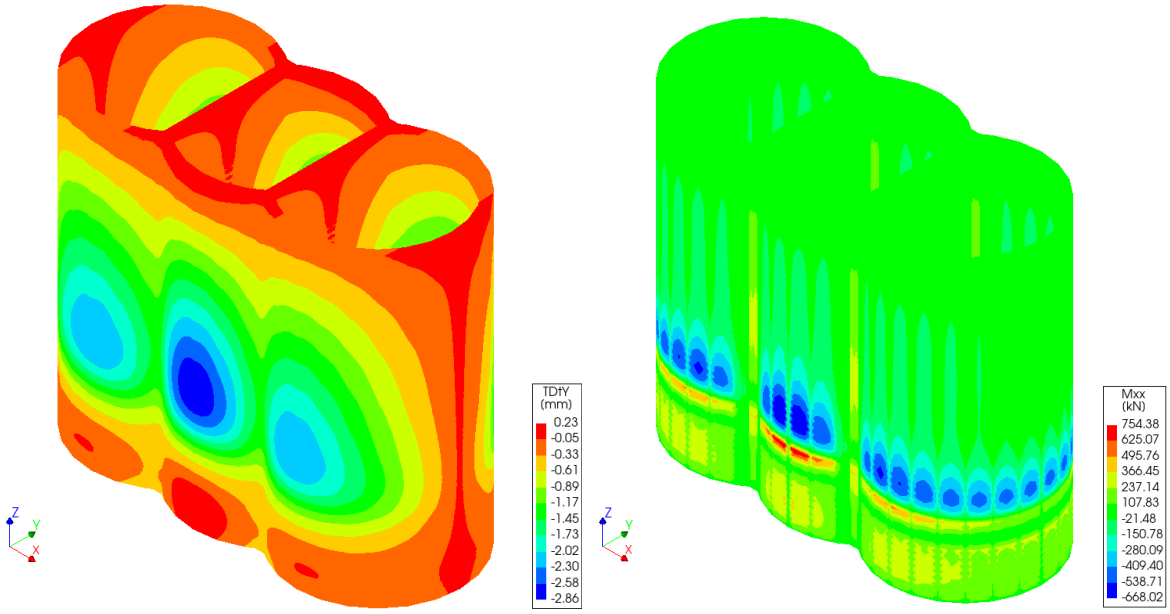

Figure 5-5: Development of deformation (left) and vertical bending moment (right) in the caterpillar shaft

- The hoop forces, on the other hand, were highest in the end-cell panels (DW-1) on either ends which gradually decreased moving towards the middle panels.

- The deformation pattern of DW-1 at different excavation stages suggests that the shaft tends to elongate outward as seen in Figure 5-6.

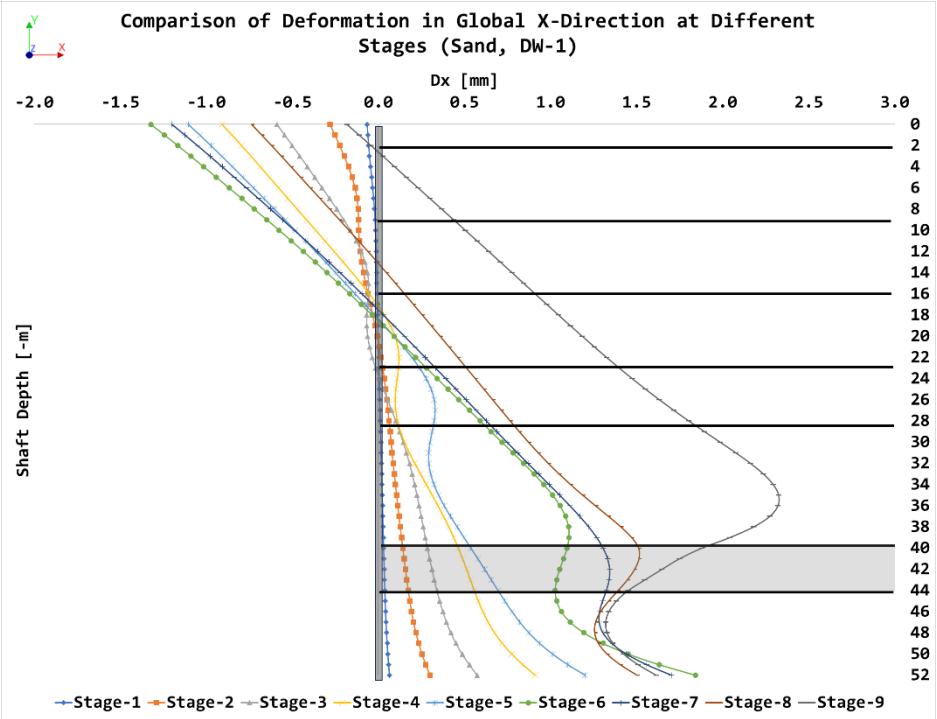

Figure 5-6: Deformation in DW-1 at different excavation stages

- When comparing the hoop forces in the circular panels with the 2D axisymmetric model, the end panels should give the closest match. However, the higher bending moments and deformations experienced in the middle panels would govern the reinforcement design of the panels.

- It is evident that the hoop forces are the main loads experienced by the circular geometry. When comparing the ratio of hoop forces developed at a stage to the initial stage, as seen in Figure 5-7, the increase in the ratio suggest the development of hoop forces in the panel as the excavation progresses. These hoop forces are the reason the shaft only deforms only 4-5mm laterally inwards suggesting that the arching effect within the structure is at play here.

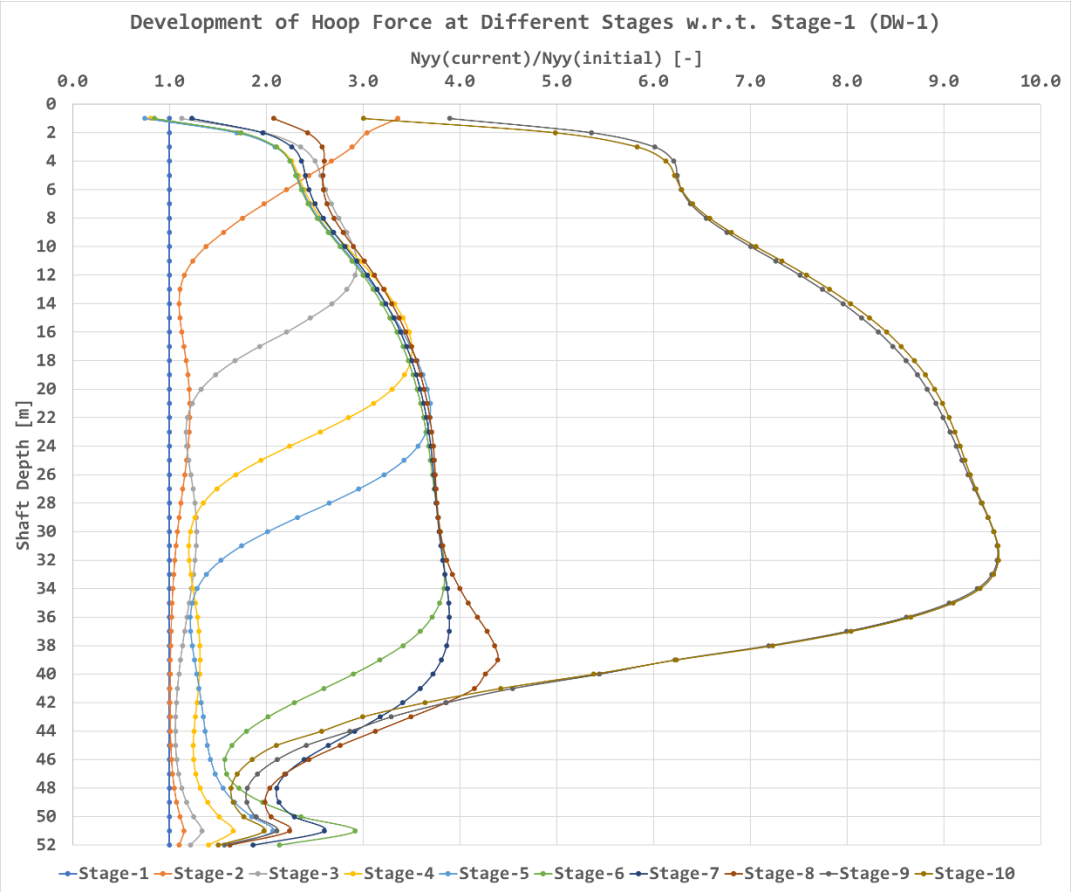

Figure 5-7: Comparison of current:initial hoop force at different stages (3D, DW-1)

5.1.2. The Y-panel

- At the Y-panel, the bending moments and the deformations are negligible up till Stage-8. From Stage-9 (dewatering) onwards, there is a noticeable increase due to increased lateral loads now acting on the shaft walls due to difference in water table levels inside and outside the shaft. These values are still considerably less because of the extensive support provided by the cross-walls all along the Y-panel length.

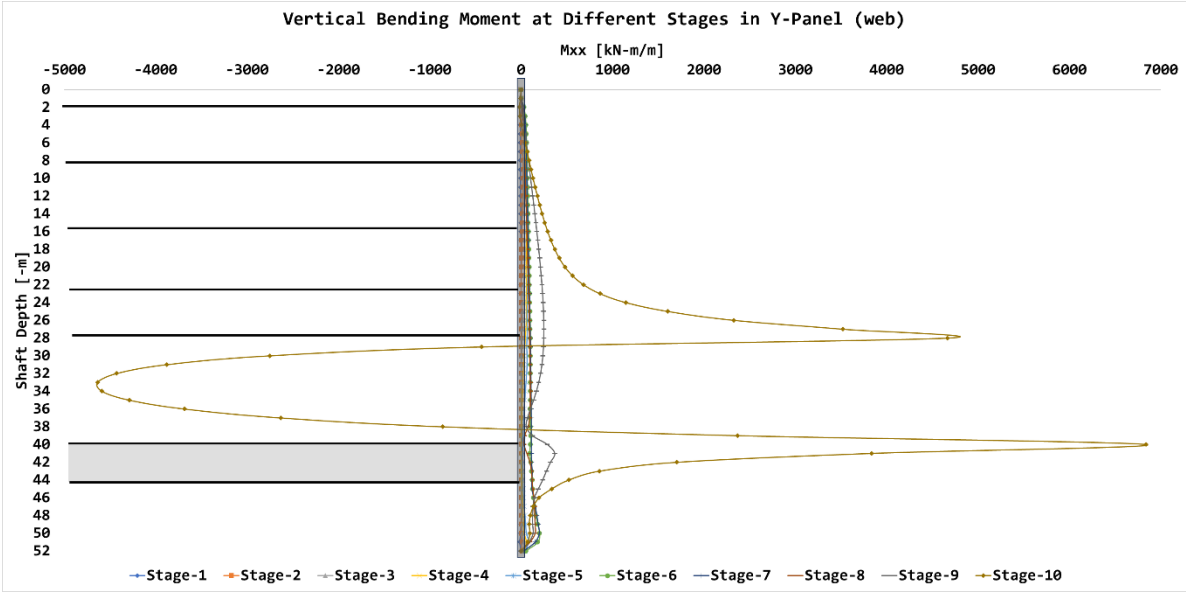

Figure 5-8: Bending moment at different stages in the Y-panel (web)

- There is also a slight movement of <0.5mm into the soil, marked by positive values of deformation, which is similar to what was observed from the field measurements taken for the Leiden parking project (see Chapter 2.1).

- Once the cross-wall is removed in Stage-10 between -28m and -40m, maximum values for forces and deformations are noticed in that section.

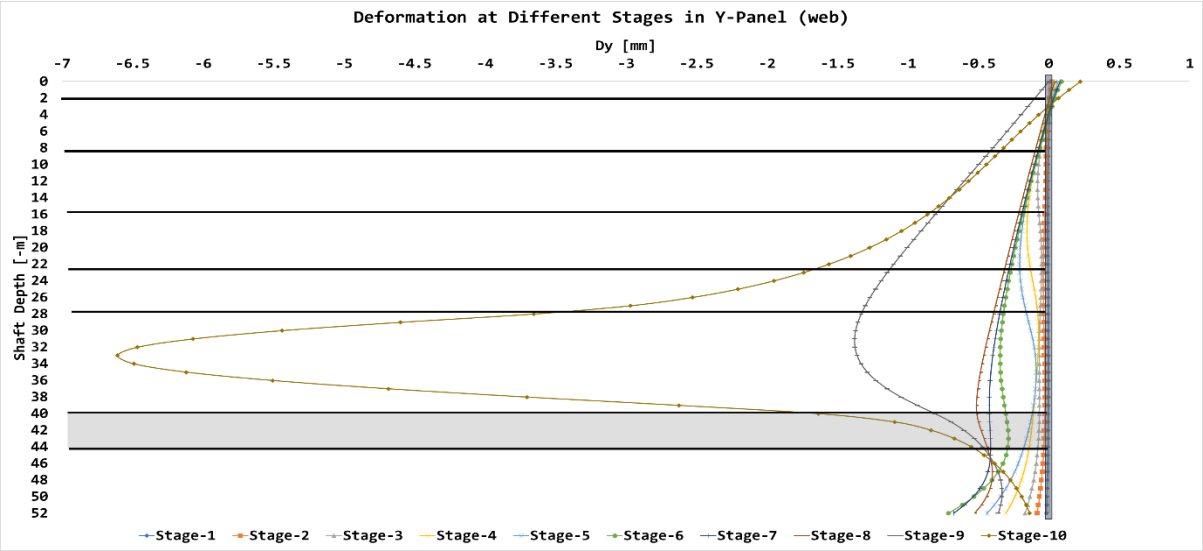

Figure 5-9: Deformation of the Y-panel (web) at different excavation stages

- Based on the results, it is obvious that the complete wall removal has significant impact on the Y-panel which would govern the design checks.

- The flanges (or wings) of the Y-panel exhibit similar structural response as the perimeter d-wall panels as those are designed as an extension of these panel; that is, the flanges maintain the same thickness (1.5m) and same internal angle (165°) as the perimeter d-wall panels. Despite the forces experienced by the middle-cell panels (DW-9 and DW-10) being a bit larger than the rest of the panels, the either flanges of the y-panel showed negligible differences in the forces as these are not very far apart; DW-8 and DW-9 also show similar results Figure 5-10.

- The hoop forces from the flanges were transferred partly in form of hoop forces in the web of the Y-panels; that is, the web also experienced the hoop forces. This is evident from gradual increase in the hoop forces as the excavation progressed. Figure 5-11 plots the ratio of hoop forces in each excavation stage (current) w.r.t. Stage-1 (initial).

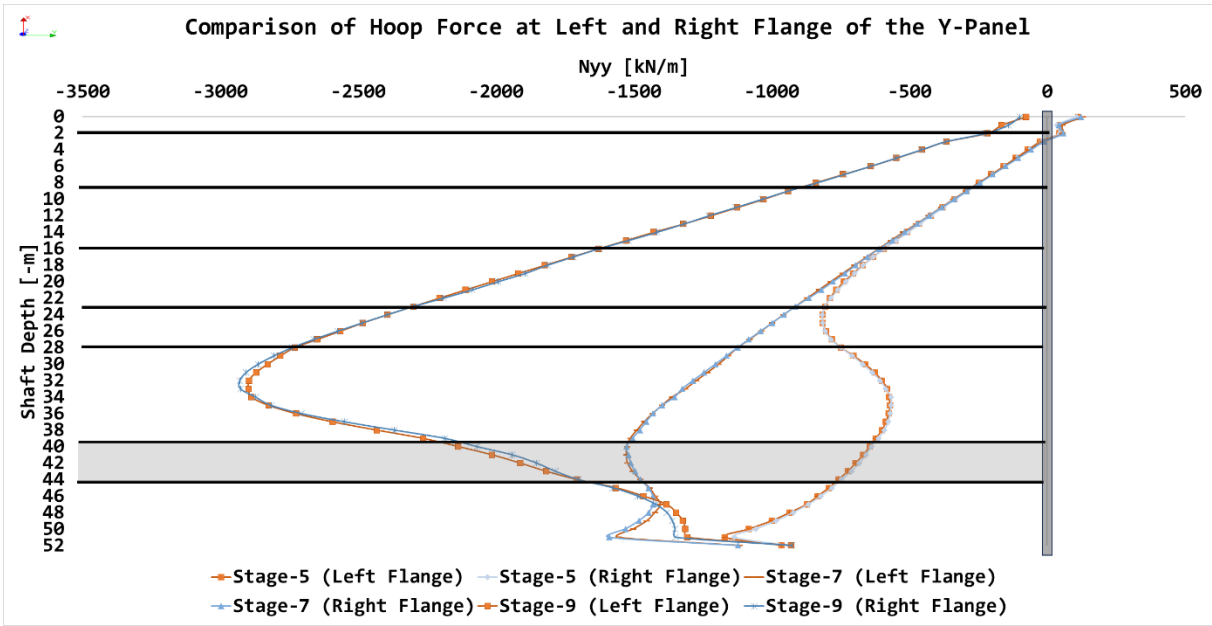

Figure 5-10: Comparison of hoop forces developed in left and right flanges of the Y-panel at different stages

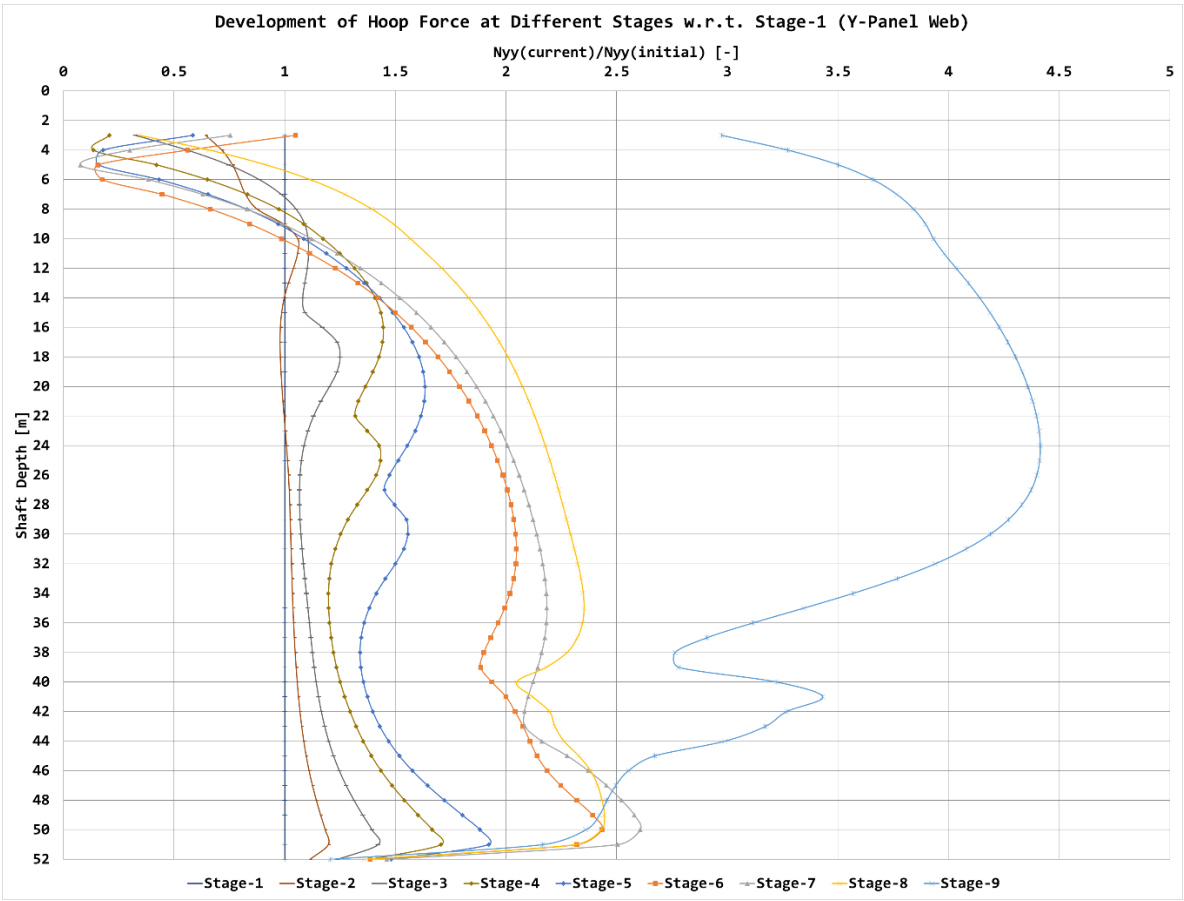

Figure 5-11: Comparison of current:initial hoop force at different stages (3D, Y-panel)

5.2. Changing Soil Strata

The stratum was progressively changed to see its effect on the shaft as discussed in Chapter 4.2.1. Key parameters like the deformation of shaft and soil, and normal and hoop forces on the shaft wall were studied.

First looking at the deformation of the panels in Figure 5-12. Across the iterations of changing soil strata, the deformation pattern seems similar. From Stage-1 to Stage-3, the movement is within 1mm, and it is seen that the upper half of the shaft moves outward while the lower half moves inwards (excavation side) making a diagonal movement. These movements are more in clay than in sand which is due to the lower soil stiffness of clay. From Stage-4 to Stage-6 the shaft continues to deform further following the diagonal deformation pattern from previous stages reaching a maximum deformation of ~1.5mm on either ends of the panel. This is a result of couple of actions experienced by the shaft: (i) the heaving of soil below the excavation level leading to loosening near the tip of the shaft and resulting in additional movement; (ii) elongation of the shaft at the shorter end due to the convergence at longer end. As the excavation increases at Stage-7 and Stage-8 the panels tend to retract to their original position marking the deformation to ~1mm at either end although the maximum deformation continues to increase which is seen just above the excavation level; in clay, this is more pronounced due to reduced soil stiffness and a lateral inward shift of the shaft is seen. In Stage-9 (dewatering), maximum deformation just above the excavation level is seen in all three cases, reaching a maximum value of ~2.4mm, and the deformation at the ends is further reduced due to lateral forces generated by the combination of soil and water loads. Similar behaviour was observed for Y-panel in all three cases, except for

elongation in the upper-half of the shaft; that is, all movements were towards excavation side.

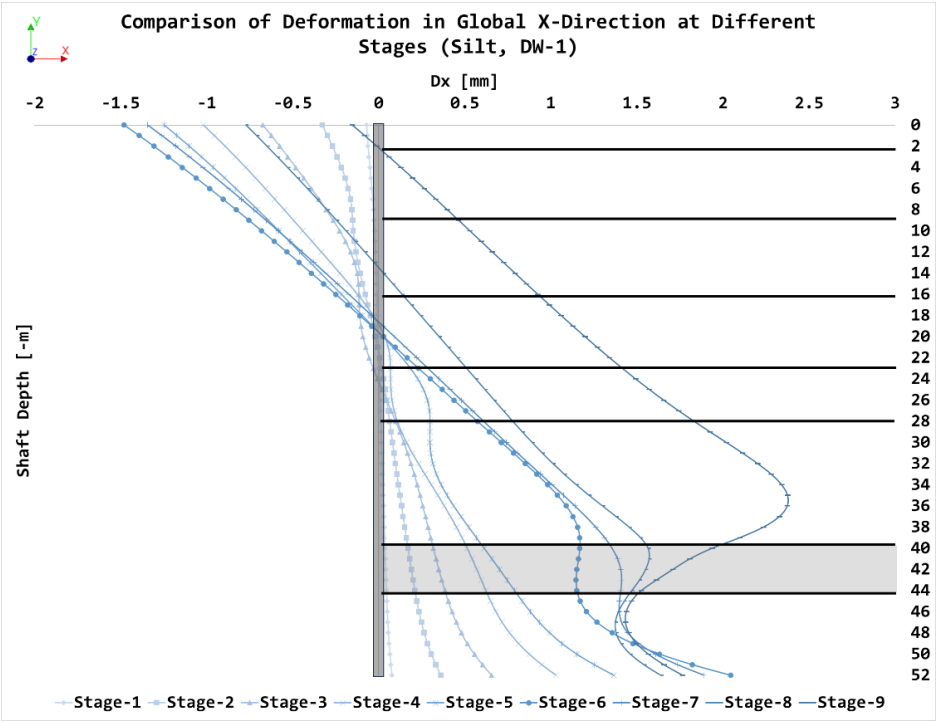

(a)

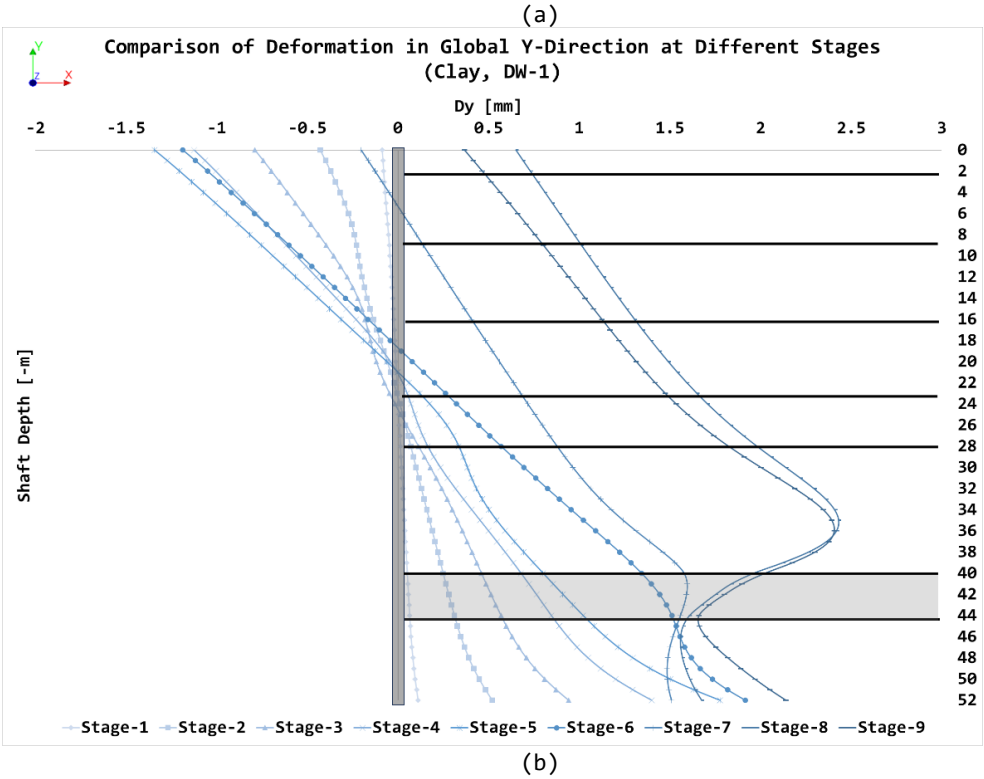

(b)

Figure 5-12: Deformation of DW-1 panel in global x-direction for (a) silt; (b) clay

Like the case with the deformations, the force pattern across all three models remains consistent except with changing magnitudes. The normal force shows a somewhat linear increase up to the excavation level and then tend to reduce thereafter at each stage (see Figure 5-13). As the deformation increases, or the entire system becomes more flexible moving from sand to clay, a reduction in the magnitude of the normal forces is seen consequently.

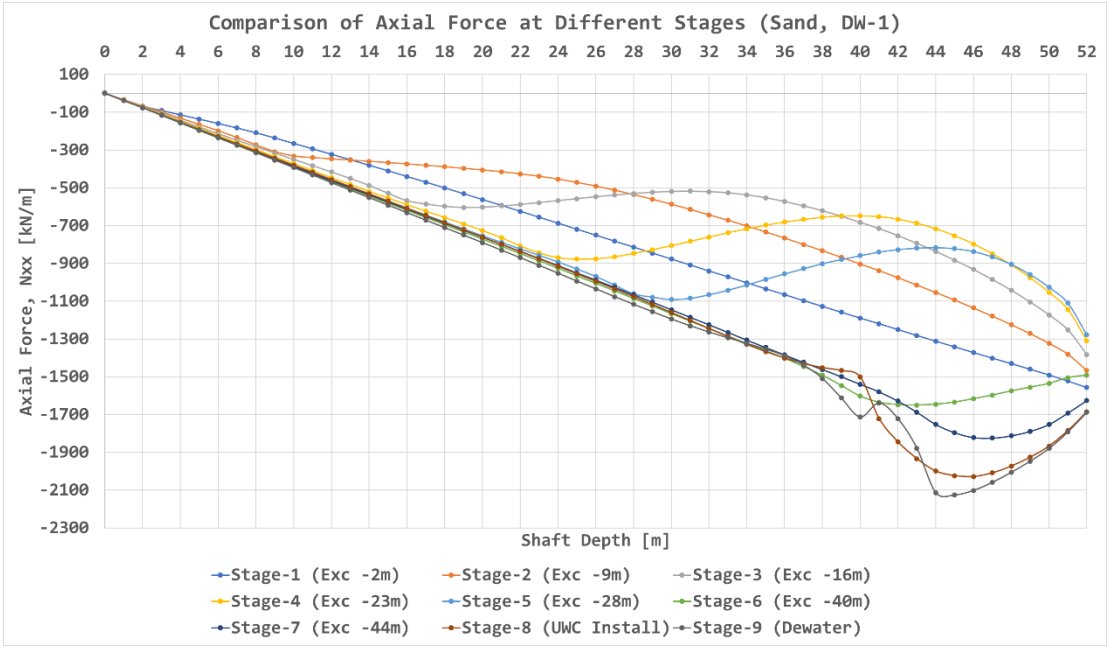

(a)

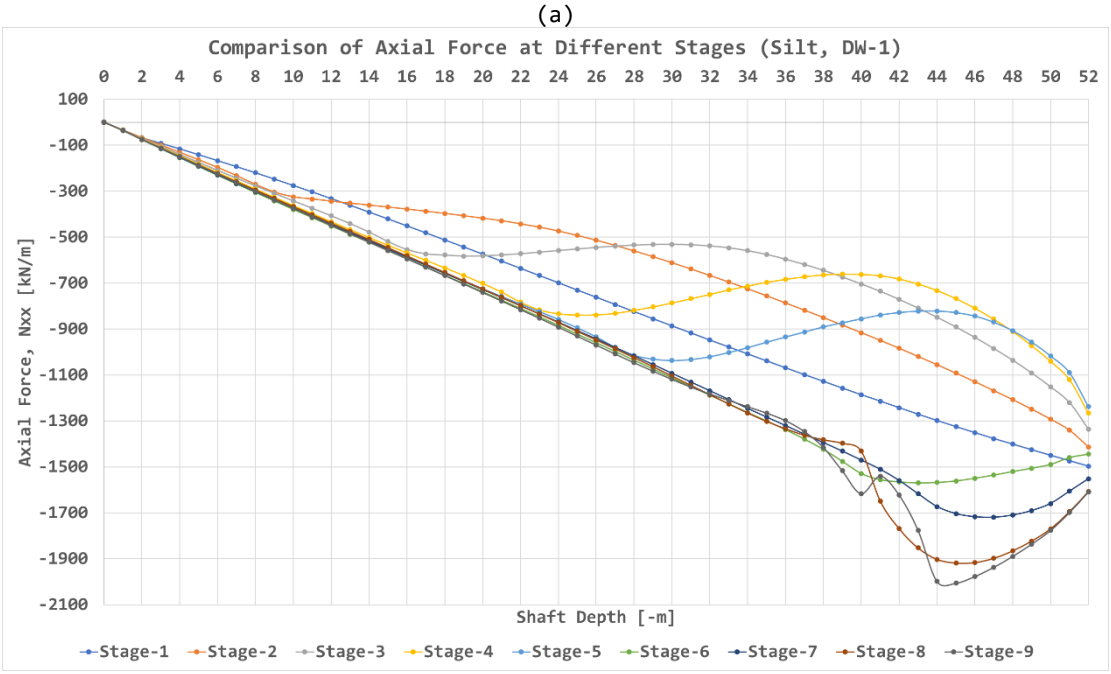

(b)

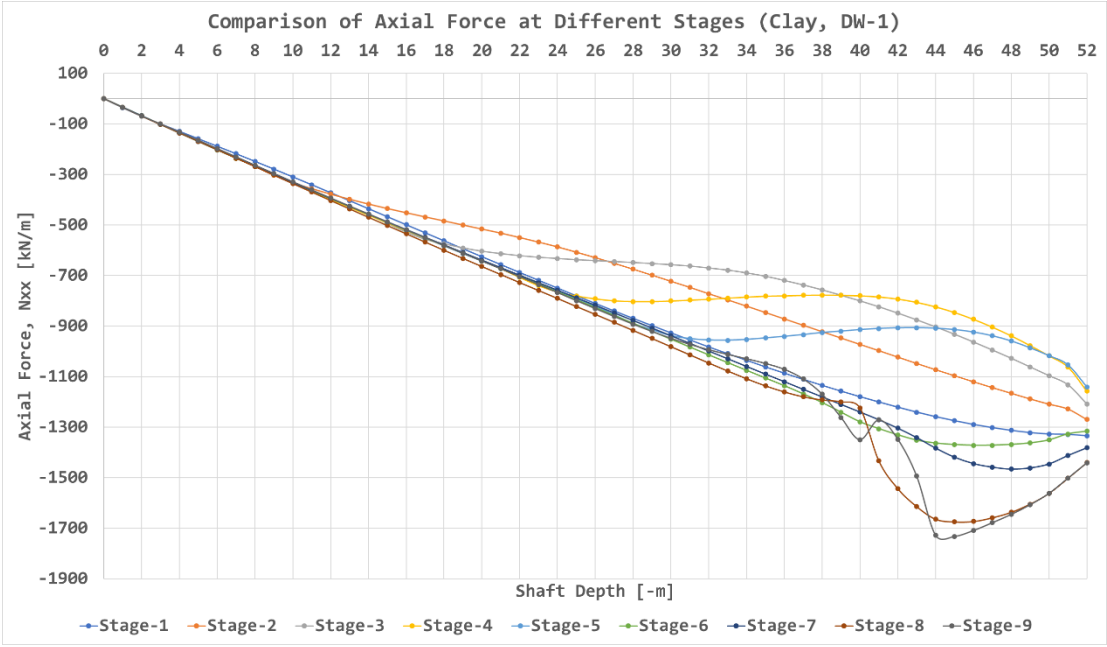

(c)

Figure 5-13: Normal force experienced by DW-1 at different excavation stages in (a) sand; (b) silt; (c) clay

Heaving of soil is experienced during excavation with maximum upward movement reported to be around 45mm for sand and about 270mm for clay at Stage-7. These values only confirm the expected behaviour from respective soil types, but the magnitude of these values is not relevant as the site conditions would be much different than what is presented here.

5.3. 3D vs. 2D Axisymmetric Model

This goal of this chapter is to present the comparison of the 2D axisymmetric model and the D-wall panels of the circular section of the shaft. From the 3D model, the D-wall panels of the circular section of the shaft were compared to the D-wall element from the 2D axisymmetric model. Three parameters are focused: Nxx (normal force), Mxx (vertical bending moment) and Nzz (hoop/tangential forces). All these parameters were collated to see a stage-wise progression in Table 5-1.

Table 5-1: Graphs showing stage wise comparison of hoop forces for D-wall panels of 3D model and 2D axisymmetric model

Stage	Nzz [kN/m]
3	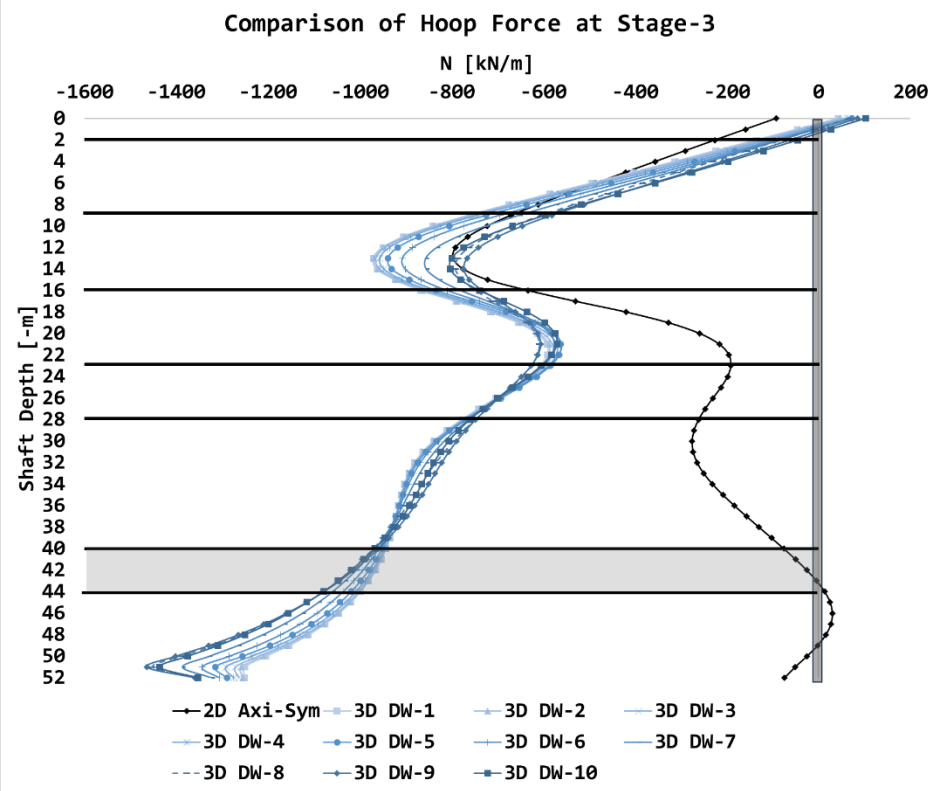
5	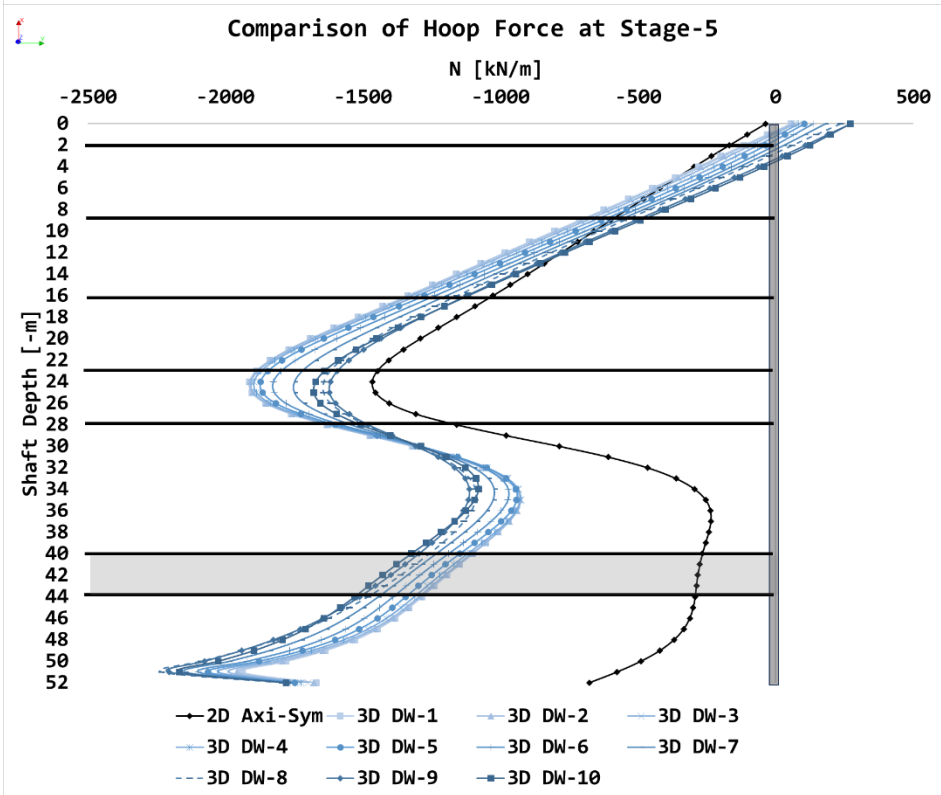

Stage	Nzz [kN/m]
7	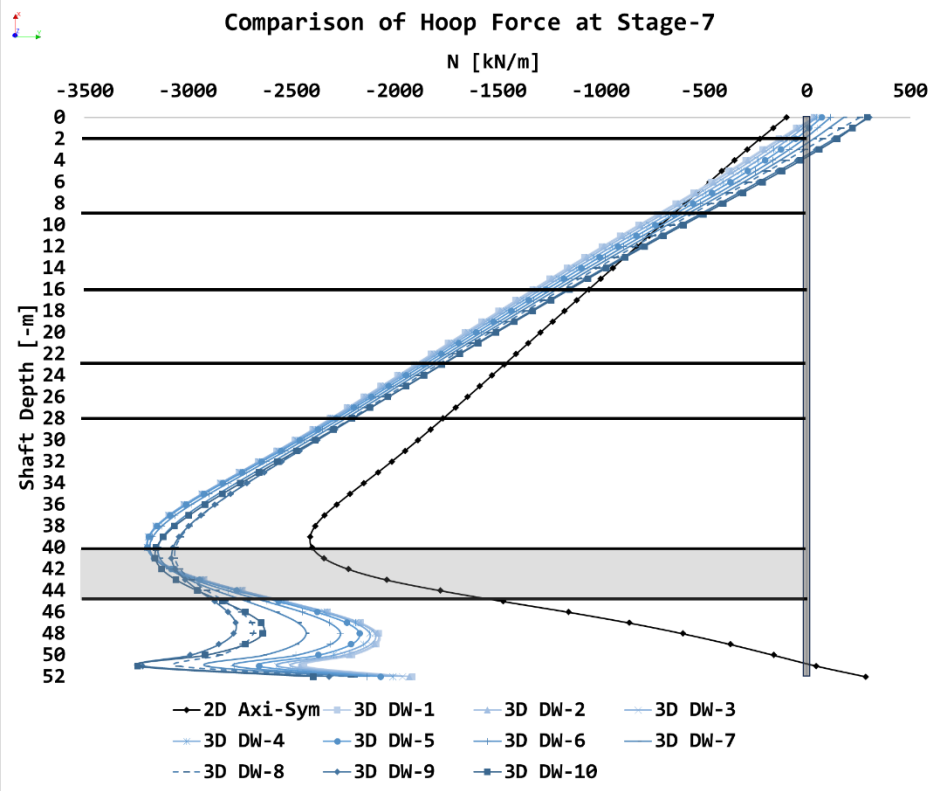
9	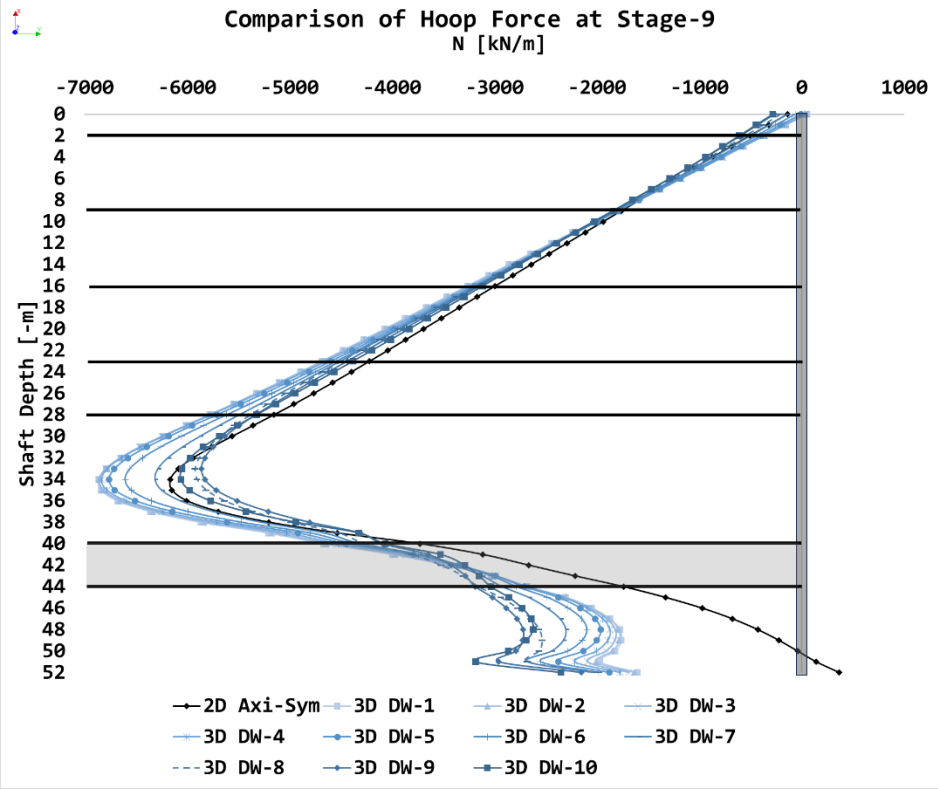

From all these stages it is evident that although the 2D and 3D models portray somewhat similar response. Magnitude is seen increasing

to maximum till the excavation level and reducing thereafter. In each stage, close to the excavated level, the hoop forces are highest for the panels of end-cells and reduces going inwards towards the panels of the middle cells; that is, DW-1 experiences largest hoop forces while DW-10 experiences the smallest. The magnitude of the response is rather underestimated by the 2D axisymmetric model. The average difference moving from the 2D axisymmetric, and 3D model is between 15-25% at various stages up to the stage-specific excavation level; below the excavation level the differences were incomparable. One possible explanation for this deviation in forces below the excavation level could be due to movement observed in the soil closer to the tip of the shaft as seen in Figure 5-6. This strange movement towards the soil side in upper part and away from soil in the lower part could be attributed to the 3D nature deformation explained earlier. In 2D case, because the deformation is uniformly inward, such a behaviour is not seen.

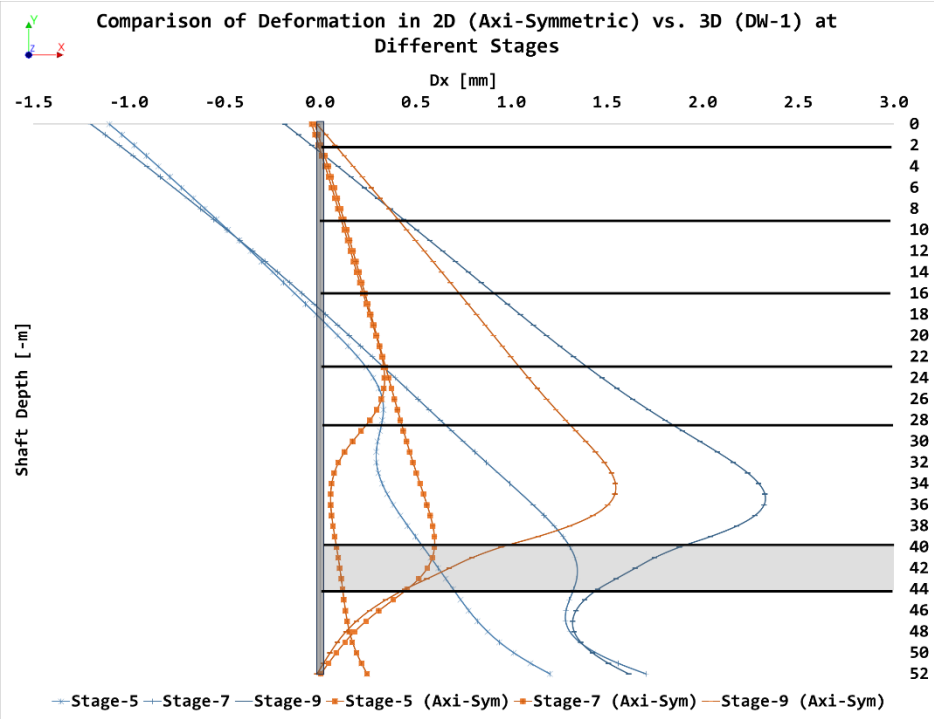

Figure 5-14: Comparison of deformation in 2D (axi-symmetric) and 3D (DW-1) at different stages

Comparing the analytical hoop forces from varying lateral earth pressure coefficients and the numerical results shows that a neutral soil state (K=0.5) best matches the results from the numerical analysis (see Figure 5-15). This response can largely be associated to the high stiffness of the shaft structure which only results in a cumulative deformation of up to 1.5-2mm which is insignificant to trigger an active or passive state of soil. The 3D analysis shows slightly higher values of hoop forces compared to the analytical and the 2D analysis which could be due to the panels pushing against the soil.

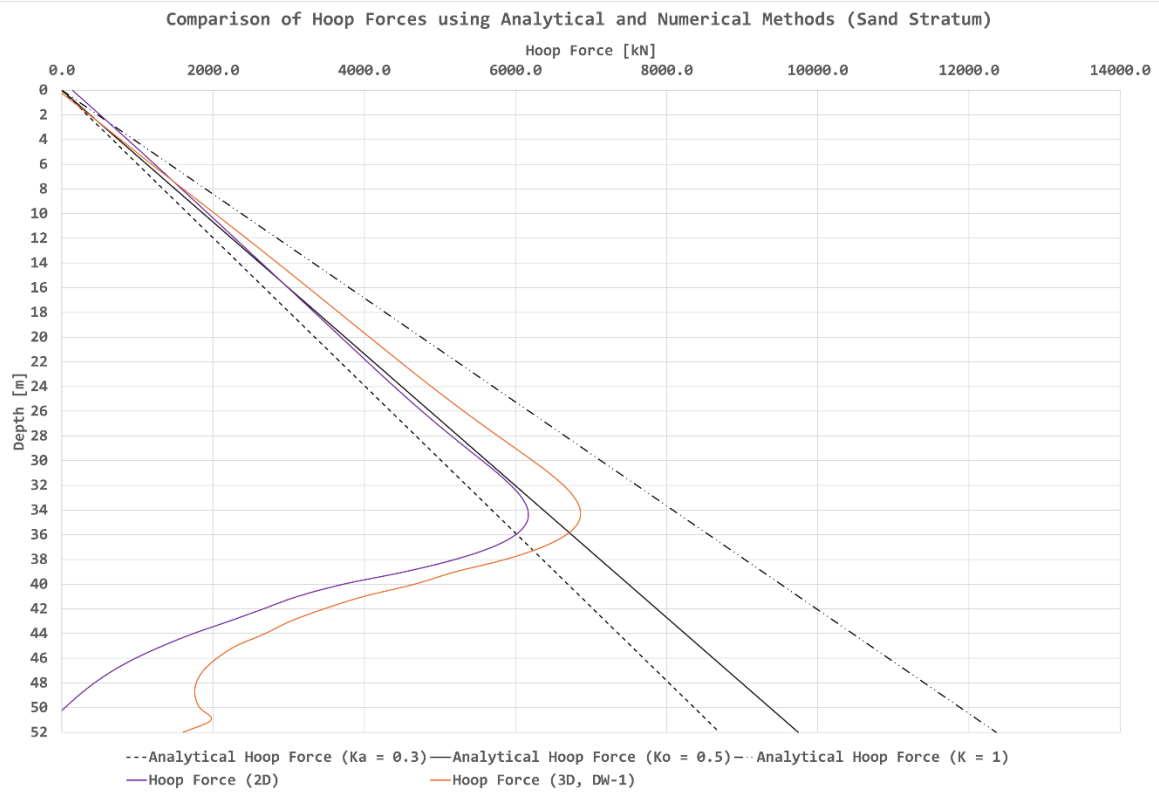

Figure 5-15: Variation of hoop forces comparing analytical and numerical results

For axial force, the 2D axisymmetric model again underestimated the values when compared with the 3D model for all perimeter d-wall panels, in all stages and at all depths. In this case, given the large differences, it is best to not use axisymmetric model for estimation

of axial forces. Figure 5-16 shows the axial force development in the permitter d-wall panels from 3D and axisymmetric model as an example.

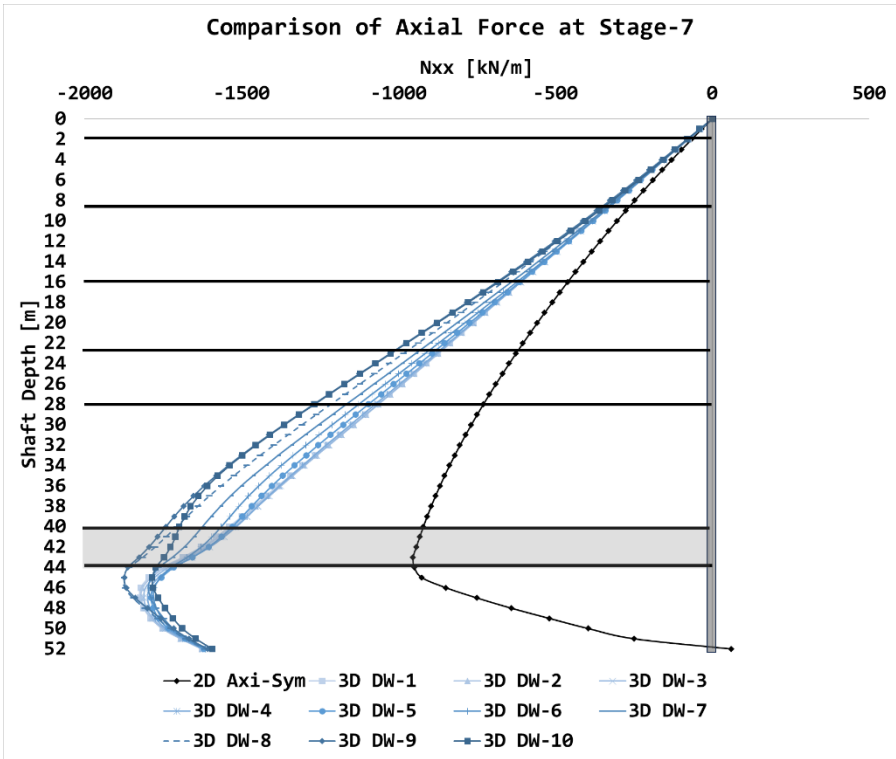

Figure 5-16: Comparison of axial forces for D-wall panels of 3D model and 2D axisymmetric model

The bending moment results estimated by the 2D analysis, as in the case of hoop forces, are underestimated when compared to the results from the 3D analysis throughout the panel depth; the difference is about 30-50% in comparison to DW-10 and about 5-10% to DW-1. The bending moment in the permitter d-wall panels are small given that most of the load experienced by these panels are tangential hoop forces. As discussed before, the highest bending moment is seen in DW-10 – the middle cell d-wall panel – while it decreases moving towards DW-1. Figure 5-17 shows this trend in bending moment at Stage-5 but is also true across all stages of excavation; panels experience the maximum bending moment in Stage-10 (see Chapter 5.6) which is used in the reinforcement design check detailed in APPENDIX-2: PANEL THICKNESS VERIFICATION.

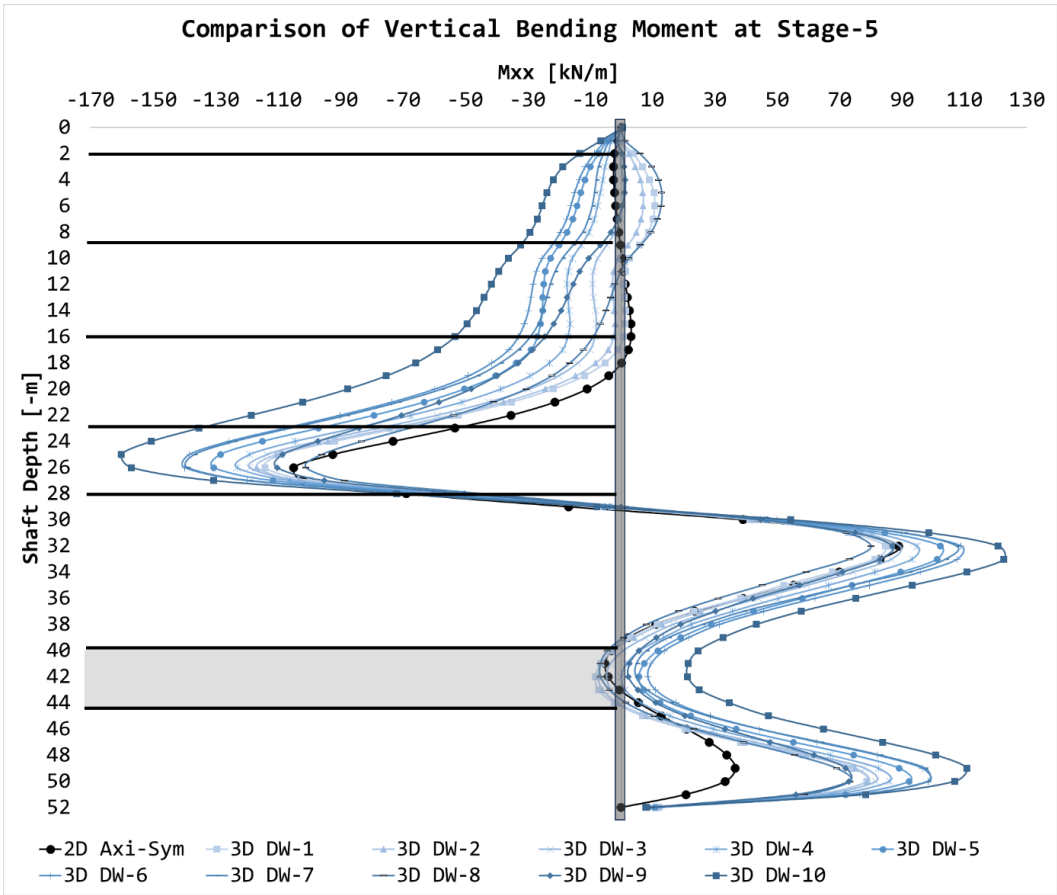

Figure 5-17: Comparison of Vertical Bending Moment development in the D-wall panels of caterpillar shaft (3D) and 2D axisymmetric model at Stage-5

In conclusion, it can be said that the 2D axisymmetric model is not an accurate representation of the 3D model in this case and it generally tends to underestimate the forces experienced by the shaft when compared with the 3D model by about 15-25% at various stages up to the excavation level for the hoop forces; below the excavation level, the results are incomparable. Axial forces show a similar trend up to the excavation level for both 2D axisymmetric and 3D model but the results are generally incomparable. Bending moments results exhibit similar behaviour in all excavation stages and at all depths are within 5-10% range for DW-1 – panel with the least bending moment – and about 45-50% range for DW-10 – panel with the most bending moment- with other panel ranging between the two. Due to the difference in the deformation behaviour of the caterpillar shaft and the circular

shaft, different force patterns are also observed. It is also evident that the structure does experience large hoop forces in the structure which results in minimal lateral deformation and bending moments in the perimeter d-wall panels of the shaft. Whether altering the stiffness of the struts (or cross-walls) reduces the discrepancies in the shaft structural behaviour is something that can be explored in future studies.

5.4. Arching Effect in Soil

The stresses in soil showed that there was practically no arching effect at play in soil throughout the excavation stages. This was confirmed by plotting ratio of $\sigma_{t(current)}/\sigma_{t(initial)}$ similar to what is seen in Figure 2-5. If the arching of soil was triggered, an increase in the ratio would be observed as the excavation progresses. A slight increase is indeed observed at Stage-9 (dewatering stage) but is practically insignificant (see Figure 5-18).

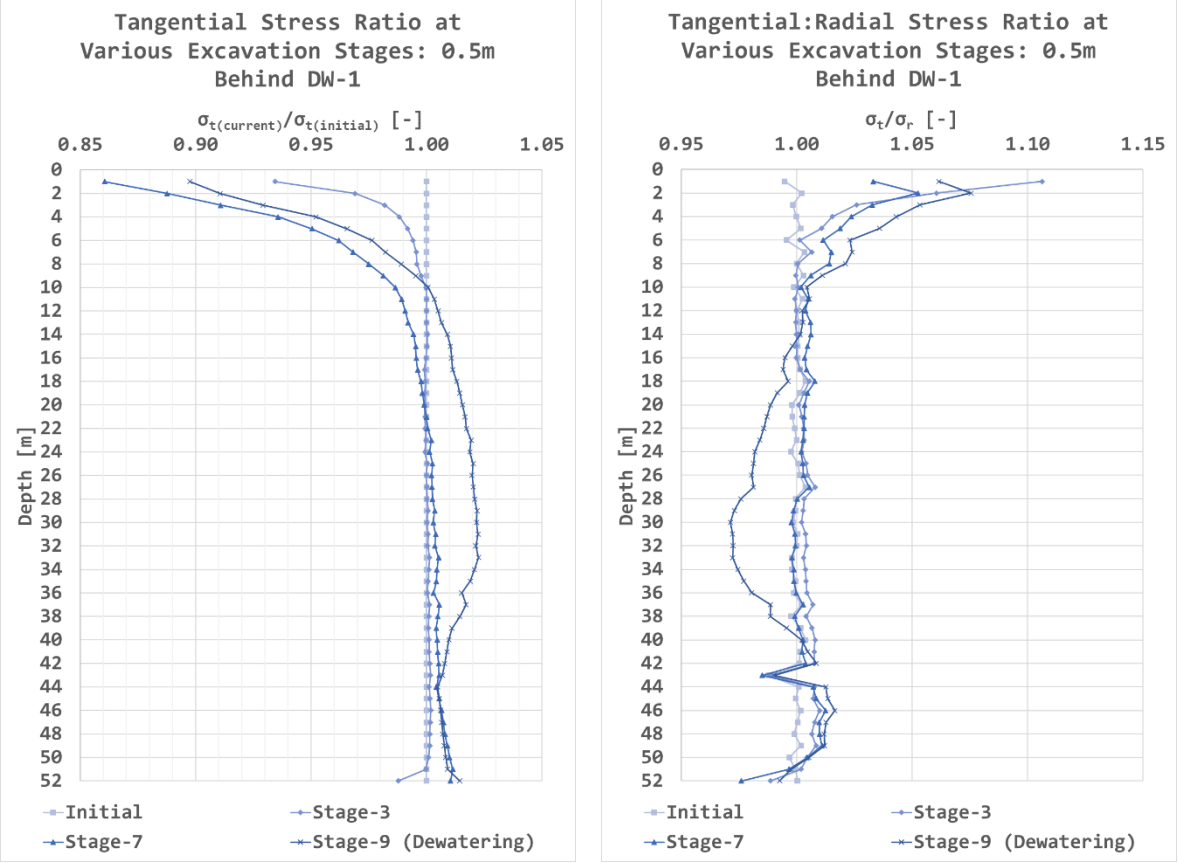

Figure 5-18: (a) Tangential stress ratio in soil at different excavation stages 0.5m behind DW-1; (b) Tangential:radial stress ratio in soil at different excavation stages 0.5m behind DW-1

When taking the same soil stress readings behind the Y-panel, similar results are seen – soil arching is not recorded when comparing tangential stress ratios in soil at different excavation stages. Additionally, when comparing tangential:radial stress ratio, it is seen that there is instead an increase in the radial stress towards the Y-panel as seen from Figure 5-19.

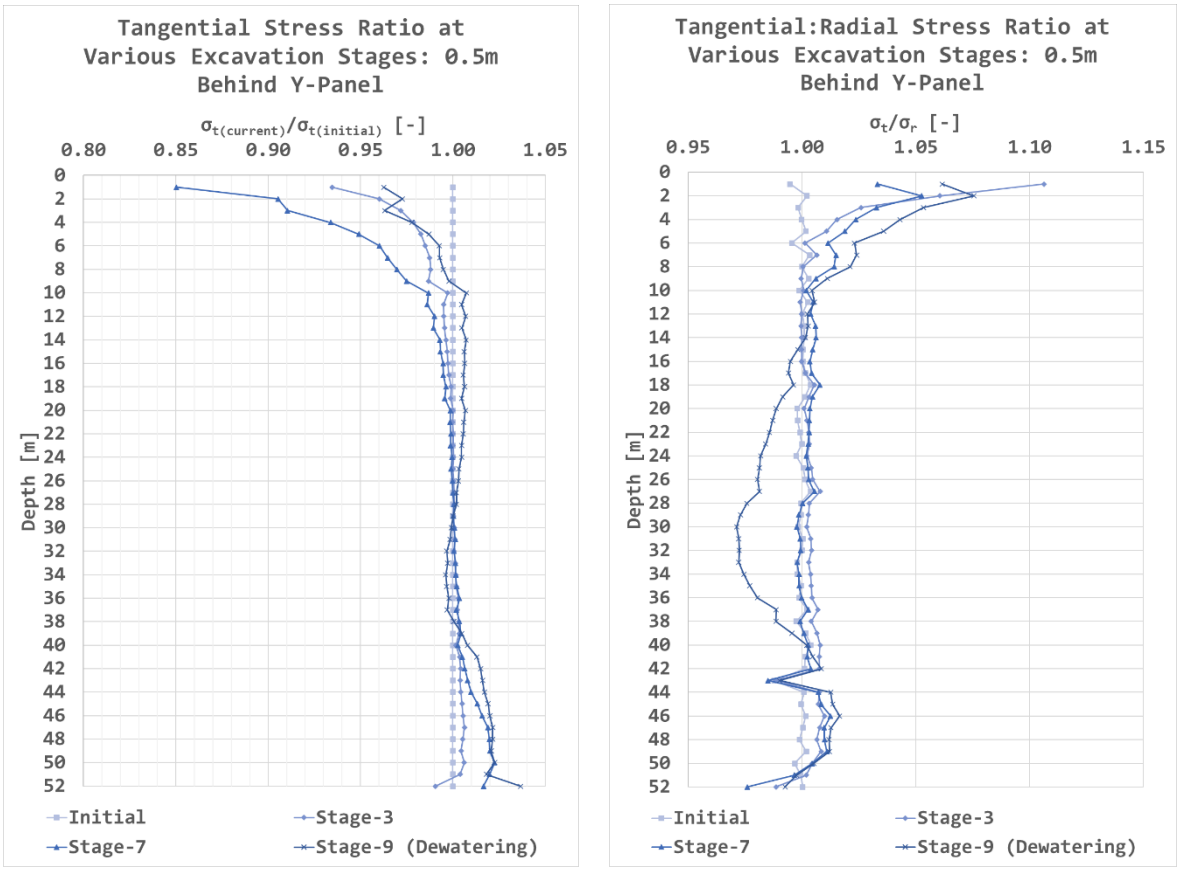

Figure 5-19: (a) Tangential stress ratio in soil at different excavation stages 0.5m behind Y-panel; (b) Tangential:radial stress ratio in soil at different excavation stages 0.5m behind Y-panel

The soil arching effect is not triggered and the horizontal forces (radial and tangential) remain almost equal throughout the excavation stages; this could be due to very rigid (or high stiffness) nature of the shaft and very low deformations which keeps the soil in the neutral state. As seen in the study by Tangjarusritaratorn et al [14], the soil arching effect is more pronounced when the shaft stiffness is low (E = 0.1 GPa) when compared to high stiffness (E = 10 GPa). To benefit from the active soil pressure and soil arching effect, the shaft would have to be made more flexible by allowing it to deform to some extent.

5.5. Comparing Buttresses

This chapter discusses what effect the Y-panel experiences when a buttress is introduced on the side facing the outer soil. The shaft with 25m diameter with no buttress was used as a control to compare the effects of adding 1m, 2m and 3m thick buttresses to the Y-panel. The results are summarised in Table 5-2.

Table 5-2: Stage-wise comparison of bending moments for different thicknesses of buttress. Note: read % change horizontal w.r.t. vertical

Mxx [% change] (max. per stage)					**Myy [% change] (max. per stage)**				
Averages					**Averages**				
Buttress thickness [m] ↓/→	**0**	**1**	**2**	**3**	**Buttress thickness [m] ↓/→**	**0**	**1**	**2**	**3**
0	0	-17	-26	-29	**0**	0	-32	-34	-34
1	-	0	-10	-14	**1**	-	0	-3	-4
2	-	-	0	-5	**2**	-	-	0	<1
Standard Deviations					**Standard Deviations**				
Buttress thickness [m] ↓/→	**0**	**1**	**2**	**3**	**Buttress thickness [m] ↓/→**	**0**	**1**	**2**	**3**
0	-	11	9	10	**0**	-	1	5	7
1	-	0	7	13	**1**	-	0	6	8
2	-	-	0	7	**2**	-	0	0	2

Note: to be read as % change from horizontal thickness w.r.t. vertical thickness. For example, the % change from 2m buttress thickness w.r.t. 1m buttress thickness is -10 for Mxx.

The addition of the buttress has a clear advantage in that the bending moments are significantly reduced in the Y-panel. For vertical bending moment, the average reduction was about 17% from having to buttress to having 1m of buttress; although, the reduction from 1m to 2m was only about 10%, and from 2m to 3m was only about 5%. It could be inferred that increasing the buttress thickness could provide diminishing returns. A similar pattern was observed for tangential bending moment as well where the reduction from having no buttress to

having 1m of buttress was about 30%; however, increasing the thickness of the buttress had insignificant effect.

For shaft deformation in global y-direction, the reduction was only 1% but this insignificant effect is because of the presence of cross-wall which makes the shaft rather rigid. The effects of buttress on the shaft deformation could be further studied in a stage-wise strut installation construction process to see if there are any meaningful benefits of it.

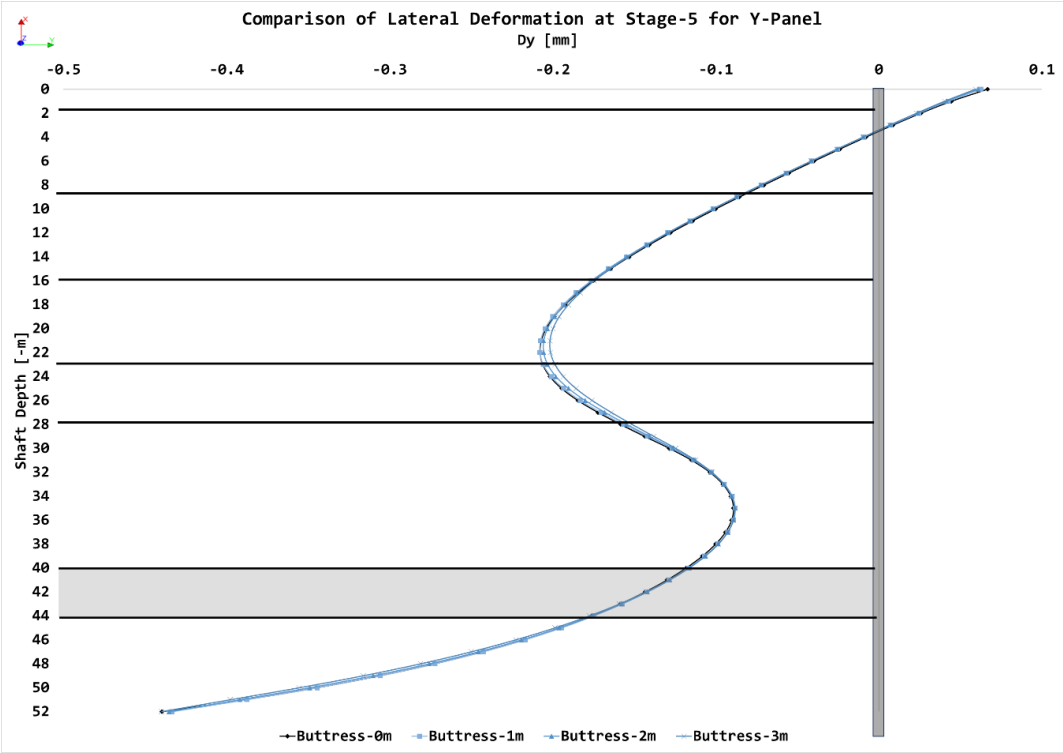

Figure 5-20: Lateral deformation of Y-panel in global y-axis for different buttress thicknesses

5.6. Stage-10: Wall Removal

The strut wall is required to be removed from -28m to -40m to make space for the TBM to be placed inside the shaft as seen from the cross-section in Figure 4-2. When the wall is removed, it is observed that there is a huge spike in the bending moment, forces and the deformation of the Y-panel; this increase is largely concentrated at

the end points at -28m and at -40m of the Y-panel as seen in Figure 5-21.

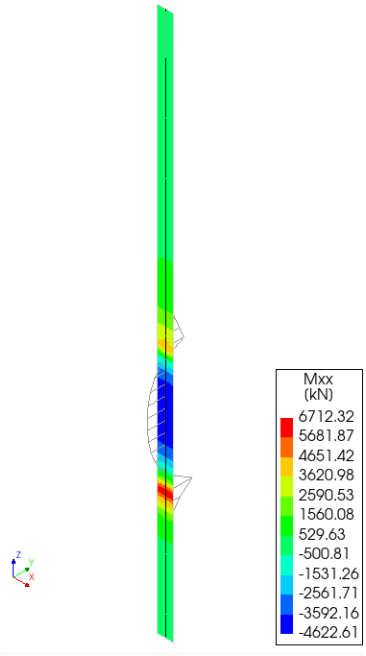

Figure 5-21: Concentrated bending moment in the Y-panel at Stage-10

These concentrated forces can be reduced significantly by avoiding removal of the entire wall to provide some buttress support to the inner side of the Y-panel as seen in Figure 5-22. By applying such a design, a significant reduction in bending moment near -28m and -40m depts where the peaks occur, as seen in Figure 5-23. A combination of buttress support on outer and inner side of Y-panel (not modelled here) could be considered to further reduce the bending moments over the entire length of the Y-panel. APPENDIX-2: PANEL THICKNESS VERIFICATION discusses the feasibility of the Y-panel.

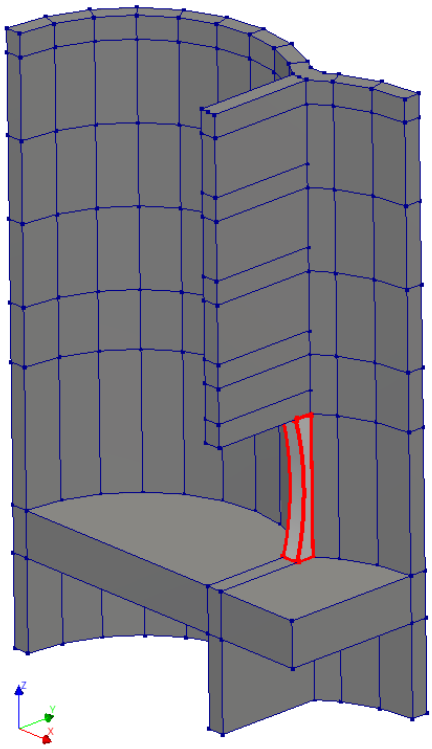

Figure 5-22: Modified wall-removal at Stage-10

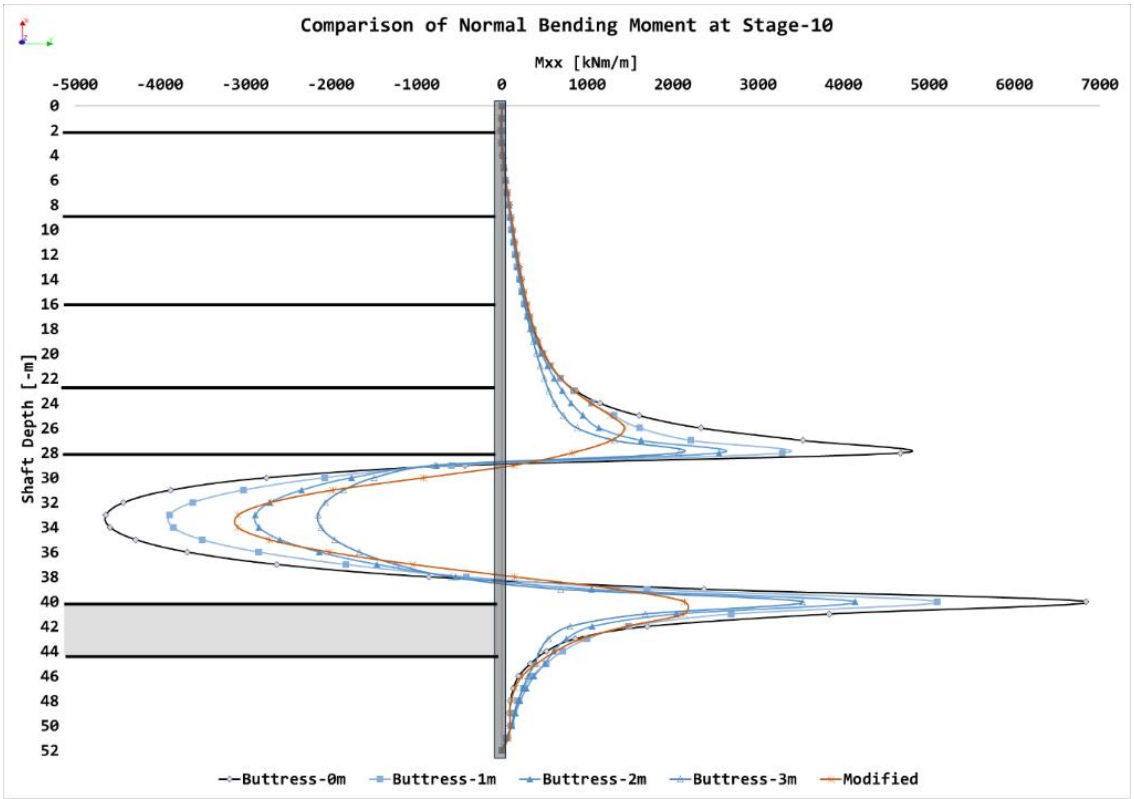

Figure 5-23: Comparison of bending moment, with modified wall (red) and buttresses of varying thicknesses, experienced in the Y-panel at Stage-10

6

CONCLUSION

The caterpillar shaft greatly benefits from the activation of the hoop forces in the structure which significantly reduce the bending moments, deformation of the shaft and the need for a dense network of stuts. The forces are transferred from the circular panels to the struts via the Y-panel. The Y-panel is the junction between two adjacent shaft cells, which can be supported using different techniques depending on what the project demands. In this study, two excavation techniques are discussed: one with cross-walls and another with struts at different levels.

The main technique discussed in this study involved the construction of cross-walls which is a D-wall connecting the two opposite Y-panels which extends till the shaft depth starting from the surface. Because this cross-wall is constructed from the surface and at the same time as the rest of the shaft structure, it significantly reduces the risks involved in excavation of unsupported structure and provide a better connection with the Y-panels. After the construction of the underwater concrete and dewatering of the shaft, these cross-walls could be demolished as required to create space for further construction.

During the excavation stages, it was observed that this caterpillar shaft deformed like an elliptical shaft – lateral inward convergence in the long edge (near Y-panels and middle-cell) and outward elongation at the shaft ends. The maximum deformation of 6.8mm were observed in the d-wall panels of the middle cell while they also generated least hoop forces of all the perimeter d-wall panels; consequently, these also generated larger bending moments. The end-cell d-wall panels, in contrast, only deformed about 2.3mm.

The highest bending moments were observed in the Y-panel when a part of the cross-wall was removed from -28m to -40m depth to create space for the TBM; these were in the range of 6000-7000 kN-m/m. These bending moments could be countered by adding a buttress on the soil

side before the commencement of the excavation. It was seen that adding just 1m thick buttress reduces the bending moments in the shaft by up to 17-30% approx.; although the delta-reduction from 1m to 2m, and 2m to 3m, thickness is significantly less when compared to 0m to 1m. Another way to reduce the large bending moments in the Y-panel, is to demolish the cross-wall only partially which could provide support to the Y-panel from the inner side. Buttress supports had a very slight effect on the deformation of the shaft in the range of 1-2% reduction due to the presence of cross-walls. The deformation of the shaft was most affected by the construction procedure chosen; that is, choosing between cross-wall and stage-wise strutting (see Appendix 1).

The extreme rigidity experienced by the shaft also meant that there was insignificant soil movement behind the shaft walls which could not trigger the soil arching effect and the soil remained in a neutral state. The shaft, however, greatly benefitted from the structural arching effect by virtue of the circular d-wall panels.

When comparing an equivalent 2D axisymmetric analysis with the circular d-wall panels of the caterpillar shaft, it was seen that the 2D axisymmetric analysis could not accurately estimate the hoop forces experienced by the circular d-wall panels of the caterpillar shaft. The axisymmetric analysis underestimated the hoop forces by 15-25% at various stages up to the excavation level at each stage and was not comparable below the excavation depth. A comparison of a 2D plane-strain model could not be done with the Y-panel as the cross-walls posed geometric limitations in the 2D model; however, an equivalent 2D plane-strain model was compared with the multi-level strut model as seen in Appendix 1. In this case, it was seen that the 2D model overestimated the deformations by up to 52% (±17%) when compared with the deformations of the Y-panel in 3D and overestimated the bending

moment by about 15% in certain cases. Thus, it could be concluded that the 2D models did not offer a reasonable estimation of forces for the caterpillar shaft given its 3D nature.

In summary, this study highlights the structural advantages of the caterpillar shaft in reducing the deformation and bending moments. The analyses show how the design choices such as cross-walls, layered struts and buttress supports influence structural performance of the shaft, specifically of the Y-panel. Additionally, the study underscores the limitations of 2D analyses in accurately predicting the behaviour of such a complex 3D structure and reinforces the need for advanced 3D modelling in the structural analysis of such a non-circular shaft. These insights should provide a foundation for future research in improving the modelling techniques and the structural design as more data becomes available.

.

7

LIMITATIONS AND FUTURE STUDIES

1. This study only performs a numerical analysis which has not been validated either through experiments or site monitoring data. However, the results align with expectations based on the literature review.

2. This study focuses on the 3-cell shaft design. Increasing the number of cells of the caterpillar shaft may create longitudinal instability which has not been studied.

3. The purpose of this shaft is to house a TBM for the construction of tunnel(s). The effect of constructing tunnel-eye(s) on the overall shaft stability can be explored in future studies.

4. There are plethora of other factors which could directly affect the stability and response of the shaft such as eccentricity of the D-wall panels, crack formation at the panel joints, addition of a capping beam, dynamic load of gantry crane to lower TBM in the shaft, break-in of the TBM etc. which were beyond the scope of the study and have not been considered here.

5. It was seen that the 2D models did not provide a reasonable estimation for the 3D model. Future studies may focus on calibration of 2D model to match the results of the 3D model, or vice versa. This could significantly reduce the effort in preparation of 3D models.

8

REFERENCES

The references provided here are presented in order of their occurrence.

[1] ITA-AITES, “Shafts – Definitions and Classifications”, ITA Report No. 26, ITA – Working Group 23 Shaft Design and Construction, ISBN: 978-2-9701242-8-3

[2] R.B. Peck, “Deep Excavations and Tunnelling in Soft Ground”, International Society for Soil Mechanics and Geotechnical Engineering, https://www.issmge.org/publications/online-library

[3] Michael Long, “Database for Retaining Wall and Ground Movements due to Deep Excavations”, Journal of Geotechnical and Geoenvironmental Engineering, February 2001, DOI: 10.1061/(ASCE)1090-0241(2001)127:3(203)

[4] Christian Moormann, “Analysis of Wall and Ground Movements Due to Deep Excavations in Soft Soil Based on a New Worldwide Database”, Japanese Geotechnical Society, Soils and Foundation, Vol. 44, No. 1, 87-98, February 2004

[5] B. New, “Settlements due to shaft construction”, Tunnels and Tunnelling International, 16-17, September 2017

[6] Faustin et al, “Case Studies of Circular Shaft Construction in London”, Proceedings of the Institution of Civil Engineers – Geotechnical Engineering 171(5): 391–404, https://doi.org/10.1680/jgeen.17.00166

[7] Qiao et al, “Deformation Characteristics of Ultra-deep Circular Shaft in Soft Soil: A Case Study”, Underground Space, Vol. 16, 239-260, June 2024, DOI: https://doi.org/10.1016/j.undsp.2023.09.006

[8] K. Terzaghi, “Theoretical Soil Mechanics”, John Wiley & Sons, 1943

[9] Feng et al, “Estimation of Arching Effect in Geosynthetic-Reinforced Structures”, Computers and Geotechnics, Vol. 87, 188-197, July 2017

[10] V.G. Berezantev, “Earth pressure on the cylindrical retaining wall”, Brussels Conference on Earth Pressure Problems, Vol. 2, 21–27, 1958

[11] Y.M. Cheng and Y.Y. Hu, “Active earth pressure on circular shaft lining obtained by simplified slip line solution with general tangential stress coefficient”, December 2004

[12] B. New, K. Bowers, “Ground Movement Model Validation at the Heathrow Express Trial Tunnel”, Tunnelling ’94, 1994 https://doi.org/10.1007/978-1-4615-2646-9_19

[13] Le et al, “Subsurface Ground Movements Due to Circular Shaft Construction”, Soils and Foundations 59 (2019) 1160–1171, July 2019

[14] Tangjarusritaratorn et al, “Numerical investigation on arching effect surrounding deep cylindrical shaft during excavation process”, Underground Space, Vol. 7, Issue 5, 944-965, October 2022

[15] Faustin, et al, “Modelling the excavation of elliptical shafts in the geotechnical centrifuge”, Physical Modelling in Geotechnics, Vol. 2, 2018

[16] A. Sandstrom and B. Elfving, “Vertical Elliptical Access Shafts - Geometrical Optimisation Through FE-Modelling”, Lund University, Thesis, 2020. ISSN 0349-4977

[17] Creten et al, “Design, Construction, and Back-Analysis of a Deep Underground Parking Garage in an Urban Environment”, International Journal of Geoengineering Case Histories, Vol. 7, Issue 1, pp. 113-116, December 2021. DOI: 10.4417/IJGCH-07-01-06

[18] U.S. Army Corps of Engineers, “Design of Sheet Pile Cellular Structures Cofferdams and Retaining Structures”, Department of the Army, Engineer Manual 1110-2-2503, September 1989

[19] Stefanizzi et al, “On Developing an Innovative, Self-supported, Cut & cover Structure for the Brooklin Station of the Sao Paulo Metro”, Proceedings of the World Tunnel Congress, International Tunnelling Association, 2014.

[20] “The World’s First 15-Cell Caterpillar-Shaped Cofferdam Design for Tuen Mun - Chek Lap Kok Link in Hong Kong”, The Singapore Engineer, September 2020, Web.

[21] S. Kanaris, “Caterpillar shaft saves carbon and space on HS2’s west London site”, New Civil Engineer, 25 August 2023, Web.

[22] A. S. Chehadeh, “Analysis and Design of Circular Shafts Using Finite Element Method”, American University of Sharjah, Thesis, June 2014. http://hdl.handle.net/11073/7717

[23] B.B. Hsiung and S. Dao, “Evaluation of Constitutive Models for Predicting Movements Caused by a Deep Excavation in Sands”, Electronic Journal of Geotechnical Engineering, December 2019.

[24] M.E. Mohamad and I.S. Ibrahim, “Interface Shear Strength of Concrete-To-Concrete Bond with and without Projecting Steel Reinforcement”, Jurnal Teknologi, Vol. 75, No. 1, Universiti Teknologi Malaysia, July 2015. https://doi.org/10.11113/jt.v75.3707

[25] J.U. Botor, “Modelling the interface in concrete-to-concrete connections between precast girders and cast-in-situ top layers”, TU Delft, Thesis, 2023. https://resolver.tudelft.nl/uuid:e556509b-49c9-42ed-b411-8d7579edfc2b

[26] W.W. Woessner and E.P. Poeter, “Hydrogeologic Properties of Earth Materials and Principles of Groundwater Flow”, The Groundwater Project, 2020. ISBN: 978-1-7770541-2-0

[27] A.I. Johnson, “Specific Yield – Compilation of Specific Yields for Various Materials”, Geological Survey Water Supply Paper 1662-D, California Department of Water Resources, 1992.

[28] Eurocode 2: EN 1992-1-1-2004

[29] V.E. Gokcek, “Diaphragm Wall Panels: Non-Linear FEM Analysis of Forces in Construction Joints”, TU Delft, Thesis, 2017.

https://resolver.tudelft.nl/uuid:757ada74-4b5c-4e0f-b713-4b029d3de94c

9

APPENDIX-1: STAGE-WISE STRUT EXCAVATION

With the limitations of designing a shaft with cross-wall in 2D plane-strain restricting a comparative study of 2D vs 3D designs, another 3D model and its equivalent 2D plain-strain were created where stage-wise installation of struts was modelled as shown in Figure 9-1 and Figure 9-2 to see if there are any similarities when the limitation of modelling the cross-wall is removed. Analysing a separate 3D model was beyond the scope of this thesis project; but, to address objective in some way, this additional effort was made. The findings of this additional model are discussed here.

In the 3D model, the struts were designed as volume elements of concrete of dimensions 1.5m x 2.0m (width x height) connecting the opposite Y-panels. The centre axes of these struts were placed, from the surface, at -1.0m, -8.0, -15.0, -22.0 and -27.0 ensuring a height clearance of 12.0m from the last strut to the UWC. The buttress at the Y-panel was not added.

In the 2D model, the Y-panel was modelled as a 'infinite shells' with a 'flat' shape definition of 1.89m thickness; 1.89m is the cross-sectional thickness of Y-panel in the model with 12.5m radius cell diameter. The struts were modelled as 'regular truss' with $3m^2$ cross-sectional area and 17.5m out-of-plane spacing to match the specifications of the 3D model. The boundary limits were the same as described for other 3D and 2D axisymmetric models, and all other parameters were the same as the main 3D model discussed in Chapter 4.

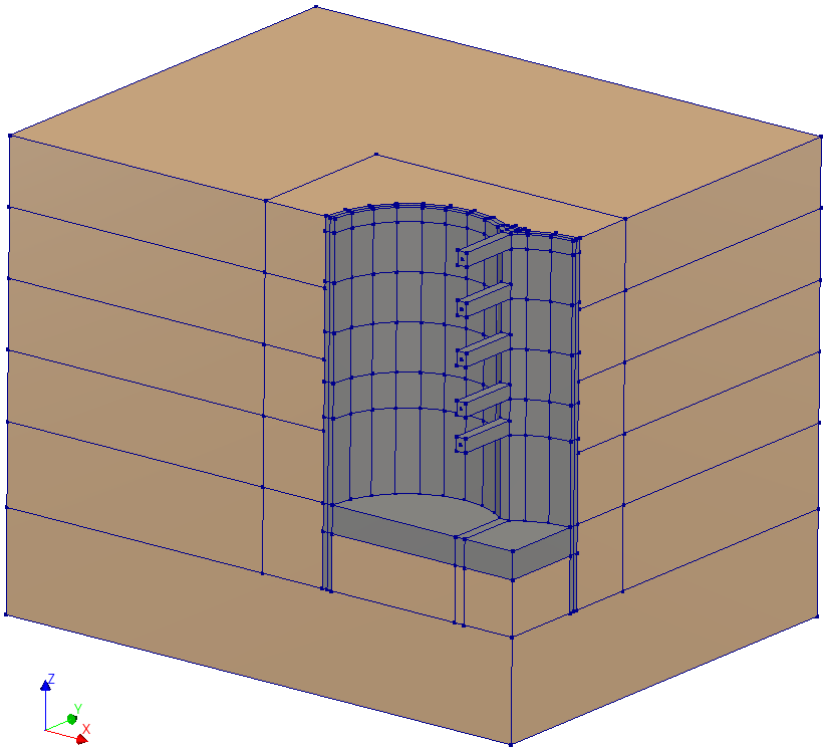

Figure 9-1: 3D model showing the stage-wise installation of struts

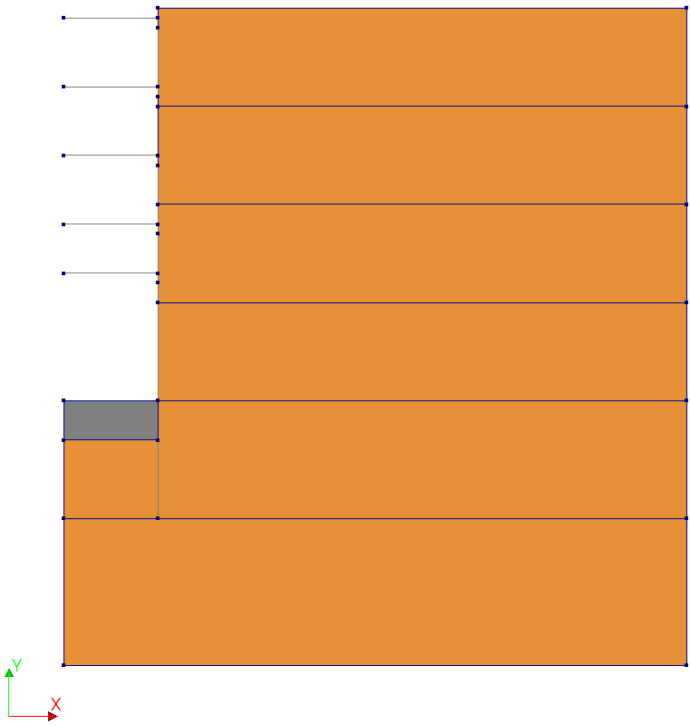

Figure 9-2: 2D plane-strain model showing the stage-wise installation of struts

In this model, a stage-wise wet excavation was executed with permanent[11] struts (instead of cross-wall); that is, excavation of soil was followed by installation of (permanent) concrete struts. An equivalent 2D model was created, which was possible in this case, and compared against the 3D model at the Y-panel section.

Stage	Description	Remarks
A	Initialisation of stresses in soil elements	Surface is considered at 0.0m elevation.
B	Installation of shaft walls and Y-panels	D-wall panels and Y-panels are installed till the depth of -52.0m. Composed elements, and structure-structure and structure-soil interfaces are also activated.
1	Excavation of inner soil till -2.0m	Hydrostatic loads are activated on the inner shaft walls till -2.0m and on the top face of unexcavated inner soil with the hydraulic head set at 0.0m to simulate wet condition for excavation
2	Strut-1 installation	First strut is installed at -1.0m
3	Excavation of inner soil till -9.0m	Hydrostatic loads are activated on the inner shaft walls till –9.0m and on the top face of unexcavated inner soil with the hydraulic head set at 0.0m
4	Strut-2 installation	Second strut is installed at -8.0m
5	Excavation of inner soil till -16.0m	Hydrostatic loads are activated on the inner shaft walls till –16.0m and on the top face of unexcavated inner soil with the hydraulic head set at 0.0m

[11] The choice of installing permanent struts, with rigid connection to the shaft, was taken to reduce the computational time of adding temporary hydraulic steel struts and replacing them with permanent struts after De-watering stage. The decision to apply rigid connection was to simplify the model. It is well acknowledged that these assumptions stray away from the real-world experience, but such an exhaustive simulation can be executed at a later stage.

Stage	Description	Remarks
6	Strut-3 installation	Third strut is installed at -15.0m
7	Excavation of inner soil till -23.0m	Hydrostatic loads are activated on the inner shaft walls till –23.0m and on the top face of unexcavated inner soil with the hydraulic head set at 0.0m
8	Strut-4 installation	Fourth strut is installed at -22.0m
9	Excavation of inner soil till -28.0m	Hydrostatic loads are activated on the inner shaft walls till –28.0m and on the top face of unexcavated inner soil with the hydraulic head set at 0.0m
10	Strut-5 installation	Fifth strut is installed at -27.0m
11	Excavation of inner soil till -40.0m	Hydrostatic loads are activated on the inner shaft walls till –40.0m and on the top face of unexcavated inner soil with the hydraulic head set at 0.0m.
12	Excavation of inner soil till -44.0m	Hydrostatic loads are activated on the inner shaft walls till –44.0m and on the top face of unexcavated inner soil with the hydraulic head set at 0.0m.
13	Installation of UWC between -40.0m to -44.0m	Hydrostatic loads are activated on the inner shaft walls till –40.0m and on the top face of UWC with the hydraulic head set at 0.0m. Interfaces connected to UWC are also activated now.
14	De-watering of shaft	Hydrostatic loads are removed from inner faces of the shaft walls. Vertical hydrostatic pressure is maintained on top face of UWC to simulate presence of tension piles.

It was seen that there were indeed some similarities in the behaviour of the 3D Y-panel and 2D plane-strain model. For example, after excavating 28m of soil and installing five levels of 2m thick struts (at -1.0, -8.0, -15.0 and -22.0 and -27.0), i.e. Stage-10, it was observed that the vertical bending moment observed in the 3D model

was like that observed in the 2D model as shown in Figure 9-3. The magnitude of the bending moment, however, varied in the two models which was expected; the plane-strain model generally seemed to overestimate the vertical bending moment, and, in this case, did so by about 15%.

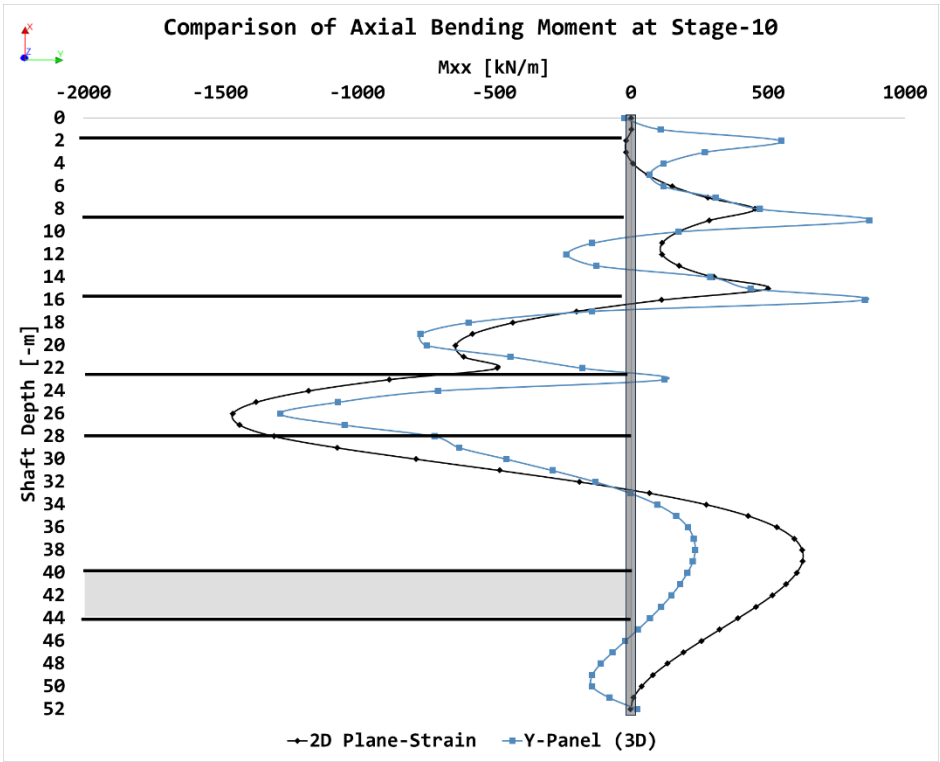

(a)

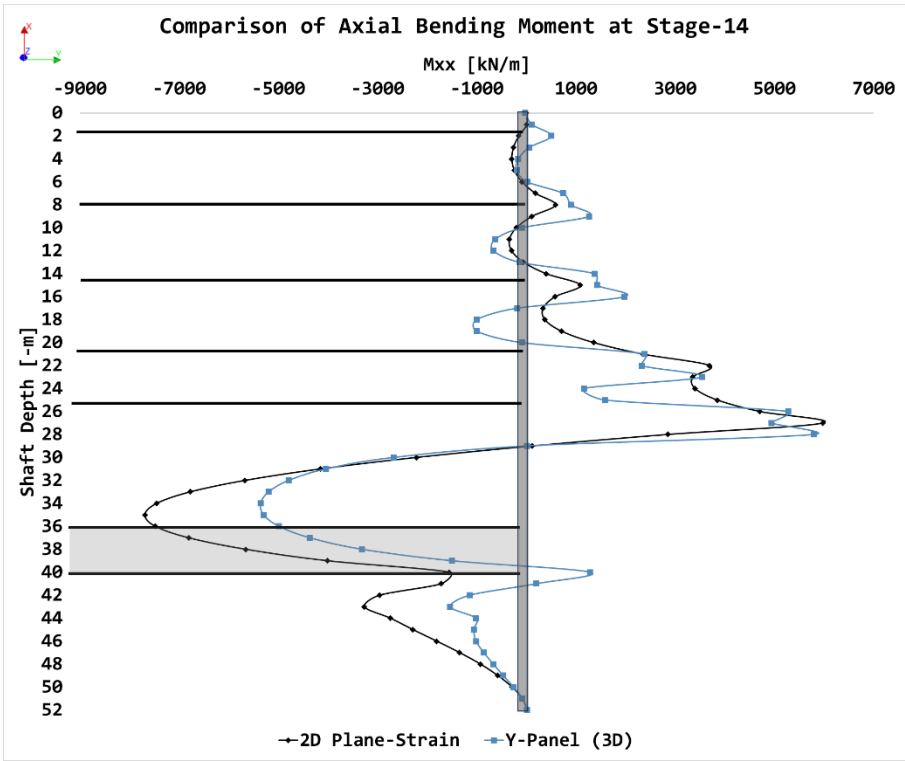

(b)

Figure 9-3: (a) vertical bending moment in 2D and 3D Y-panel after 28.0m of soil excavation; (b) vertical bending moment in 2D and 3D Y-panel after de-watering stage.

The plane-strain model also overestimated the deformation in the Y-panel when compared to the 3D model by about 52% (± 17%) above the excavation surface, whereas the plane-strain model underestimated deformations below the excavation level. Despite the differences in the values, the deformation pattern was largely similar in both cases – increasing till the excavation level then decreasing below the excavated surface as seen in Figure 9-4. The maximum deformation experienced by the Y-panel in the 3D model was ~23mm at the dewatering stage between -28.0m and -40.0m which was expected given that the entire 12m length was unsupported. This could be reduced by adding temporary struts or by adding buttress support.

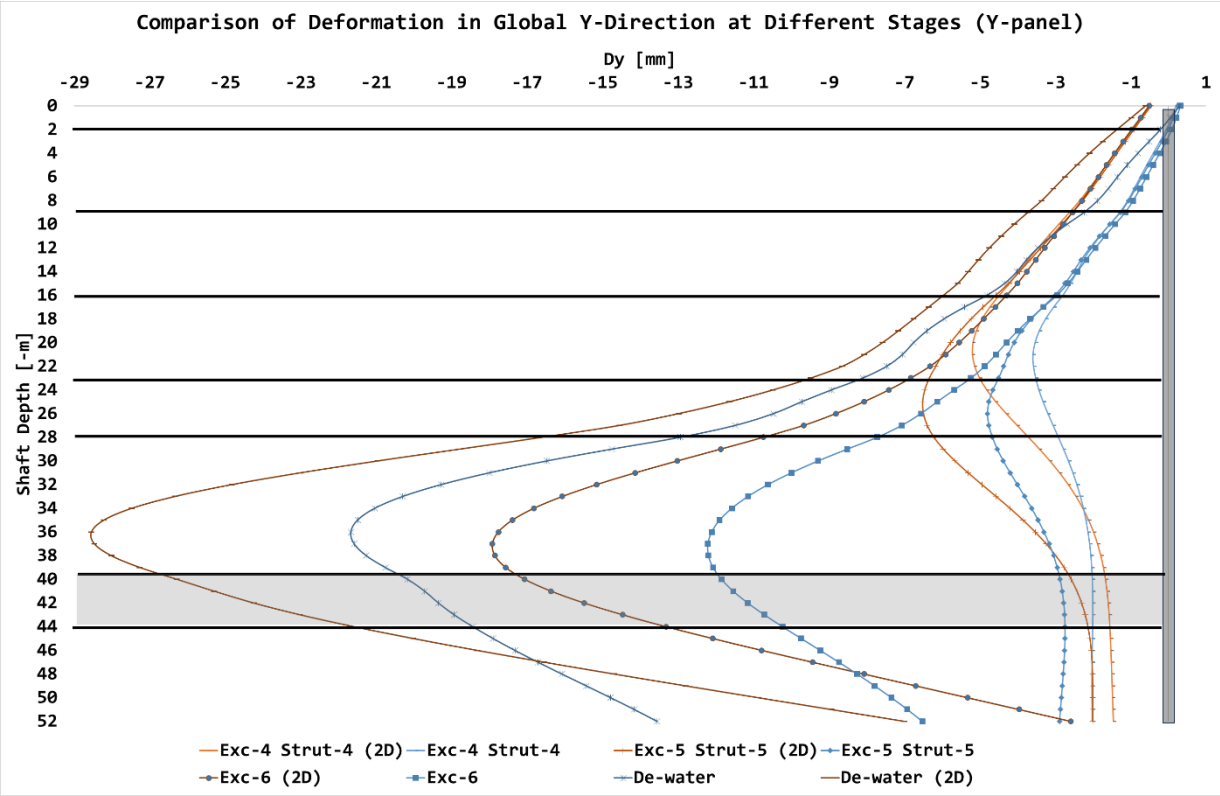

Figure 9-4: Comparison of lateral deformation of Y-panel at different stages in 2D and 3D models

At the strut locations, large bending moment could be seen developed. These moments could be reduced by adopting a (winged) corbel design as seen in Figure 2-12. When comparing these with the results from the 2D Plane-Strain analysis, it is seen that the two results are mostly comparable, although, the 2D model tends to overestimate the bending moment at unsupported lengths by about 15-20%.

10

APPENDIX-2: PANEL

THICKNESS VERIFICATION

The thickness of the shaft walls used in the analyses was initially chosen as a conservative estimate before the modelling process to ensure it did not constraint the analysis. After deriving the forces, the adequacy of the thickness could be evaluated to determine whether it was over-designed or under-designed.

To achieve this, the minimum required area of reinforcement was calculated as per Eurocode 2 <insert reference> followed by comparative study of the characteristic loads against the interaction diagram.

The panels were treated as 'columns' considering the axial loads and bending moments acting on the structure. The minimum required reinforcement area was calculated using Eq: 8 to account for the crack-control and using Eq: 9 to account for minimum steel area for longitudinal bars for a column cross-section [28].

$$A_{s,min} * \sigma_s = k_c * k * f_{ct,eff} * A_{ct}$$

Eq: 8

$$A_{s,min} = max(\frac{0.10 * N_{ED}}{f_{yd}}; 0.002 * A_c)$$

Eq: 9

The general cross-section used for the calculation of the steel reinforcement is shown in Figure 10-1. The input parameters are detailed in Table 10-1.

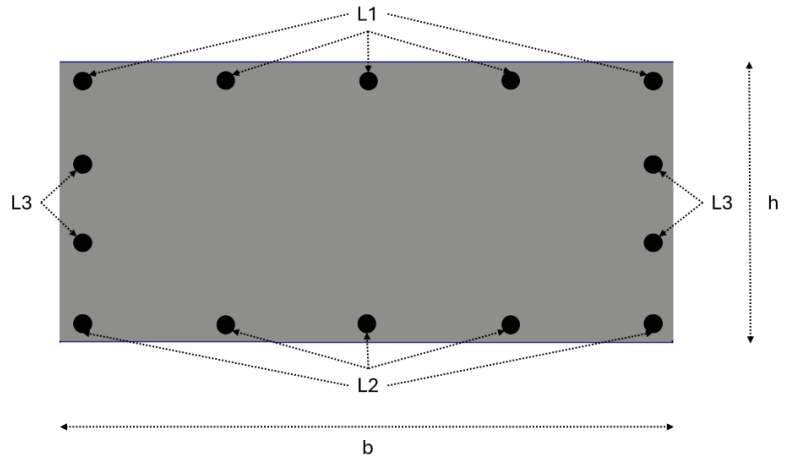

Figure 10-1: General cross-section of a reinforced concrete column

10.1. Perimeter D-wall Panels

The trapezoidal geometry of the panel was simplified to a rectangular shape of 1.5 (h) x 3.2 (b) metres for the ease of calculation. The bending moments and axial force from DW-10 at Stage-10 were used for the calculations presented in Table 10-1.

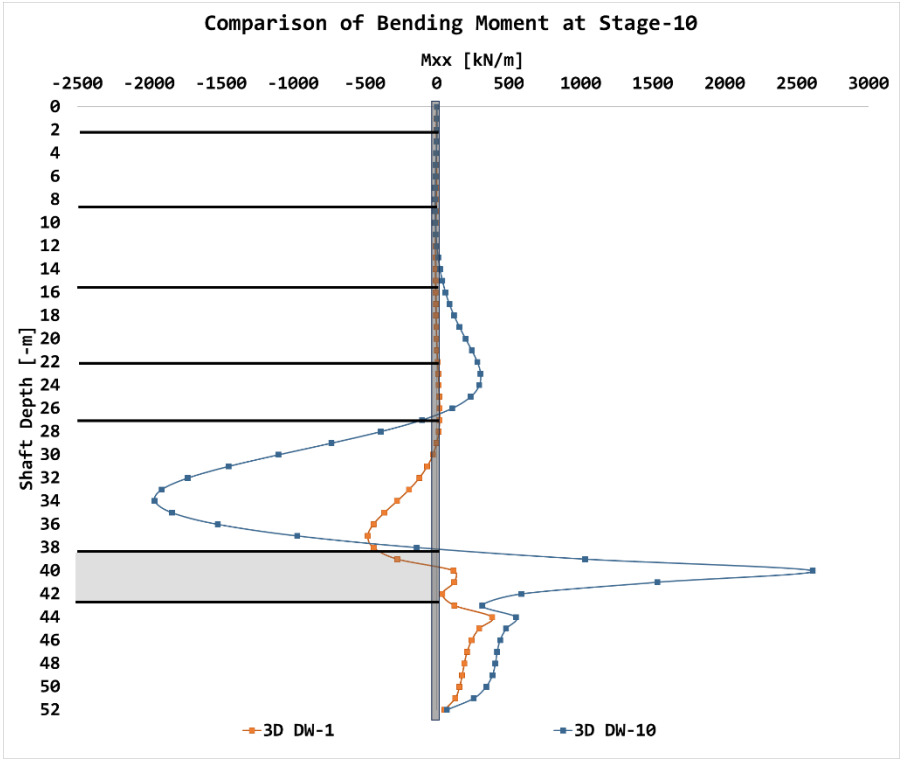

Figure 10-2: Maximum bending moment experienced by DW-1 and DW-10 (in Stage 10)

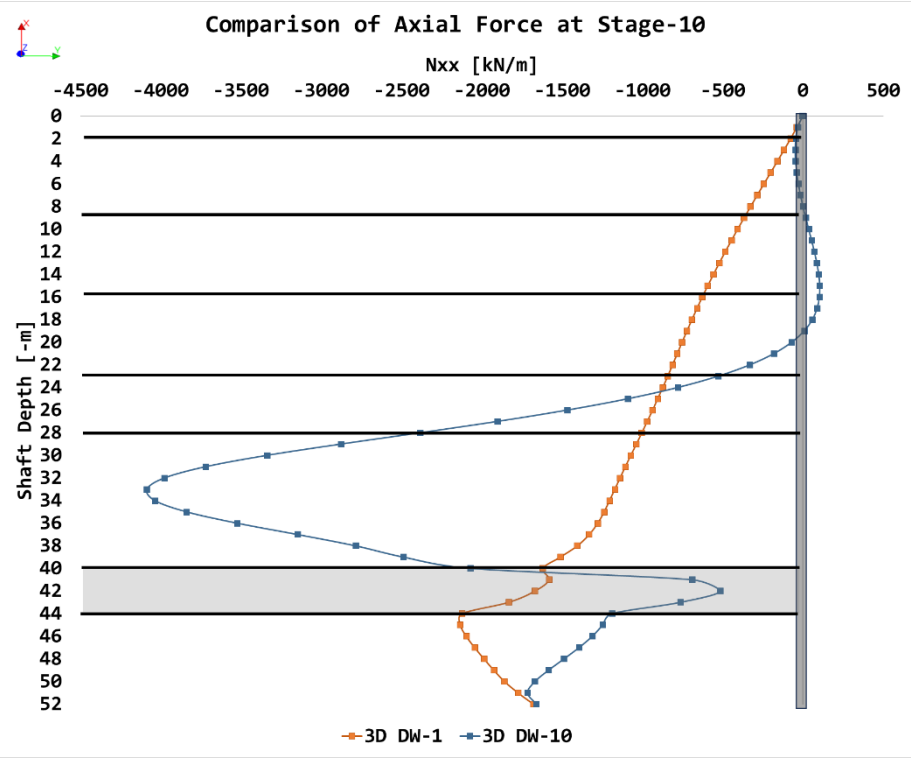

Figure 10-3: Maximum axial force experienced in DW-1 and DW-10 (in Stage-10)

Table 10-1: Summary of calculations for minimum reinforcement area required for a column cross-section

	Minimum Steel Area Required for Crack Control	Minimum Steel Area Required for Column Cross-Section	Minimum Steel Area Required for M-N Design Values
Reference	Eq: 8	Eq: 9	Chapter 6.1 [28]
N_{ED} [MN]	-1.49	-1.49	-1.49
M_{ED} [kN-m]	3000	3000	3000
f_{ck} [MPa]	30	30	30
f_{yk} [MPa]	500	500	500
α_{cc}	1	1	1
γ_c	1.5	1.5	1.5
γ_s	1.15	1.15	1.15
$\epsilon_{ud}/\epsilon_{uk}$	0.9	0.9	0.9
Stress-strain behaviour	Perfectly plastic	Perfectly plastic	Perfectly plastic
σ_s (or f_{yd}) [MPa]	434	434	-
k_c	0.40	-	-
k	0.65	-	-
$f_{ct,eff}$ [MPa]	2.9	-	-
A_{ct} [m2]	2.4	-	-
Concrete Cover [mm]	75+5	75+5	75+5
b [m]	3.2	3.2	3.2
h [m]	1.5	1.5	1.5
$A_{s,min}$ [mm^2]	4163.4	9600	6242
$A_{s,provided}$	7536	**10053**	6280

	Minimum Steel Area Required for Crack Control	Minimum Steel Area Required for Column Cross-Section	Minimum Steel Area Required for M-N Design Values
Bar Arrangement	L1: ϕ20 * 8 L2: ϕ20 * 8 L3: ϕ20 * 8	**L1: $\boldsymbol{\phi}$20 * 12** **L2: $\boldsymbol{\phi}$20 * 12** **L3: $\boldsymbol{\phi}$20 * 8**	L1: ϕ20 * 6 L2: ϕ20 * 6 L3: ϕ20 * 8
h [m]	1.2	1.2	1.2
$A_{s,min}$ [mm^2]	3331.3	7680	8992
$A_{s,provided}$	3768	8164	**9420**
Bar Arrangement	L1: ϕ20 * 4 L2: ϕ20 * 4 L3: ϕ20 * 4	L1: ϕ20 * 10 L2: ϕ20 * 10 L3: ϕ20 * 6	**L1: $\boldsymbol{\phi}$20 * 12** **L2: $\boldsymbol{\phi}$20 * 12** **L3: $\boldsymbol{\phi}$20 * 6**
h [m]	1.0	1.0	1.0
$A_{s,min}$ [mm^2]	-	-	**11930**
$A_{s,provided}$	-	-	**11930**
Bar Arrangement	-	-	**L1: $\boldsymbol{\phi}$20 * 16** **L2: $\boldsymbol{\phi}$20 * 16** **L3: $\boldsymbol{\phi}$20 * 6**

Note:

- All partial factors are as per the general Eurocode and do not account for National Annexes.
- Only the minimum required of eccentricity as per Eurocode is considered in the calculations (e=h/30).
- These calculations only consider the requirement for longitudinal reinforcement. Checks for tranversal reinforcement, shear reinforcement, bar lapping, etc. are beyond the scope of this study.

From the Table 10-1, it is evident that the panel thickness of 1.5m for the circular section is overdesigned for the required design M-N values as the area of steel required for the cross-section governs. To resist the M-N forces experienced by the panel, a minimum steel area of 6280mm^2 suffices for a 1.5m thick panel. By reducing the panel thickness to 1.2m, it is seen that the characteristic M-N values now govern the minimum area required for the reinforcement and leads to a reduction of about 633mm^2 (or two ϕ20 bars). Further, reducing the panel thickness to 1.0m leads to an increased reinforcement area to

11930mm^2. From this preliminary analysis, it could be concluded that 1.2m thickness for the panel is most optimal, although other options are also feasible. Figure 10-4 and Figure 10-5 show the interaction diagram for the two panel thicknesses. Mostly, the characteristic values derived from the analyses lie around the 'balanced' failure zone while all values lie within the failure envelop.

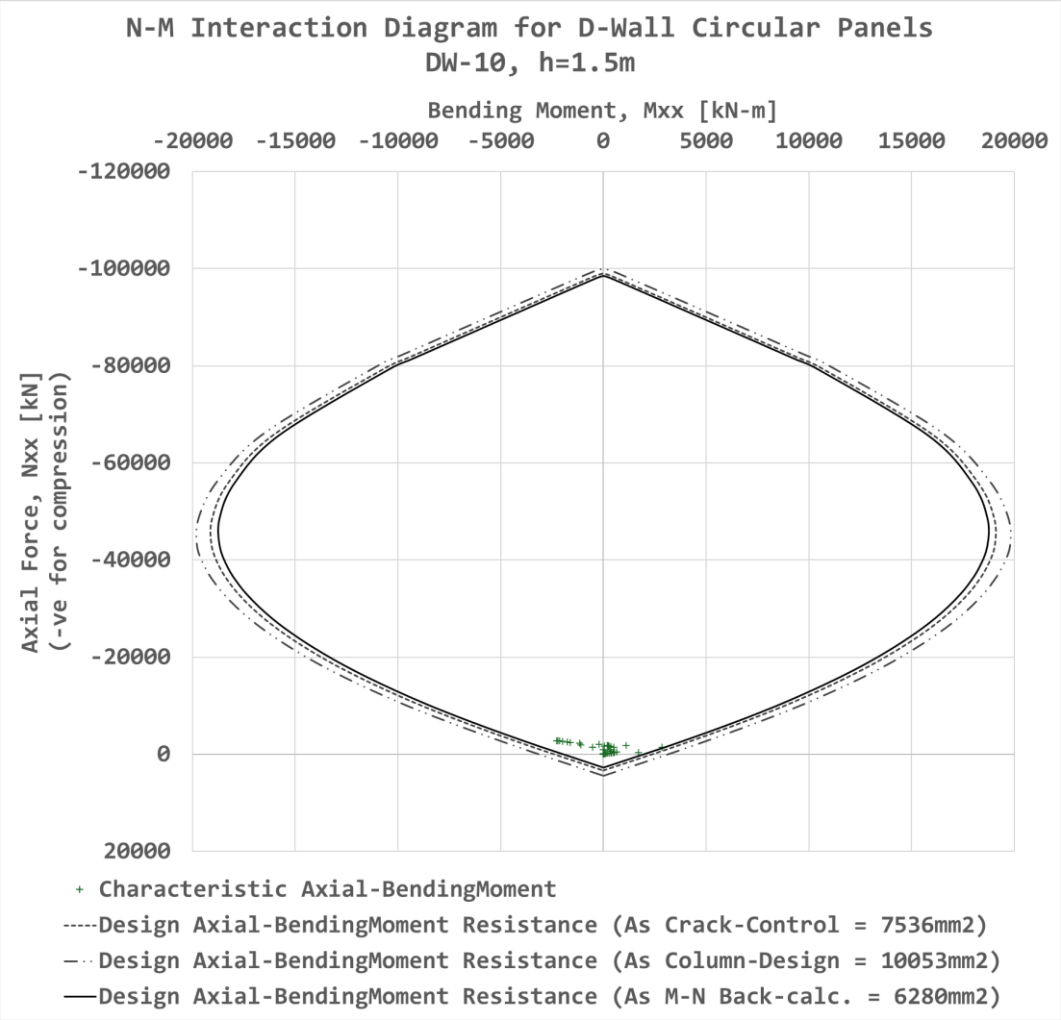

Figure 10-4: M-N interaction diagram for DW-10 (1.5m thickness)

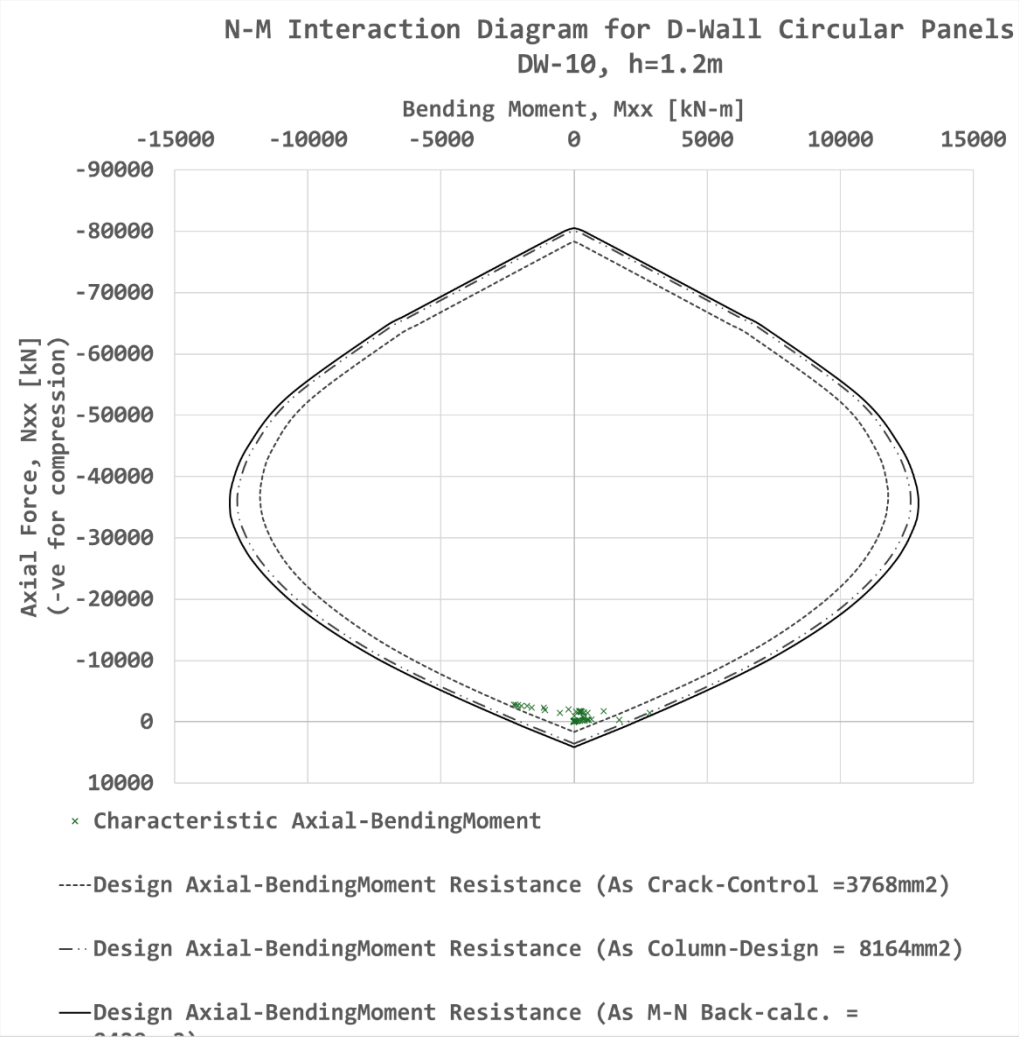

Figure 10-5: M-N interaction diagram for DW-10 (1.2m thickness)

10.2. Y-Panel

The same exercise when conducted for the Y-panel. As per the Eurocode guideline, the web and the flange of the Y-panels should be analysed individually; here, only the cross-section of the web, with h = 1.89m and b = 1.5m, was considered. This cross-section resulted in a minimum required steel area of 25491mm^2 governed by the M_{ED}-N_{ED} forces; the calculation was like that of the circular panel considered in the previous chapter – 25m diameter, 3-cell shaft with no buttress support and uniform sand stratum at Stage-10 excavation. The M-N combination from depths -28m to -40m were the most critical in this

case (see Figure 5-23), which is expected given that the cross-wall is excavated at those depths. However, when considering the M-N forces with buttress support on the inner side, the required reinforcement area for this web of Y-panel reduces to 9918mm^2 as shown in Figure 10-6 which is a more realistic scenario. Given the large differences in the required reinforcement area, the importance of the buttress support, especially in the zone where the wall is removed, cannot be understated. The reduced reinforcement requirement not only benefits economically but would also make fabrication and lowering of reinforcement cage more feasible at site.

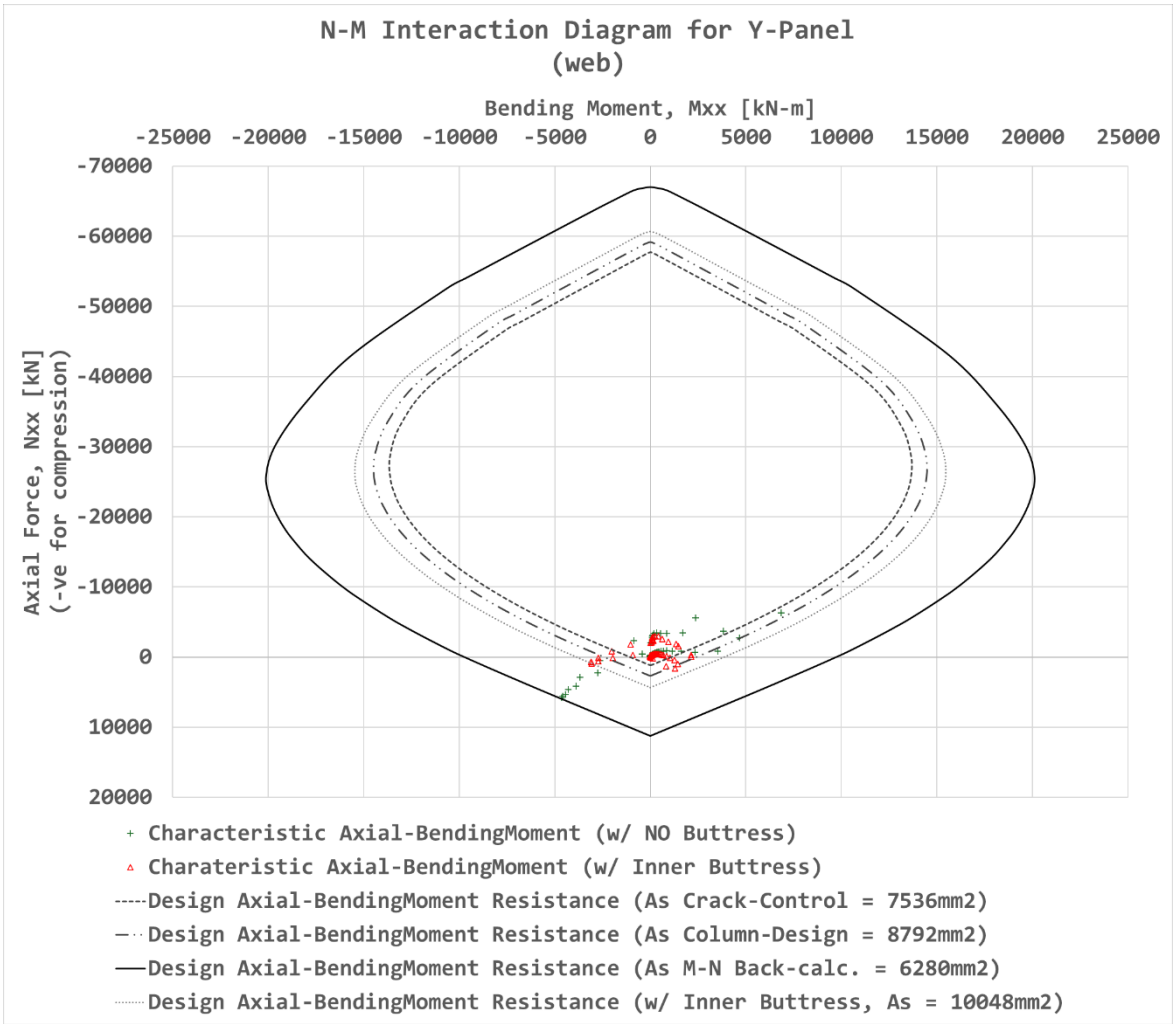

Figure 10-6: M-N interaction diagram for Y-Panel (web)

From the interaction diagram, it is also seen that the bending moment experienced by the panel is about 2-2.5 times that of the moment experienced by the circular panels; adding the buttress support reduces the moment experienced by the Y-panel significantly, consequently, also reducing the required steel area. For the most part, the failure of the panel tends to be governed more by the bending moment than by the axial force.

In the current design-state, the thickness of the circular panels matches that of the Y-panel; however, if the thickness of the circular panels is reduced (to 1.2m) while the Y-panel thickness remains 1.5m, the uneven thicknesses could generate additional eccentric loads and may affect the join-stability between the Y-panel and the circular panels [28].

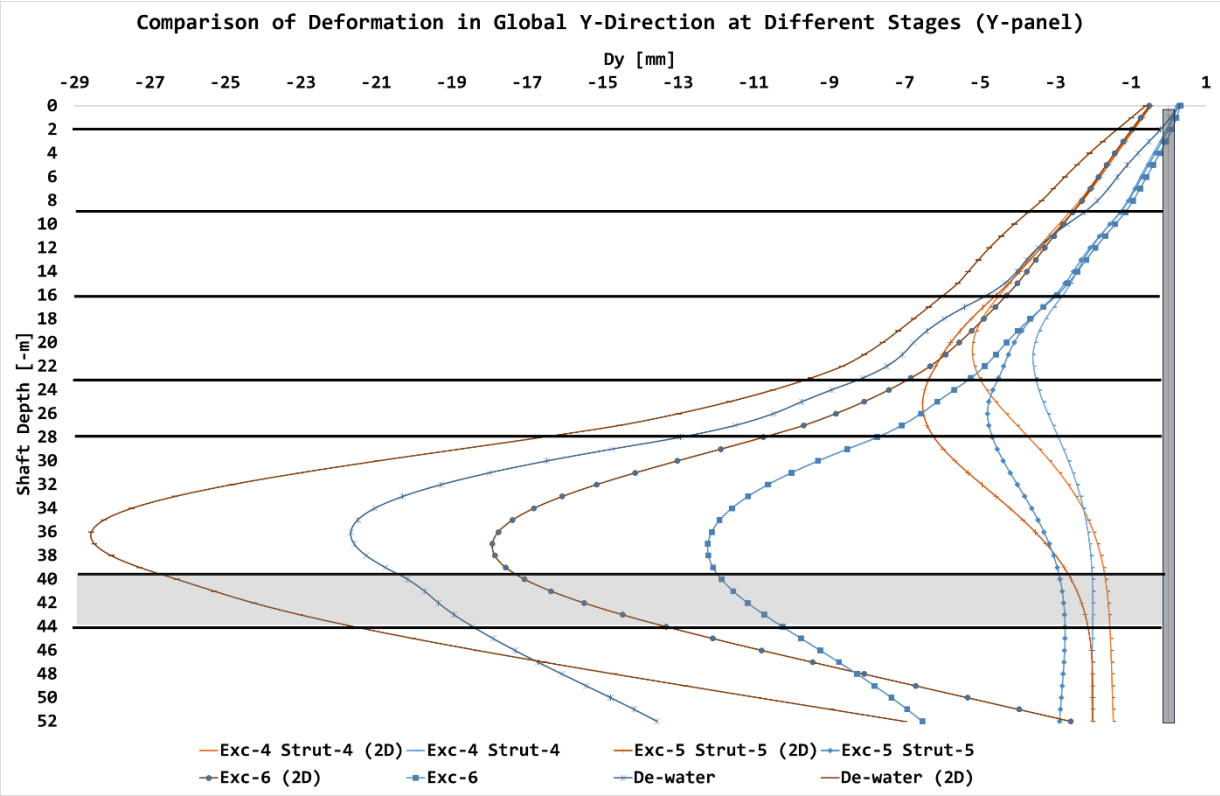

Figure 10-7: Comparison of lateral deformation of Y-panel at different stages in 2D and 3D models

At the strut locations, large bending moment could be seen developed. These moments could be reduced by adopting a (winged) corbel design as seen in Figure 2-12. When comparing these with the results from the 2D Plane-Strain analysis, it is seen that the two results are mostly comparable, although, the 2D model tends to overestimate the bending moment at unsupported lengths by about 15-20%.